Development of a novel method for β-hexosaminidase A purification and investigation of the transport of an engineered enzyme across the blood-brain barrier

By

Kristen Bouma

A Thesis submitted to the Faculty of Graduate Studies of

The University of Manitoba

in partial fulfillment of the requirements for the degree of

Master of Science

Department of Microbiology

University of Manitoba

Winnipeg, Manitoba, Canada

Abstract

Tay-Sachs disease (TSD) and Sandhoff disease (SD) are severe autosomal recessive genetic disorders caused by loss-of-function mutations in the *HEXA* and *HEXB* genes encoding the heterodimeric enzyme β-hexosaminidase A (HexA). Deficiencies in HexA lead to the pathological accumulation of GM2 ganglioside (GM2) in the central nervous system (CNS). An engineered enzyme called HexM was previously developed based on the key features of the α- and the β-subunits of HexA as a potential therapeutic for these genetic disorders. Currently all treatments for TSD and SD are palliative in nature as there are no cures available. One of the biggest challenges in developing a therapeutic is the limited permeability of the blood-brain barrier (BBB), which impedes the delivery of molecules, including HexM, to the CNS. To this end, HexM variants were generated by genetically fusing the enzyme to peptide tags derived from apolipoprotein B (3371-3409) and E $(159\text{-}167)_2$, known to facilitate the transport of lysosomal proteins across the BBB. The resulting HexM-ApoB and HexM-ApoE proteins were purified from a human embryonic kidney 293T cell line deficient in *HEXA* and *HEXB* (HEK293T-ABKO) after transfection with overexpression cassettes. The fusion proteins were kinetically active and stable in several buffer conditions, however, did not cross an *in vitro* BBB model consisting of human brain endothelial cells. To further therapeutic research on TSD and SD, a novel method of recombinantly producing HexA was developed. The HEK293T-ABKO cells were transfected with plasmids encoding *HEXA* and *HEXB* with a C-terminal FLAG-tag and a His_6 tag, respectively. The enzyme could be isolated in a two-step purification procedure and was found to be kinetically active. This method provides a convenient means of obtaining HexA, rather than the traditional process of isolating the enzyme from human placentas, and can further be developed to generate HexA mutants in sufficient quantities for structural studies.

Acknowledgements

I would like to begin by thanking my supervisor Dr. Brian Mark for his guidance and support throughout my time as his student. I am deeply grateful for all of the knowledge and the invaluable advice he provided me over the course of my graduate training. I would also like to thank my committee members, Dr. Gerd Prehna and Dr. Michael Czubryt for all of their insightful comments and suggestions.

I would like to extend my gratitude to Dr. Willard Costain and Eric Brunette at the National Research Council of Canada for their contributions on the blood-brain barrier work. I would also like to recognize the Canadian Institutes for Health Research, Research Manitoba and the Canadian Glycomics Network for their financial support which made this research possible.

I would like to thank all members of the Mark lab for all of their guidance and for providing a wonderful work environment. Thank you to Veronica Larmour and Graeme Benzie for training me in biochemical and molecular biology techniques. I would also like to express my gratitude to Vince Jung for formally training me on how to establish and maintain mammalian cell lines. Thank you to Ankoor Patel for all the help troubleshooting and for your friendship both in and out of the lab. I would like to extend my thanks to the rest of the students, faculty and staff within the Department of Microbiology for providing me with a positive graduate experience.

Finally, I would like to thank my family for their unwavering love and support.

Table of Contents

List of Tables

List of Figures

List of Abbreviations

AAV2/8	Adeno-associated virus serotype 2/8
Ab	Antibody
AMT	Adsorptive-mediated transport
AnP	Antarctic Phosphatase
ApoB	Apolipoprotein B
ApoE	Apolipoprotein E
ASA	Arylsulfatase A
ASA-ApoE	Arylsulfatase A-apolipoprotein E
BBB	Blood-brain barrier
BBBD	Blood-brain barrier disruption
BCNU	1,3-bis(2-chloroethyl)-1-nitrosourea
bFGF	Basic fibroblast growth factor
Bis-Tris	Bis(2-hydroxyethyl)amino-tris(hydroxymethyl)methane
BMECs	Brain microvascular endothelial cells
BMT	Bone marrow transplantation
CAG	Chicken β-actin
CDM-HD	Chemically defined medium for high density
CD-MPR	Cation-dependent mannose 6-phosphate receptor
CMV	Cytomegalovirus
CNS	Central nervous system
CPP	Cell-penetrating peptide
CRISPR	Clustered regularly interspaced short palindromic repeats
CSF	Cerebrospinal fluid
DLS	Dynamic light scattering
DMEM	Dulbecco's modified Eagle medium
DMSO	Dimethyl sulfoxide
DNA	Deoxyribonucleic acid
DOC	Degree of conversion
dNTP	Deoxynucleoside triphosphate
ERAD	Endoplasmic reticulum-association degradation
ERT	Enzyme replacement therapy
FBS	Fetal bovine serum
FDA	United States Food and Drug Administration
FUS	Focused ultrasound
GalNAc	*N*-acetyl-β-galactosamine
GFP	Green fluorescent protein
GLUT1	Glucose transporter 1
GM1	GM1 ganglioside
GM2	GM2 ganglioside
GM3	GM3 ganglioside
GM4	GM4 ganglioside
GM2AP	GM2 activator protein
HBSS	Hanks' balanced salt solution
HEK 293T	Human embryonic kidney 293T
HEPES	4-(2-hydroxyethyl)-1-piperazineethanethanesulfonic acid

HexA	β-hexosaminidase A
HexB	β-hexosaminidase B
HexM	β-hexosaminidase M
HexM-ApoB	β-hexosaminidase M-apolipoprotein B
HexM-ApoE	β-hexosaminidase M-apolipoprotein E
HexS	β-hexosaminidase S
HIV TAT	Human immunodeficiency virus trans-activator of transcription
HRP	Horseradish peroxidase
IDUA	α-L-iduronidase
IDUA-ApoE	α-L-iduronidase-apolipoprotein E
IDUA-RTB	α-L-iduronidase-ribosome-inactivating toxin B subunit
IGF2R	Insulin-like growth factor 2 receptor
IUBMB	International Union of Biochemistry and Molecular Biology
IUPAC	International Union of Pure and Applied Chemistry
k_{cat}	Catalytic rate constant
K_m	Michaelis constant
LDLR	Low-density lipoprotein receptor
LRP1	Low-density lipoprotein receptor-related protein 1
LRP2	Low-density lipoprotein receptor-related protein 2
LSD	Lysosomal storage disorders
MCT1	Monocarboxylate transporter 1
MHC	Major histocompatibility complex
MPS I	Mucopolysaccharidosis type I
MPS IIIA	Mucopolysaccharidosis type IIIA
MPS IIIB	Mucopolysaccharidosis type IIIB
MUG	4-Methylumbelliferyl 2-acetamido-2-deoxy-β-D-glucopyranoside
MUGS	4-Methylumbelliferyl 6-sulfo-2-acetamido-2-deoxy-β-D-glucopyranoside
M6P	Mannose 6-phosphate
NAGLU	α-*N*-acetylglucosaminidase
Nickel-NTA	Nickel-nitrilotriacetic acid
NRC	National Research Council of Canada
NRR	Normalized reaction rate
ORF	Open reading frame
PBS	Phosphate-buffered saline
PEG	Polyethylene glycol
PEI	Polyethylenimine
PCR	Polymerase chain reaction
R_f	Retention factor
RFU	Relative fluorescence units
RTB	Ribosome-inactivating toxin B subunit
rtTA	Reverse tetracycline transactivator
scAAV9	Self-complementary adeno-associated virus serotype 9
SD	Sandhoff disease
SDS-PAGE	Sodium dodecyl sulfate polyacrylamide gel electrophoresis
SGSH	N-sulfoglucosamine sulfohydrolase
SV40	Simian vacuolating virus 40

SV40Δ90	Attenuated simian vacuolating virus 40 early promoter
tetO	Tetracycline operator
T_m	Melting temperature
TRE	Tetracycline response element
TSD	Tay-Sachs disease
UV	Ultraviolet
v-ATPase	Vacuolar adenosine triphosphatase
V_{max}	Maximum enzyme velocity
4-MU	4-methylumbelliferone

1. Introduction

1.1. Gangliosides and disease

Gangliosides were first discovered in the 1930s by the German scientist Ernst Klenk. He was examining post-mortem human brain tissue obtained from individuals diagnosed with what was known at the time as "amaurotic idiocy" (Sachs, 1896; Konrad Sandhoff & Harzer, 2013). Amaurotic idiocy was clinically characterized by having impaired vision, muscle weakness (Tay, 1881), intellectual disabilities (Sachs, 1896) and high quantities of lipid-laden cells. These cells were primarily located within the nervous system and in visceral organs (Norman & Wood, 1941). It was found that in some forms of amaurotic idiocy, gangliosides were the primary type of lipid accumulating within the cells (Sandhoff & Harzer, 2013). Amaurotic idiocy is now referred to as Tay-Sachs disease (TSD), named after the ophthalmologist Waren Tay, who first described a characteristic "cherry red" spot observed in the macula of patients (Tay, 1881) and for the neurologist Bernard Sachs, who further described the physiological changes associated with the disease (Sachs, 1887, 1896). Sachs also noted the hereditary nature of the disorder (Sachs, 1896).

While patients diagnosed with TSD have cells overloaded with gangliosides, these lipids are a normal component of the plasma membrane in all mammalian cells. The quantity of gangliosides is greatest in neuronal cells, where they are a significant glycolipid on the plasma membrane (Schnaar, 2016; Svennerholm, 1980). Gangliosides are glycosphingolipids with one or more sialic acid residues attached to a carbohydrate. Variations in the sugar residues attached to the ceramide base differentiates various gangliosides from each other (Ledeen & Wu, 2018; Schnaar, 2016; Svennerholm, 1964). Gangliosides actively play a role in cellular processes such as apoptosis, cell signaling, differentiation and adhesion (Malisan & Testi, 2002; Sandhoff &

Harzer, 2013). They also play a role in infectious disease by acting as receptors for toxins and viruses. GM1 ganglioside (GM1) is considered to be the main receptor for the cholera toxin (Holmgren *et al.*, 1973; Jobling *et al.*, 2012). Trisialoganglioside GT1b, one of the four major gangliosides found within the brain (Svennerholm, 1964), is thought to be a receptor for the Merkel cell polyomavirus, which is suspected to be a causative agent of Merkel cell carcinoma (Erickson *et al*., 2009). Gangliosides are also known to act as receptors for influenza virus (Cutillo *et al.*, 2020; Vrijens *et al.*, 2019).

Gangliosides are constantly being synthesized and degraded by cells. Biosynthesis of these glycosphingolipids begins with the formation of ceramide. *De novo* synthesis of ceramide occurs in the smooth endoplasmic reticulum with the condensation of palmitoyl-CoA and serine to form 3-keto-dihydrosphinganine (Hanada *et al.*, 1990, 1992), which is then reduced to generate dihydrosphinganine (**Fig. 1.1**). Dihydrosphinganine is then acylated to form dihydroceramide. A desaturase introduces a trans-4,5 double bond to dihydroceramide to generate ceramide (Wang *et al.*, 1991). Ceramide is then transported to the Golgi apparatus, where it is further modified by the sequential addition of carbohydrate moieties to generate glucosylceramide (Futerman & Pagano, 1991; Jeckel *et al*., 1992) then lactosylceramide (Brandli *et al.*, 1988). Most gangliosides are synthesized from lactosylceramide. The exception is GM4, which is synthesized from galactosylceramide (Sandhoff & Kolter, 2003). GM3 ganglioside (GM3) is synthesized by the addition of a sialic acid to lactosylceramide (Preuss *et al.*, 1993). Glycosyltransfterases then converts GM3 into more complex gangliosides, including GM2 ganglioside (GM2) and GM1 (Sango *et al.*, 1995).

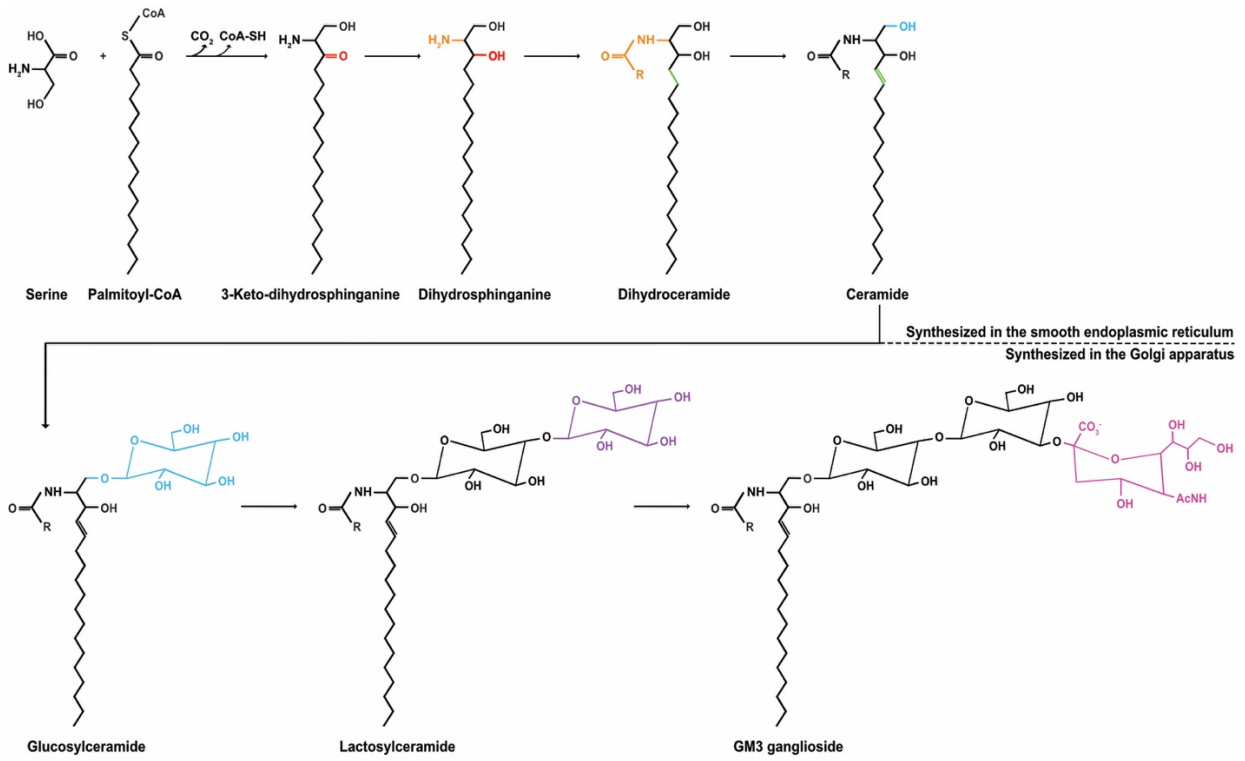

Figure 1.1. The biosynthetic pathway of gangliosides. Synthesis begins in the smooth endoplasmic reticulum with the condensation of serine and palmitoyl-CoA, which forms 3-keto-dihydrosphinganine. Reduction of 3-keto-dihydrosphinganine generates dihydrosphinganine, which is then acylated to produce dihydroceramide. A double bond is inserted in dihydroceramide to generate ceramide. Ceramide is transported to the Golgi apparatus and glucosylceramide is formed by the addition of a glucose residue. A terminal lactose residue is added to form lactosylceramide and GM3 ganglioside is produced by the addition of a sialic acid moiety. Additional sugar residues are added to form more complex gangliosides. Changes to the intermediates in the pathway are shown by various colours.

While few diseases are caused by errors in ganglioside synthesis, defects in ganglioside catabolism can result in fatal neurodegenerative diseases (Sandhoff & Harzer, 2013). The enzyme GM1-β-galactosidase removes a terminal β-D-galactose residue from GM1 (**Fig. 1.2**). This results in the production of GM2 (Okada & O'Brien, 1968; Wilkening *et al.*, 2000). The terminal *N*-acetyl-β-galactosamine (GalNAc) residue is removed from GM2 by the enzyme β-hexosaminidase A (HexA), to produce GM3 (Gravel *et al.*, 2001; Okada & O'Brien, 1969; Sandhoff, 1969). Sialidase then removes a *N*-acetylneuraminic acid residue from GM3,

converting it into lactosylceramide (Lieser *et al.*, 1989), which can be degraded by galactosylceramidase and GM1-β-galactosidase. Both of these enzymes are capable of removing a β-D-galactose residue from lactosylceramide, which forms glucocerebroside (Zschoche *et al*., 1994). Glucocerebrosidase cleaves the glucose moiety of glucosylceramide, forming ceramide (Vaccaro *et al*., 1997). Ceramidase cleaves off the fatty acid on ceramide, forming sphingosine (Bernardo *et al.*, 1995; Linke *et al*., 2001). Saposin B, Saposin C, Saposin D and GM2 activator protein (GM2AP) are co-enzymes that are involved in the degradation pathway. Loss-of-function mutations in the enzymes or co-enzymes mentioned above can result in metabolic disorders (Sandhoff & Harzer, 2013).

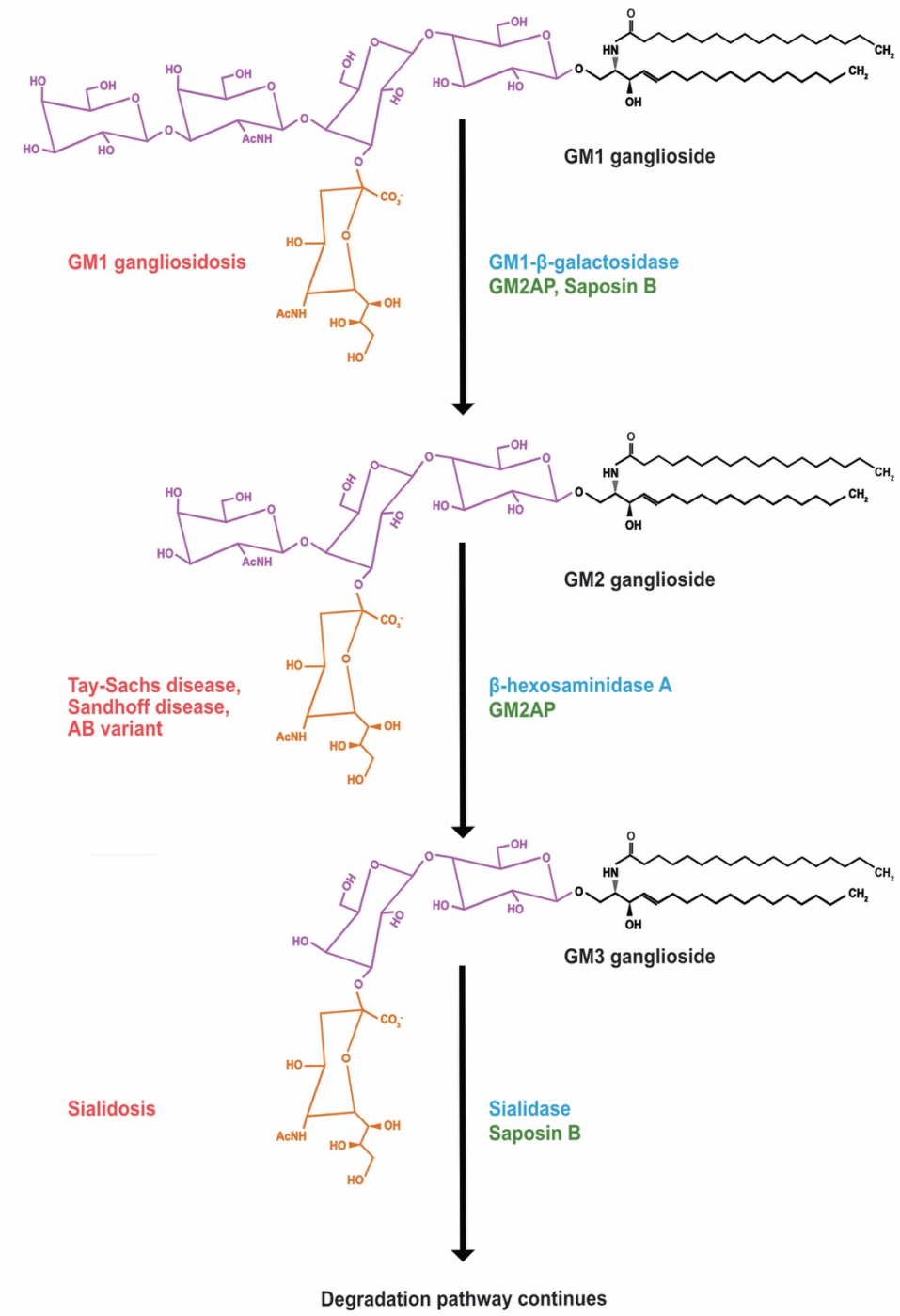

Figure 1.2. The degradation pathway of GM1 ganglioside to GM3 ganglioside. GM1-β-galactosidase cleaves the terminal galactose residue from GM1 ganglioside, forming GM2 ganglioside. The *N*-acetyl-β-galactosamine (GalNAc) residue of GM2 is cleaved by the enzyme β-hexosaminidase A. This produces GM3 ganglioside, which is further degraded to sphingosine in a multi-step process. Enzymes involved in the ganglioside degradation pathway are shown in teal and co-enzymes are in green. Metabolic disorders associated with the enzymes and co-enzymes are denoted in red. The neutral core sugars are indicated in purple and the sialic acid residue is shown in orange. Image modified from Sandhoff & Harzer (2013).

There are two nomenclatures used to name gangliosides. The first is the standardized nomenclature recommended by the International Union of Pure and Applied Chemistry (IUPAC) and by the International Union of Biochemistry and Molecular Biology (IUBMB) (Chester, 1999). The second is a shorthand naming system first proposed in 1963 by Lars Svennerholm. In this nomenclature, the first letter indicates the series of the ganglioside. Each series has a unique neutral sugar core conformation and sequence. The letter "G" denotes that a ganglioside is part of the ganglio-series (Svennerholm, 1963), which has a Galβ1-3GalNAcβ1-4Galβ1-4Glc sugar core (**Fig. 1.2**) (Kuhn & Wiegandt, 1963). The second letter in the name indicates the total number of sialic acid residues in the ganglioside. The letter "M" is for mono. Therefore, GM1, GM2 and GM3 are all ganglio-series gangliosides with one sialic acid residue, which is attached to the inner galactose residue (**Fig. 1.2**) (Svennerholm, 1963). In comparison, GT1b, the ganglioside which is believed to be a receptor for Merkel cell polyomavirus, is a ganglio-series ganglioside but has three sialic acid residues, indicated by the letter "T" (**Fig. 1.3)** (Kuhn & Wiegandt, 1963; Svennerholm, 1963). A number was assigned to the name based on the migration pattern of human brain gangliosides on a thin-layer chromatogram. The more complex gangliosides had a slower migration patten and thus a smaller retention factor (R_f) value and were therefore assigned a smaller number. As GM1 is more complex than GM2 and GM3 (**Fig 1.2**), it was given a lower number in its name (Svennerholm, 1963). In the IUPAC system, each monosaccharide residue, as well as any other substituents (such as sialic acid) in the ganglioside are named and the positions linking the residues are indicated. Under the IUPAC nomenclature, GM1 is named Galβ1-3GalNAcβ1-4(Neu5Acα2-3)Galβ1-4GlcβCer (Chester, 1999). While the IUPAC nomenclature is more comprehensive and there are some exceptions to the Svennerholm

nomenclature, the naming system propositioned Svennerholm is used more frequently and will be used for the purpose of this thesis.

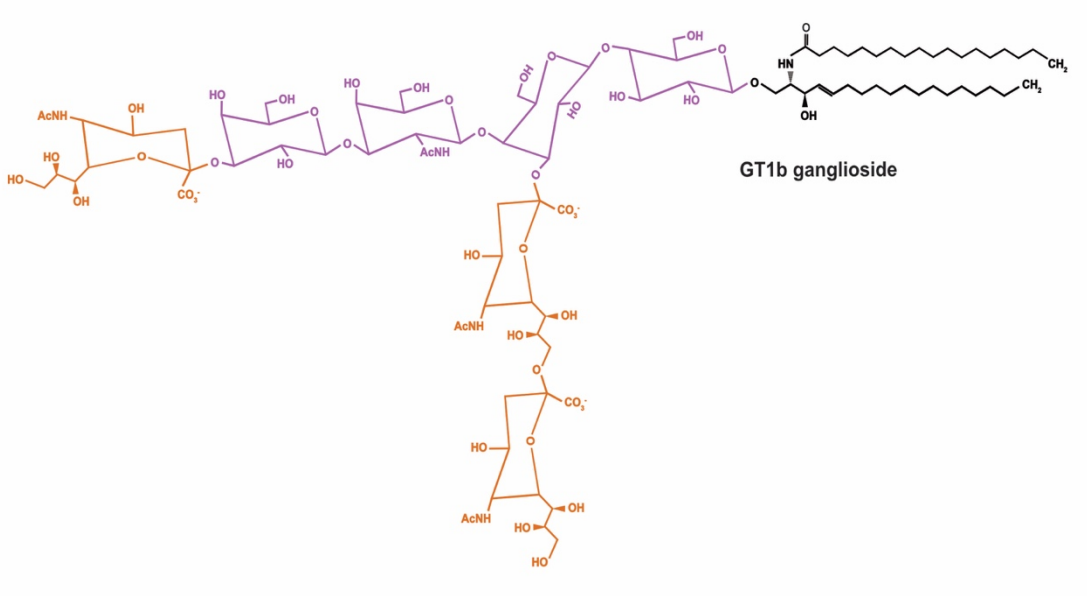

Figure 1.3. Structure of GT1b ganglioside. GT1b is a ganglio-series ganglioside with three sialic acid moieties, shown in orange. One of the moieties is attached to the terminal galactose residue and two residues are attached to the internal galactose. The neutral core sugars are shown in purple. Image modified from Kolter (2012).

1.2. Human β-hexosaminidase

The enzyme responsible for degrading GM2 is β-hexosaminidase A (HexA), a heterodimeric lysosomal enzyme composed of an α- and a β-subunit (**Fig 1.4a**) (Lemieux *et al.*, 2006). While HexA is the only human enzyme capable of hydrolyzing GM2, there are two other naturally occurring lysosomal β-hexosaminidase isoforms that exist. β-hexosaminidase S (HexS) is a homodimer comprised of two α-subunits and is not usually detected in human tissue due to

low stability and it does not appear to have any physiological relevance (Beutler *et al*., 1975; Mahuran & Lowden, 1980). The other isoform is β-hexosaminidase B (HexB), which is a highly stable β-subunit homodimer that is abundant in cells but its biochemical role remains unclear (**Fig 1.4b**) (Gravel *et al.*, 2001; Srivastava & Beutler, 1973).

The evolutionarily related *HEXA* and *HEXB* genes (~60% sequence identity) respectively encode for the α- and the β-subunits (**Fig 1.4c**) (Korneluk *et al.*, 1986; Proia, 1988). A third gene, *GM2A*, encodes for the co-enzyme GM2AP which is necessary for extracting GM2 from intralysosomal membranes (**Fig 1.5**). GM2AP then presents the glycosphingolipid to HexA for hydrolysis (Mark *et al*., 2003).

The α- and β-subunits are not functional as monomers; dimerization is required for proper β-hexosaminidase enzymatic activity (Mahuran & Lowden, 1980). The α-subunit present in HexA and HexS has a positively charged binding pocket which can accommodate the negatively charged sialic acid residue present in GM2 (Lemieux *et al*., 2006; Sharma *et al*., 2001). In contrast, the β-subunit binding pocket is negatively charged (Mark *et al.*, 2003). Only HexA is efficient at hydrolyzing negatively charged substrates such GM2 ganglioside; however, both HexA and HexB are capable of degrading neutral substrates (Hou *et al*., 1996; Kytzia & Sandhoff, 1985). Regions of both the α-subunit and the β-subunit are required for GM2AP to interact with HexA and for the proper positioning of GM2 within the active site (Meier *et al.*, 1991).

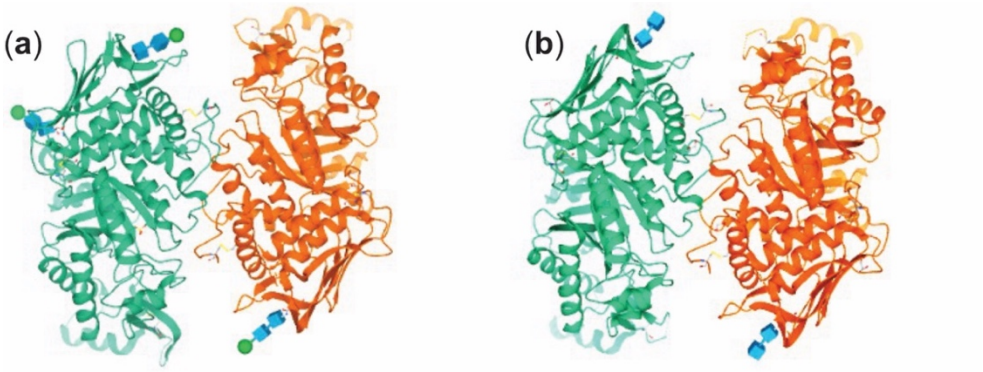

(c)

```
α   1   MTSSRLWF-------SLLLAA------------------AFAGRAT--------ALWPWP  27
β   1   MELCGLGLPRPPMLLALLLATLLAAMLALLTQVALVVQVAEAARAPSVSAKPGPALWPLP  60
α  28   QNFQTSDQRYVLYPNNFQFQYDVSSAAQPGCSVLDEAFQRYRDLLFGSGSWPRPYLTGKR  87
β  61   LSVKMTPNLLHLAPENFYISHSPNSTAGPSCTLLEEAFRRYHGYIFGFYKWHHEPAEFQA  120
α  88   HTLEKNVLVVSVVTPGCNQLPTLESVENYTLTINDDQCLLLSETVWGALRGLETFSQLVW  147
β 121   KTQVQQLLVSITLQSECDAFPNISSDESYTLLVKEPVAVLKANRVWGALRGLETFSQLVY  180
α 148   KSAEGTFFINKTEIEDFPRFPHRGLLLDTSRHYLPLSSILDTLDVMAYNKLNVFHWHLVD  207
β 181   QDSYGTFTINESTIIDSPRFSHRGILIDTSRHYLPVKIILKTLDAMAFNKFNVLHWHIVD  240
α 208   DPSFPYESFTFPELMRKGSYNPVTHIYTAQDVKEVIEYARLRGIRVLAEFDTPGHTLSWG  267
β 241   DQSFPYQSITFPELSNKGSYS-LSHVYTPNDVRMVIEYARLRGIRVLPEFDTPGHTLSWG  299
α 268   PGIPGLLTPCYSGSEPSGTFGPVNPSLNNTYEFMSTFFLEVSSVFPDFYLHLGGDEVDFT  327
β 300   KGQKDLLTPCYSRQNKLDSFGPINPTLNTTYSFLTTFFKEISEVFPDQFIHLGGDEVEFK  359
α 328   CWKSNPEIQDFMRKKGFGEDFKQLESFYIQTLLDIVSSYGKGYVVWQEVFDNKVKIQPDT  387
β 360   CWESNPKIQDFMRQKGFGTDFKKLESFYIQKVLDIIATINKGSIVWQEVFDDKAKLAPGT  419
α 388   IIQVWREDIPVNYMKELELVTKAGFRALLSAPWYLNRISYGPDWKDFYIVEPLAFEGTPE  447
β 420   IVEVWKDSA---YPEELSRVTASGFPVILSAPWYLDLISYGQDWRKYYKVEPLDFGGTQK  476
α 448   QKALVIGGEACMWGEYVDNTNLVPRLWPRAGAVAERLWSNKLTSDLTFAYERLSHFRCEL  507
β 477   QKQLFIGGEACLWGEYVDATNLTPRLWPRASAVGERLWSSKDVRDMDDAYDRLTRHRCRM  536
α 508   LRRGVQAQPLNVGFCEQEFEQT  529
β 537   VERGIAAQPLYAGYCNHE--NM  556
```

Figure 1.4. Sequence alignment and structures of the α- and β-subunits. (a) Heterodimeric HexA structure (PDB: 2GJX). The α-subunit is shown in teal and the β-subunit is in orange. (b) Structure of the homodimeric HexB (PDB: 1NOU). One β-subunit is shown in orange and the other in teal. (c) Sequence alignment of the α- and β-subunits of human HexA. The underlined amino acid residues are cleaved post-translationally. The amino acids highlighted in yellow, are identical in the two subunits. Sequence alignment was generated using basic local alignment search tool (BLAST).

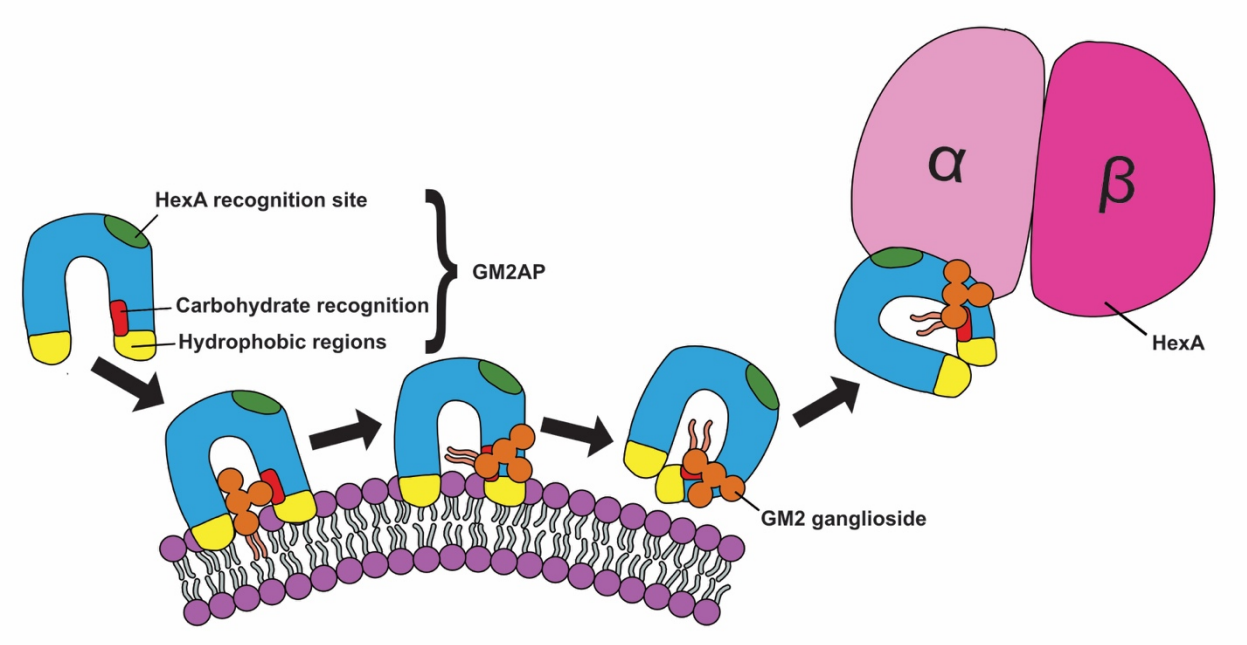

Figure 1.5. Mechanism of GM2 extraction from intralysosomal membranes and presentation to HexA for degradation. Hydrophobic regions of GM2AP (yellow) are inserted into the membrane (purple). Specific sites within the GM2AP cavity (red) recognize GM2 (orange). Once GM2 is properly positioned, GM2AP changes from an open to a closed conformation. The closed conformation exposes more hydrophobic regions of GM2AP and favours the release of the GM2AP-GM2 complex from the membrane. The complex can then interact with HexA (pink) where the GalNAc moiety is cleaved from GM2. Image modified from Sandhoff & Harzer (2013).

1.3. Lysosomal storage disorders

The lysosome was first discovered in 1955 in Christian de Duve's laboratory (de Duve *et al.*, 1955), which had been researching a specific glucose-6-phosphatase (Appelmans *et al.*, 1955). Their attempts to localize and purify this enzyme eventually led to the discovery of the lysosome (de Duve *et al.*, 1955) and Christian de Duve was awarded a share of the Nobel Prize in Physiology or Medicine in 1974 for this discovery (de Duve, 1975).

Since then, the lysosome has been extensively characterized. It is a membrane bound organelle present in almost all eukaryotic cells and contains approximately 50 different degrative

enzymes, including the β-hexosaminidase isoenzymes (Journet *et al.*, 2002). An internal pH of 4.5-5 is maintained within the organelle by the lysosomal vacuolar adenosine triphosphatase (v-ATPase) as the degrative enzymes function optimally at an acidic pH (Ohkuma *et al.*, 1982). The lysosome is often described as being the recycling centre of the cell as macromolecules are transported to the organelle for degradation (Alroy & Lyons, 2014). Extracellular macromolecules are transported to the lysosome by endocytosis (Bright *et al.*, 2005; Luzio *et al*., 2007), while intracellular macromolecules segregated during autophagy are also transported to the lysosome to be broken down. Once the macromolecules are degraded, their components can further be used by the cell (Luzio *et al.*, 2007). In addition to degrading biomolecules, the lysosome plays a role in several different physiological processes including the downregulation of surface receptors (Beguinot *et al.*, 1984), loading antigens onto major histocompatibility complex (MHC) class II molecules (Gao *et al*., 2017), inactivating pathogenic organisms (Gao *et al.*, 2017; Pauwels *et al.*, 2017), plasma membrane repair (Reddy *et al*., 2001) and bone remodeling (Erkhembaatar *et al.*, 2017).

The variety of physiological roles played by the lysosome is reflected in the diversity of diseases caused by errors in normal lysosomal function. Lysosomal storage disorders (LSD) are a group of metabolic diseases caused by defects in the degradation pathway and the subsequent accumulation of various biomolecules. Most LSDs are caused by mutations in genes encoding for hydrolytic lysosomal enzymes, causing a partial or complete deficiency in activity and resulting in the accumulation of the corresponding substrate. However, some LSDs are caused by defects in non-enzymatic proteins or in lysosomal membrane proteins (Alroy & Lyons, 2014; Platt *et al.*, 2012). LSDs are all autosomal recessive genetic disorders, except for Fabry disease and mucopolysaccharidosis type II, which are X-liked recessive disorders (Meikle *et al*., 1999;

Ozand & Al-essa, 2012) Currently, over 40 different LSDs have been described (Futerman & van Meer, 2004; Journet *et al.*, 2002; Meikle *et al*., 1999), including diseases caused by mutations in the genes which encode for HexA (*HEXA* [α-subunit] and *HEXB* [β-subunit]) and the co-enzyme GM2AP (*GM2A*). More disorders may be characterized in the future, as a better understanding of lysosomal functions and the proteins involved is gained (Palmieri *et al*., 2011; Platt *et al*., 2018).

Although LSDs are grouped together, the age of onset, the severity and the symptoms are different for each disease. A common feature of several LSDs is the involvement of the central nervous system (CNS) in the pathology of the disease (Ozand & Al-essa, 2012; Platt *et al.*, 2012). Visceromegaly, the enlargement of the abdominal organs, is also commonly observed in patients diagnosed with LSDs (Ozand & Al-essa, 2012). The onset of LSDs often begins at a young age and death may occur within the first few years of life. However, there are some cases in which LSDs develop at a later stage and patients have a normal lifespan (Platt *et al.*, 2012).

1.4. GM2 gangliosidoses

Tay-Sachs disease (TSD), Sandhoff disease (SD) and the AB variant are clinically similar LSDs collectively referred to as the GM2-gangliosidoses. They are called GM2-gangliosidoses as each of these diseases are characterized by defects in GM2 catabolism and the subsequent accumulation of the ganglioside (Conzelmann & Sandhoff, 1978; de Baecque *et al.*, 1975). TSD and SD are respectively caused by loss-of-function mutations in the *HEXA* and *HEXB* genes encoding for the α- and β-subunits of HexA, and are heritable neurodegenerative disorders (Gravel *et al.*, 2001). Deficiencies in GM2AP, caused by mutations in the *GM2A* gene, results in

an extremely rare form of GM2-gangliosidosis known as the AB variant (Conzelmann & Sandhoff, 1978; de Baecque *et al.*, 1975).

Although TSD and SD are relatively rare in the general population, an increased incidence rate is observed in specific population groups. The carrier rate of TSD in the Ashkenazi Jewish population is 1 in 30 with an incidence rate of 1 in 3900 births. In the Eastern French-Canadian population, the carrier rate is 1 in 14 (Maegawa *et al*., 2006; Meikle *et al.*, 1999). The carrier rate of SD is 1 in 7 the Cyprus Christian Maronite community (Drousiotou *et al.*, 2000). Among northern Saskatchewan communities, the carrier rate is estimated to be 1 in 15, with an incidence rate of 1 in 390 (Fitterer *et al*., 2014).

The onset of symptoms and the severity of TSD and SD is determined by the amount of residual HexA activity (Leinekugel *et al*., 1992). The most common and severe manifestation of the GM2-gangliosidoses is the infant-onset form. In patients with this form of the disease, almost no HexA activity (<0.5% of normal) is detected (Conzelmann *et al*., 1983; Sandhoff & Christomanou, 1979). Although the accumulation of GM2 begins prior to birth, during the gestation period, babies are born asymptomatic and disease characteristics become apparent by 6 months of age. Commonly observed symptoms include a distinctive “cherry-red” spot in the eyes, an increased startle response, seizures, the loss of motor skills and vision loss (Ozand & Al-essa, 2012). Death typically occurs within the first few years of life in patients affected by the infant-onset form of TSD and SD (Mahuran, 1999). In contrast to the infant-onset form, the juvenile-onset form is a relatively uncommon form of GM2 gangliosidosis. The age of onset of the juvenile form is between 2 to 15 years old (Maegawa *et al*., 2006). Symptoms include intellectual impairments, gait abnormalities, muscle spasticity and seizures (Ozand & Al-essa, 2012). The late-onset form of GM2 gangliosidosis is variable in both the symptoms exhibited

and the age at which they begin. Individuals may be affected by muscle weakness, slurred speech, an unsteady gait and neurological disorders (Neudorfer *et al*., 2005). Between 1-10% of normal HexA activity is observed in patients with the juvenile-onset and adult-onset forms of the GM2 gangliosidoses (Leinekugel *et al*., 1992). Currently, the standard medical care for each form of TSD and SD is palliative in nature, as there are no effective treatments available (Ou *et al.*, 2020).

1.5. Potential therapies

To date, multiple therapeutic approaches for TSD and SD have been investigated, each demonstrating various degrees of success. The use of bone marrow transplantation (BMT) has been proposed as a potential treatment for LSDs. However, limited results displaying the effectiveness of BMT on disorders primarily affecting the CNS have been obtained thus far (Hoogerbrugge *et al.*, 1995; Norflus *et al*., 1998). Substrate reduction therapy is another possible therapeutic approach, but neurological deterioration was nonetheless observed in a clinical trial assessing the potential of miglustat to prevent substrate accumulation in individuals diagnosed with the juvenile-onset form of GM2 gangliosidosis (Maegawa *et al*., 2009). Miglustat is a drug that partially inhibits the function of the enzyme (ceramide glucosyltransferase) which synthesizes glucosylceramide (**Fig. 1.1**), and therefore preventing ganglioside synthesis to some extent as well (Platt *et al.*, 1994). Gene therapy is an approach which has shown some promise in murine models (Osmon *et al*., 2016; Walia *et al.*, 2015).

Another potential treatment for TSD and SD is pharmacological chaperone therapy. Certain *HEXA* and *HEXB* mutations result in a misfolded enzyme with a functional active site capable of hydrolyzing GM2. Although still functional, these enzymes are often eliminated

through the endoplasmic-reticulum-associated protein degradation (ERAD) pathway due to their misfolding (Tropak & Mahuran, 2007). Pharmacological chaperones are small molecules that act as antagonists or inhibitors which can bind to misfolded HexA in the endoplasmic reticulum, ensuring the protein is folded in the proper conformation and not marked for degradation (Tropak *et al*., 2007; Yam *et al.,* 2005). Once in the lysosome, the high quantity of GM2 is believed to favour the interaction of HexA with its natural substrate (Tropak *et al*., 2004). Pharmacological chaperone therapy is thought to be a potential treatment for those with the juvenile and adult-onset forms of GM2 gangliosidoses. Pyrimethamine has been found to stabilize HexA in certain fibroblast cell lines, including cells with the αG269S mutation, the most common form of adult-onset TSD (Maegawa *et al*., 2007; Tropak *et al*., 2004).

Enzyme replacement therapy (ERT) experiments have demonstrated that intracerebroventricular injection of recombinant HexA can reduce GM2 accumulation within the CNS in Sandhoff disease mice models (Tsuji *et al.*, 2011). Development of ERTs for lysosomal storage disorders relies on the mannose 6-phosphate (M6P) pathway for the delivery of exogenous protein to cells. Most lysosomal enzymes are post-translationally modified, which ensures proper trafficking from the rough endoplasmic reticulum, where the proteins are synthesized, to the lysosome. The enzymes are glycosylated in the endoplasmic reticulum and transported to the Golgi apparatus. The proteins are then phosphorylated and acquire a terminal M6P residue, which at physiological pH, binds to the cation-dependent mannose 6-phosphate receptor (CD-MPR) or the insulin-like growth factor 2 receptor (IGF2R) within the Golgi. The enzyme is then transported through the endosomal system until it reaches the lysosome, where the acidic pH favours the uncoupling of the enzyme-receptor complex. Exogenous enzyme with a M6P residue can bind to IGF2R or CD-MPR on the plasma membrane, triggering the

endocytosis and transport of the protein to the lysosome (Sands & Davidson, 2006). This is especially useful for lysosomal storage disorders, including the GM2 gangliosidoses, as the enzyme is delivered directly to the organelle where substrate accumulation occurs. It has been hypothesized that if exogenously administered β-hexosaminidase activity levels could reach a "critical threshold" of approximately 10% of normal activity within neuronal cells, accumulation of GM2 could be prevented (Leinekugel *et al*., 1992).

1.6. HexM

To help overcome challenges posed by heterodimeric HexA for use in of a gene therapy or ERT to treat GM2 gangliosidoses, a hybrid enzyme named β-hexosaminidase M (HexM) has been developed (**Fig. 1.6**) (Tropak *et al.*, 2016). HexM is a homodimer comprised of two artificial μ-subunits, which are modified α-subunits where a total of 22 amino acid substitutions were made to bring the critical features of the β-subunit into the α-subunit. Thus, μ-subunit was designed to contain essential features from the α and β-subunits of HexA. One of the key aspects included in the μ-subunit design was the α-subunit active site required for GM2 degradation. Another critical feature included in the μ-subunit design were regions of the α- and β-subunits needed for the enzyme to interact with the GM2-GM2AP complex. The α-subunit dimerization interface was replaced by the β-subunit interface to promote highly stable HexM dimer formation (Tropak *et al.*, 2016).

HexM addresses a key difficulty faced when trying to develop a gene therapy for TSD and SD, which is the large open reading frame (ORF) required to encode the *HEXA* and *HEXB* genes (Tropak *et al*., 2016; Walia *et al.*, 2015). To ensure sufficient enzyme production, both genes must be delivered to a neuron to produce enough of the α- and the β-subunit to form the

active HexA dimer. However, the ORF of both subunits (~3.2 kb) exceeds the packaging capacity constraints (~2.2 kb) of the self-complementary adeno-associated virus serotype 9 (scAAV9), the most efficient viral vector reported to improve gene delivery to the CNS (Dashkoff *et al*., 2016; Foust *et al.*, 2009; Gray *et al*., 2011). In contrast, the μ-subunit of HexM is encoded by a single gene (~1.6 kb) that is within the packaging capacity of scAAV9 (Tropak *et al*., 2016).

The heterodimeric nature of HexA also presents an obstacle in the development of an ERT. ERT requires large quantities of enzyme and HexA (α/β-subunits) would need to be isolated from the two other naturally occurring isoforms, HexB (β/β-subunits) and HexS (α/α-subunits), which are not capable of GM2 degradation (Kresse *et al.*, 1981). Additionally, HexA is somewhat unstable and re-dimerization can result in conversion to the more stable HexB over time. Fortunately, HexM has the stability of HexB engineered into it and does not interconvert into an alternate isoform that is incapable of cleaving GM2 (Tropak *et al.*, 2016).

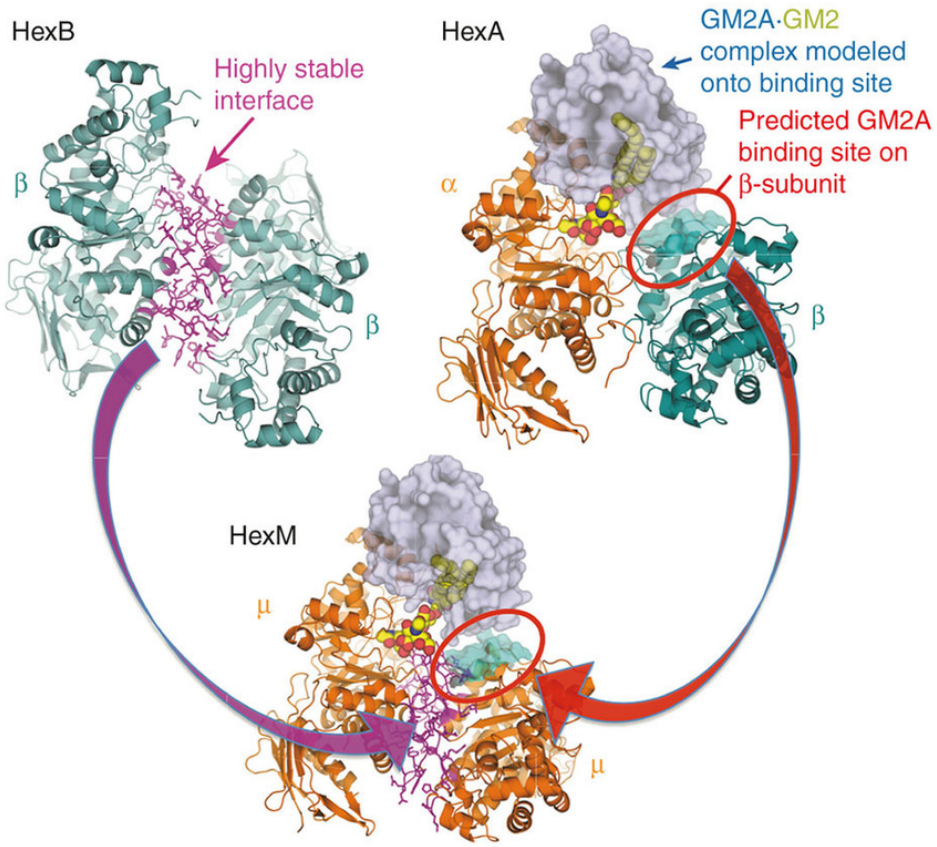

Figure 1.6. Model of HexM interacting with the GM2AP-GM2 complex. Critical elements of the α- and β-subunits required for GM2AP interaction were included in the construction of the artificially engineered μ-subunit. Shown in magenta is the stable interface that forms between two β-subunits. The α-subunit is shown in orange and the β-subunit in teal. It has been predicted that both of the HexM active sites are able to simultaneously interact with a GM2:GM2AP complex, shown in gray. Reproduced from Tropak *et al.* 2016.

1.7. The problem posed by the blood-brain barrier

The blood-brain barrier (BBB) plays a key role in maintaining CNS homeostasis by protecting the nervous system from pathogens and toxins, while also mediating the transfer of essential molecules and ions from the blood vessels to neural tissues. Small hydrophilic molecules (<500 Da) are generally capable of diffusing across the endothelial cells of the BBB (Oller-Salvia *et al*., 2016). Polar molecules and larger molecules are transported to the CNS by

specialized transporters (Kalaria *et al*., 1988; Smith *et al*., 1987). While the BBB is an essential component in protecting the brain from infection, it can render the delivery of therapeutics to treat diseases of the CNS difficult. Potential strategies to circumvent the BBB and deliver therapeutically relevant quantitates of drugs are currently being developed as possible therapeutic options for diseases that primarily affect the CNS, such as Alzheimer's disease, certain types of cancers and several LSDs (Oller-Salvia *et al*., 2016).

Blood vessels are responsible for transporting oxygenated blood from the heart to each organ of the body, including the brain, and for removing metabolic waste and carbon dioxide from bodily tissues. The term BBB refers to the unique properties of the capillaries responsible for supplying blood to the CNS. The combination of cells that make up the BBB results in a semipermeable barrier which tightly regulates the passage of substances from the circulatory system to the CNS (Daneman & Prat, 2015).

The walls of blood vessels are formed by endothelial cells (**Fig. 1.7**) (Coomber & Stewart, 1985). In the CNS, microvessels are lined with specialized endothelial cells called brain microvascular endothelial cells (BMECs) and are continuous nonfenestrated vessels (Coomber & Stewart, 1985). BMECs are the main component of the BBB and have several unique properties compared to other endothelial cells. Low levels of vesicles are observed in BMECs in comparison to peripheral endothelial cells, which limits the transport of molecules across the BBB (Coomber & Stewart, 1985). BMECs are adjoined by tight junctions which link the plasma membrane of two cells together via the extracellular regions of different transmembrane molecules (Brightman & Reese, 1969; Reese & Karnovsky, 1967; Westergaard & Brightman, 1973). The transmembrane molecules play a role in the size and charge selectivity of the BBB (Colegio *et al*., 2002, 2003; Van Itallie *et al.*, 2001). Endothelial cells throughout the remainder

of the body may be linked by gap junctions, but these do not confer the same properties to the cells as tight junctions (Brightman & Reese, 1969). It is thought that there are higher quantities of mitochondria present in BMECs than in peripheral endothelial cells, which helps supply the cells with enough ATP for transporting molecules across the BBB (Oldendorf *et al.*, 1977). BMECs mainly express two types of transporters, efflux transporters and specific nutrient transporters. The efflux transporters pump lipophilic molecules which are generally capable of diffusing across the BBB back towards the circulatory system (Cordoncardo *et al*., 1989; Thiebaut *et al.*, 1989). The specific nutrient transporters mediate the entry of essential nutrients into the brain. These transporters can also be used to remove excess nutrients and certain metabolic waste products from the CNS (Cordoncardo *et al.,* 1989*;* Kalaria *et al.*, 1988; Smith *et al*., 1987). Glucose primarily enters the CNS by glucose transporter 1 (GLUT1) and is transported at a higher rate than what can be phosphorylated during the first step of glycolysis. The excess sugar is subsequently removed from the brain by GLUT1 (Hladky & Barrand, 2018). Lactate, a cellular waste product formed during glycolysis, is removed from the CNS by monocarboxylate transporter 1 (MCT1) (Wang *et al*., 2019). However, MCT1 can also be used to transport lactate and lactic acid into the CNS, as these molecules can be used to generate energy (Chiry *et al.*, 2006). Finally, under normal conditions, BMECs express low levels of leukocyte adhesion molecules compared to other endothelial cells (Henninger *et al.*, 1997; Stins *et al*., 1997). These adhesion molecules are cell surface receptors that mediate interactions between leukocytes and endothelial cells. The quantity of immune cells capable of entering the CNS is limited due to the lower expression levels of these adhesion molecules in BMECs. This is advantageous as it helps prevent strong inflammatory responses which may be damaging to the CNS. However, the expression of leukocyte adhesion molecules in BMECs increases with

infections (Roe *et al*., 2014). Together, the differences observed in BMECs compared with endothelial cells present in other tissues contributes to the tight regulation of the BBB and homeostasis within the CNS.

Astrocytes and pericytes are the other cells that play a key role in the structure and physiology of the BBB. Pericytes are embedded within the basal lamina on the abluminal surface of microvessels, including the capillaries that vascularize the CNS. These cells have long cytoplasmic processes which extend over the blood vessels and neural tissue capillaries contain the highest concentration of pericytes in the human body (Armulik *et al.,* 2011). Pericytes are muscle-like cells which contain α-smooth muscle actin, a contractile protein found in vascular smooth muscle cells (Alarcon-Martinez *et al*., 2018), along with tropomyosin and myosin, two other contractile proteins (Joyce *et al.*, 1985a, 1985b). The presence of contractile proteins in pericytes allows for vasoconstriction and vasodilation, both of which cause changes in the diameter of capillaries responsible for supplying blood to the CNS. Variations in the diameter of blood vessels result in the quantity of oxygen and nutrients delivered to the CNS to be changed based on physiological demands (Alarcon-Martinez *et al.*, 2018). Pericytes play a role in the postnatal formation of the BBB and are thought to also play a role in the immunological defence of the CNS (Daneman *et al*., 2016). Pericytes are capable of phagocytosis and express Fc receptors which are used to trigger antibody-dependent phagocytosis (Balabanov *et al.*, 1996). Astrocytes are glial cells which surround the blood vessels of the brain (**Fig. 1.7**) (Abbott *et al*., 2006) and play an important role in maintaining water homeostasis in the CNS (Frigeri *et al*., 1995; Nielsen *et al*., 1997; Rash *et al.*, 1998). Astrocytes are also capable of transmitting signals from neurons to brain capillaries, including relaying signals to pericytes which results in vasoconstriction or vasodilation (Gordon *et al.*, 2011).

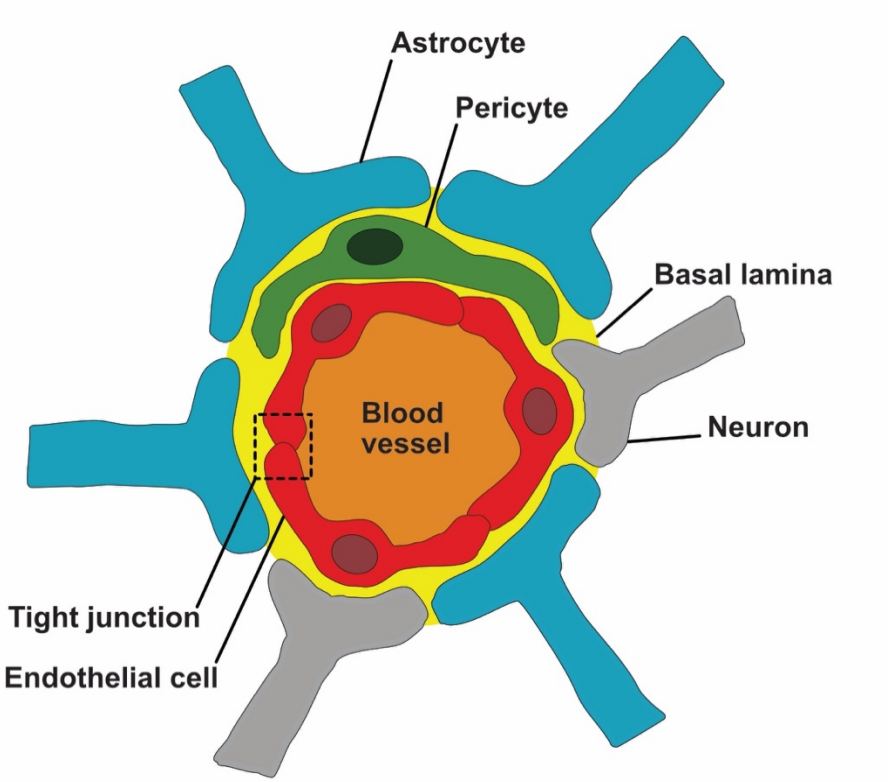

Figure 1.7. Blood-brain barrier model. The walls of the blood vessels are formed by endothelial cells (red). Tight junctions adjoin neighbouring endothelial cells and contribute to the selectivity of the BBB. Pericytes (green) are embedded in the basal lamina (yellow) and provide structural support for the endothelial cells. Astrocytes (teal) surround blood vessels and relays signals from neurons (grey) to blood vessels. Endothelial cells, pericytes and astrocytes collectively form the BBB. Image modified from Abbott *et* al., 2006.

1.8. Brain delivery methods

1.8.1. Direct drug delivery methods

Direct drug delivery methods are a group of clinical procedures in which drugs are administered directly into the CNS, bypassing the BBB. While these methods are invasive, they allow for clinically relevant amounts of therapeutics to be delivered to the brain (Marshall *et al.*, 2015), without subjecting the rest of the body to large quantities of the drug, which may be toxic in other tissues (Soderquist & Mahoney, 2010). Direct drug delivery methods include

intracerebral implantation, intraparenchymal injection, biological tissue delivery, intrathecal injections, and intraventricular administration.

Intracerebral implantation involves surgically opening the skull to insert a biodegradable polymeric reservoir containing a therapeutic drug. The drug is slowly released into the brain in a controlled manner. The physiochemical properties of the drug determine how far the therapeutic will penetrate into the CNS. The polymeric reservoir may need to be refilled once all the drug has been released (Brem *et al.*, 1995; Grossman *et al*., 1992). Intracerebral implants have been approved by the United States Food and Drug Administration (FDA) for the delivery of 1,3-bis(2-chloroethyl)-1-nitrosourea (BCNU) to treat glioma (U.S. Food and Drug Administration, 1996).

Intraparenchymal injections involve the delivery of therapeutics to the brain directly by injecting therapeutic agents into the brain tissue. The administration of the treatment is usually localized and may not diffuse through the brain tissue effectively (Hrabe *et al.*, 2004; Nicholson *et al.*, 2011). Not only is this method invasive, but it can also result in infection or brain damage.

Another method of delivering drugs to the CNS is biological tissue delivery. This method involves implanting biological material such as tissues from the peripheral nervous system, tissues from other organs or laboratory generated cell lines directly into the brain or the spinal cord. The implanted tissues are capable of producing and secreting the required therapeutic, which is thought to be taken up by neighbouring cells (Lu *et al.*, 2014). Biological tissue delivery had been investigated extensively as a potential treatment for Parkinson's disease (Harris *et al.*, 2020). However, the use of biological tissue delivery has also been investigated as a potential therapeutic approach for the LSD mucopolysaccharidosis type IIIB (MPS IIIB). MPS IIIB is caused by mutations in the *NAGLU* gene, resulting in deficiencies of the enzyme α-*N*-

acetylglucosaminidase (NAGLU). Mouse embryonic fibroblasts lacking *NAGLU* were reprogrammed to induced pluripotent stem cells, which were then differentiated into neural stem cells. The neural stem cells which were subsequently transduced with the *NAGLU* gene and grafted into the brain of newborn MPS IIIB mice. A reduction in lysosomal storage was observed in brain cells near the engraftment sites. Ideally, using patient-derived cells will minimize the likelihood of immune rejection of the implanted biological tissue (Clarke *et al*., 2018).

In addition to administrating therapeutics straight into brain tissue to bypass the BBB, it is possible to administer drugs directly into the cerebrospinal fluid (CSF). Intrathecal injections involve the administration of therapeutics to the CSF surrounding the spinal cord. Therapeutic agents are delivered via a catheter inserted into the lumbar subarachnoid space. The catheter is attached to a pump which infuses the therapeutic molecules (Soderquist & Mahoney, 2010). Historically, intrathecal injections have most commonly been used to deliver analgesia and anesthesia to relieve chronic and acute pain, especially with cancer (Leavens *et al.*, 1982; Penn & Paice, 1987; Sommer *et al*., 2020). There are several advantages of using intrathecal injections to deliver therapeutics to the CNS besides bypassing the BBB. Often lower quantities of drugs can be administered due to the proximity of the spinal cord to the brain (Bottros & Christo, 2014; Deer *et al*., 2019; Hayek & Hanes, 2014; Mercadante, 1999). Therapeutics may also be less likely to encounter certain degradative enzymes when injected in the CSF than in the blood (Spector *et al.*, 2015). However, while this method does bypass the BBB, the CSF is separated from the brain parenchyma by a layer of cells which therapeutics need to cross. The CSF-brain barrier also has a smaller surface area than the BBB, which may limit drug delivery to the CNS.

Intraventricular delivery is similar to intrathecal injections, except the catheter is placed into the ventricle system of the brain, which is filled with CSF (Cohen-Pfeffer *et al.*, 2017). This

administration route has been used to deliver drugs for certain types of cancer, meningitis and for severe pain management (Leavens *et al*., 1982; Lin *et al*., 2012; Toyokawa *et al*., 2013; Wei *et al*., 2017). In terms of LSDs, intraventricular delivery has been used in clinical trials for the delivery of sulfoglucosamine sulfohydrolase (SGSH), the deficient enzyme in patients diagnosed with mucopolysaccharidosis IIIA (MPS IIIA) (identifier NCT02060526). Clinical trials have also been performed to assess the administration of recombinant iduronate-2-sulfatase by intraventricular delivery to patients with mucopolysaccharidosis II (identifier NCT02055118).

1.8.2. Blood-brain barrier disruption techniques

Blood-brain barrier disruption (BBBD) techniques encompass different methods that result in the temporary disruption of the BBB, therefore allowing therapeutic agents to reach the CNS. Two mechanisms of BBBD include the intra-arterial injection of osmotic agents and the use of focused ultrasound in conjunction with microbubbles.

Intra-arterial administration of osmotic agents to disrupt the BBB was initially conceptualized in the 1970s (Rapoport, 1970) and first used on patients in 1980 (Neuwelt *et al.*, 1980). Mannitol is the most commonly employed osmotic molecule for intra-arterial administration as a BBBD technique (Doolittle *et al*., 1998; Doolittle *et al.*, 2000; Fortin *et al.*, 2007; Neuwelt *et al*., 1980). The injection of osmotic molecules results in the dehydration of BMECs and consequently the tight junctions are temporarily opened, increasing the permeability of the BBB for as long as 8 hours in humans (Rapoport *et al*., 1971; Siegal *et al*., 2000). It has been estimated that the administration of an osmotic agent can increase the delivery of therapeutics to the CNS up to 100 times (Miller, 2002; Siegal *et al.*, 2000). However, the intra-arterial injection of osmotic agents is rarely used in a clinical setting as it increases the risk of

seizure and strokes, generally requires anesthesia, and the potential passage of toxins or pathogens to the CNS. Administration of osmotic agents is also not specific to BMECs and can cause the temporary dehydration of other endothelial cells, which can result in undesirable effects on the body (Rodriguez *et al*., 2015).

High-intensity focused ultrasound (FUS) is a non-invasive approach used to thermally ablate tissue and has been approved to treat prostate cancer pain in Canada and has been used to treat patients with tremor-dominant Parkinson's disease, essential tremor and neuropathic pain. The use of high-intensity FUS is also being investigated as a potential treatment for other forms of cancer, especially ones with tumors that are hard to reach, such as brain cancer and intestinal cancers (Foley *et al.,* 2013). In comparison to high-intensity FUS, low-intensity FUS is being investigated as a BBBD technique. As a mechanism for BBBD, microbubbles are administered intravenously in conjunction with the transcranial delivery of low-intensity ultrasound waves (Abrahao *et al*., 2019; Rezai *et al.*, 2020) The microbubbles have a diameter of 1 to 10 μm and consist of fluorocarbon gas encased in lipids (McDannold *et al.*, 2006). The low-intensity FUS causes the acoustic cavitation of the microbubbles, which consequently results in mechanical forces applied to BMECs and the transient opening of the BBB without causing damage to the cells (Rodriguez *et al*., 2015). The BBB closes within 24 hours after low-intensity FUS and microbubbles (Abrahao *et al*., 2019; Rezai *et al*., 2020). One of the advantages of using FUS and microbubbles as a BBBD method is the size of the disruption can be altered based on the size of the microbubbles and the frequency of ultrasound waves (Chen & Konofagou, 2014; Vlachos *et al*., 2011). The combination of low intensity FUS and microbubbles have been tried recently in humans, including a 2019 study in patients with amyotrophic lateral sclerosis (Abrahao *et al.*, 2019). Further human studies were conducted in 2020 in patients with early Alzheimer's disease

(Rezai *et al*., 2020). Both studies demonstrated the effectiveness of FUS in humans but did not try administering a therapeutic in conjunction with the ultrasound (Abrahao *et al*., 2019; Rezai *et al.*, 2020).

1.8.3. Blood-brain barrier shuttle peptides

The notion of BBB shuttle peptides originated in the mid-1980s and was based on the specific receptor transcytosis systems on the BBB, which allowed numerous peptides to enter the CNS. The idea was that chimeric proteins could be generated where one region was from a protein that could not normally cross the BBB and the other region was the receptor binding domain of a protein that could cross the barrier (Pardridge, 1986). Not only does the term BBB shuttle peptides encompass these chimeric proteins, but has been expanded to include small molecules, nanoparticles and genetic material fused to ligands capable of binding to receptors on BMECs (Oller-Salvia *et al*., 2016). One downfall of using BBB shuttle peptides to deliver therapeutics to the CNS is that the ligand portion of the compound competes with endogenous substrates for binding to the receptors on the blood vessels. However, BBB shuttle peptides are relatively easy to synthesize and tend to have low immunogenicity. Since the concept of BBB shuttle peptides was first proposed, an assortment of peptides which bind to different transporters on the BBB have been explored (Oller-Salvia *et al*., 2016).

Some of these shuttle peptides include the receptor binding domains of apolipoprotein B (ApoB) and apolipoprotein E (ApoE) (Böckenhoff *et al*., 2014; Sorrentino *et al*., 2013; Wang *et al*., 2013). Apolipoproteins are a group of proteins which associates with lipids in order to form liposomes. Several processes in lipid metabolism are mediated by apolipoproteins. The formation of liposomes aids in the transport of lipids in the circulatory system and in CSF due to

the amphipathic properties of apolipoproteins. Apolipoproteins also facilitate the transport of lipids by binding to cell-surface receptors, resulting in lipoprotein uptake. There are different classes and sub-classes of apolipoproteins with different functions. ApoB and ApoE are of particular interest for use as BBB shuttle peptides. ApoB binds to low-density lipoprotein receptors (LDLR) and low-density lipoprotein receptor-related protein 2 (LRP2) while ApoE interacts with LDLR, low-density lipoprotein receptor-related protein 1 (LRP1) and LRP2. Although some success in using ApoB as a BBB shuttle peptide has been observed, greater efficacy was observed when using ApoE peptides. This may be attributed to ApoE binding to more receptors, notably LRP1, which is overexpressed on the luminal side of the BBB.

Derivatives of both ApoB and ApoE have been used in previous studies aiming to deliver lysosomal enzymes across the BBB. ApoB (3371-3409) and six variations of the receptor binding domain of ApoE were fused to α-L-iduronidase (IDUA), which when deficient results in mucopolysaccharidosis type I (MPS I), an LSD which affects cells within the CNS. Transcytosis across a BBB model comprised of bovine brain capillary endothelial cells on collagen-coated Transwell inserts was observed for two of the IDUA-ApoE variants, which were ApoE (159-167)$_2$ and ApoE (159-173). These two IDUA-ApoE fusion proteins were then tested in MPS I mice models, by injecting DNA into the tail-vein. A liver specific promoter was used to ensure the proteins were crossing the BBB and that the proteins were not being formed within the CNS. Mice injected with the IDUA-ApoE fusion proteins exhibited a 10-to-30-fold increase in IDUA within brain tissues than mice injected with an IDUA-myc control. These findings illustrate that the IDUA-ApoE proteins were delivered across the BBB in a receptor dependent manner (Wang *et al*., 2013). The receptor binding domain of ApoB (3371-3409) was fused to a modified N-SGSH, an enzyme which when deficient results in the LSD MPS IIIA (Sorrentino *et al.*, 2013;

Spencer *et al*., 2011; Spencer & Verma, 2007). The fusion proteins were delivered to MPS IIIA mice using adeno-associated virus serotype 2/8 (AAV2/8) vectors with a liver-specific human thyroxine binding globulin (TBG) promoter, which was administered by retro-orbital injections. A 10-15% increase in brain SGSH activity was observed in mice injected with the modified SHSH-ApoB enzyme when compared to mice injected with green fluorescent protein (GFP). This resulted in the correction of some of the pathological signs in the MPS III mice, along with improved behaviour (Sorrentino *et al*., 2013). In another study, the receptor binding domain of ApoB (3371-3409) and two versions of ApoE (148-170) and $(159\text{-}167)_2$ were fused to the lysosomal protein arylsulfatase A (ASA). A linker sequence was added downstream of the ASA sequence, upstream of the BBB shuttle peptide. Compared to wild-type ASA, the ASA-Apo fusion proteins significantly crossed an *in vitro* BBB model consisting of primary porcine brain capillary endothelial cells growing on a microporous membrane. However, in ASA-knock out mice, only ASA-ApoE $(159\text{-}167)_2$ significantly crossed into the CNS (Böckenhoff *et al*., 2014).

Other key peptides being developed as brain delivery vectors for protein transport include the human immunodeficiency virus trans-activator of transcription (HIV TAT) protein, Angiopep-2 (Oller-Salvia *et al.*, 2016) and the ribosome-inactivating toxin B subunit (RTB) lectin (Acosta *et al*., 2015; Ou *et al.*, 2018). HIV TAT belongs to the cell-penetrating peptide (CPP) family, a group of cationic peptides capable of crossing cell membranes without requiring receptors or causing damage to the membrane (Frankel & Pabo, 1988; Madani *et al.*, 2011). HIV TAT can enter cells due to a transduction domain (Vivès *et al*., 1997). When large proteins are attached to CPPs, they are transported into the cell by endocytosis and it is thought that the complex is transported across the BBB by adsorptive-mediated transport (AMT) (Oller-Salvia *et al.*, 2016). Angiopep-2 is a peptide developed based on the Kunitz domain of aprotinin *(*Demeul*e*

et al., 2008a) and interacts with LRP1 to cross the BBB (Demeule *et al.*, 2008b). A conjugate of paclitaxel and Angiopep-2 (ANG1005) reached phase II clinical trials for the treatment of breast cancer in patients with recurrent brain metastases (identifier NCT02048059) and recurrent high-grade glioma (identifier NCT01967810).

RTB is the nontoxic B chain of the heterodimeric ricin AB toxin. RTB is a lectin which binds to glycolipids and glycoproteins with a terminal galactose on the cellular membrane and mediates the entry of the ricin A chain into mammalian cells. Both chains are required to produce a toxic effect (Rutenber *et al.*, 1987). RTB has been reported to utilize several different uptake mechanisms to enter cells, however, the predominant route is through AMT mechanisms, rather than receptor mediated transport. Similar to HIV TAT, these AMT mechanisms may be used to deliver therapeutics across the BBB (Sandvig *et al*., 2011). MPS I mice were intravenously injected with an IDUA-RTB fusion protein and IDUA activity was measured (Ou *et al.*, 2018). IDUA-RTB is capable of entering human cells and degrading glycosaminoglycan, the substrate which accumulates when IDUA is deficient (Acosta *et al*., 2015). A reduction in glycosaminoglycan was observed in the brain cortex and cerebellum of mice injected with IDUA-RTB. IDUA activity was detected in the CNS after a single injection while improvement in neurocognition was observed in treated mice after 8 weekly infusions (Ou *et al*., 2018).

1.9. The *piggyBac* protein expression system

To retrain the post-translational modifications acquired by lysosomal enzymes, including HexA, a non-bacterial expression system is needed to produce recombinant protein. The *piggyBac* transposon-based expression system is a technique used to generate stably transfected mammalian cell lines (Li *et al.*, 2013). Up to 15 copies of the gene of interest can be inserted into

the genome of the host cell (Wang *et al.*, 2008). Protein overexpression in the transfected cells is doxycycline inducible (Li *et al.*, 2013).

Both adherent and suspension cell lines can be transfected using the *piggyBac* system, which requires 3 different plasmids (**Fig. 1.8**). The first is pB-T-RfA, a plasmid encoding a Gateway Reading Frame cassette A (Li *et al*., 2013). This cassette facilitates the insertion of genes into pB-T-RfA using the Gateway Cloning System (**Fig. 1.9**), ensuring that the reading frame of the gene is maintained and that the sequence is inserted into the vector in the correct orientation. Genes of interest are PCR amplified to add *att*B sites on both ends of the sequence. A BP Clonase enzyme mix mediates a recombination reaction between the *att*B sites on the PCR product and the *att*P sites on a donor vector (ThermoFisher Scientific, 2003). The donor vector encodes the ccdB protein, a toxin that inhibits *E. coli* DNA gyrase, which is lethal in most strains of the bacteria (Couturier *et al.*, 1998). This gene is used as a selectable marker to eliminate any bacteria transformed with the donor vector. The BP recombination reaction results in the formation of an entry clone with the gene of interest flanked by *att*L sites (ThermoFisher Scientific, 2003). The cassette in pB-T-RfA (destination vector) encodes *ccd*B and a chloramphenicol resistance gene, which are flanked by *att*R sites (Li *et al*., 2013). A second recombination reaction, mediated by the LR Clonase enzyme mix, exchanges the DNA between the *att*L and *att*R sites (ThermoFisher Scientific, 2003). This results in the gene of interest being inserted into pB-T-RfA (expression clone).

A puromycin resistance gene, which is regulated by an attenuated simian vacuolating virus 40 early promoter (SV40Δ90), is also present on pB-T-RfA (**Fig. 1.8**). Expression of the gene of interest is driven by the tetracycline response element (TRE) promoter (Li *et al*., 2013), which is comprised of a series of eight repeating tetracycline operator (tetO) elements placed

with a shortened minimal cytomegalovirus (CMV) promoter (Agha-Mohammadi *et al*., 2004). The second plasmid required for the *piggyBac* expression system is pB-RB, a vector which encodes the reverse tetracycline transactivator (rtTA) inducer, which is constitutively expressed by a strong CMV promoter (Li *et al.*, 2013). In the presence of tetracycline, or a derivative such as doxycycline, the rtTA inducer will bind to one of the tetO elements of the TRE promoter, which initiates transcription of the gene of interest encoded on pB-T-RfA (Gossen *et al.*, 1995). A blasticidin S resistance gene, constitutively expressed by the simian vacuolating virus 40 (SV40) promoter, is also present on pB-RB. The pBase plasmid encodes for PBase, the transposase responsible for inserting transposons into mammalian cells (Li *et al.*, 2013). Expression of PBase is mediated by the constitutive chicken β-actin (CAG) promoter (Wang *et al.*, 2008). A puromycin resistance gene is also present on pBase. However, it has been demonstrated that no puromycin resistant cells were obtained when cells were transfected only with pB-RB and pBase, indicating that the PBase transposase does not integrate into the genome (Li *et al.*, 2013).

High and nearly identical protein expression was observed in cells transfected using the *piggyBac* system. Because of this efficiency, bulk cell cultures can be used, rather than the time-consuming traditional method of selecting an individual clone with the best protein expression and expanding (Li *et al.,* 2013).

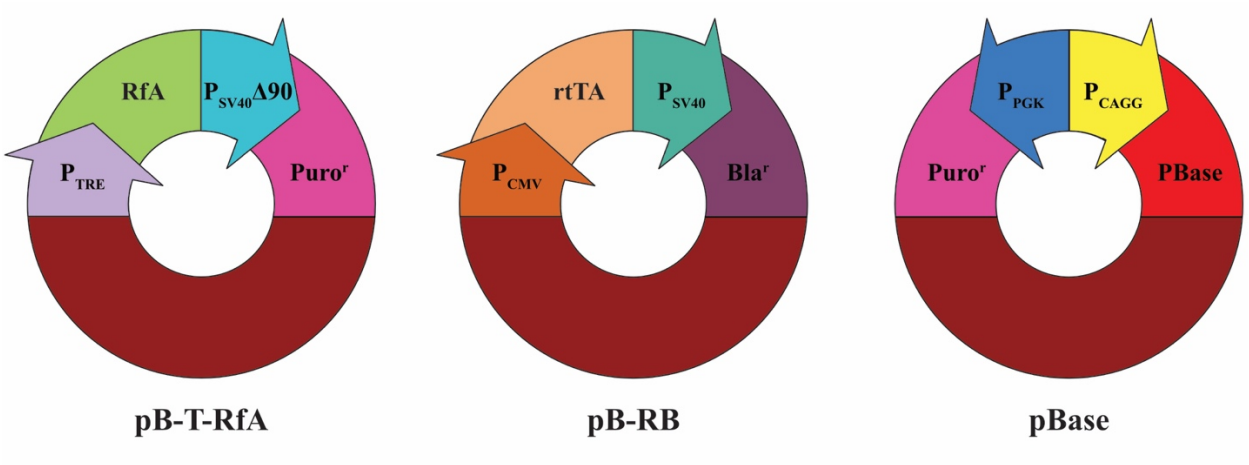

Figure 1.8. Diagram of the plasmids used for the *piggyBac* transposon-based mammalian cell expression system. Three plasmids are required for protein expression using the *piggyBac* system. The pB-T-RfA plasmid encodes a puromycin resistance gene along with a Gateway Reading Frame cassette A, which can be replaced with a gene for protein overexpression. The pB- RB plasmid encodes a strong cytomegalovirus promoter which constitutively expresses the reverse tetracycline transcactivator (rtTA) gene (Li *et al.*, 2013). In the presence of doxycycline, rtTA binds to the tetracycline response element (TRE) promoter upstream of the gene of interest, allowing for inducible protein production (Gossen *et al*., 1995). A blasticidin resistance gene is also encoded on pB-RB. The pBase plasmid encodes for PB transposase, which integrates the genes from pB-T-RfA and pB-RB into the host cell genome. The PB transposase gene is constitutively expressed under the control of a chicken β-actin promoter coupled with cytomegalovirus immediate-early enhancer. Reproduced from Li *et al.* (2013).

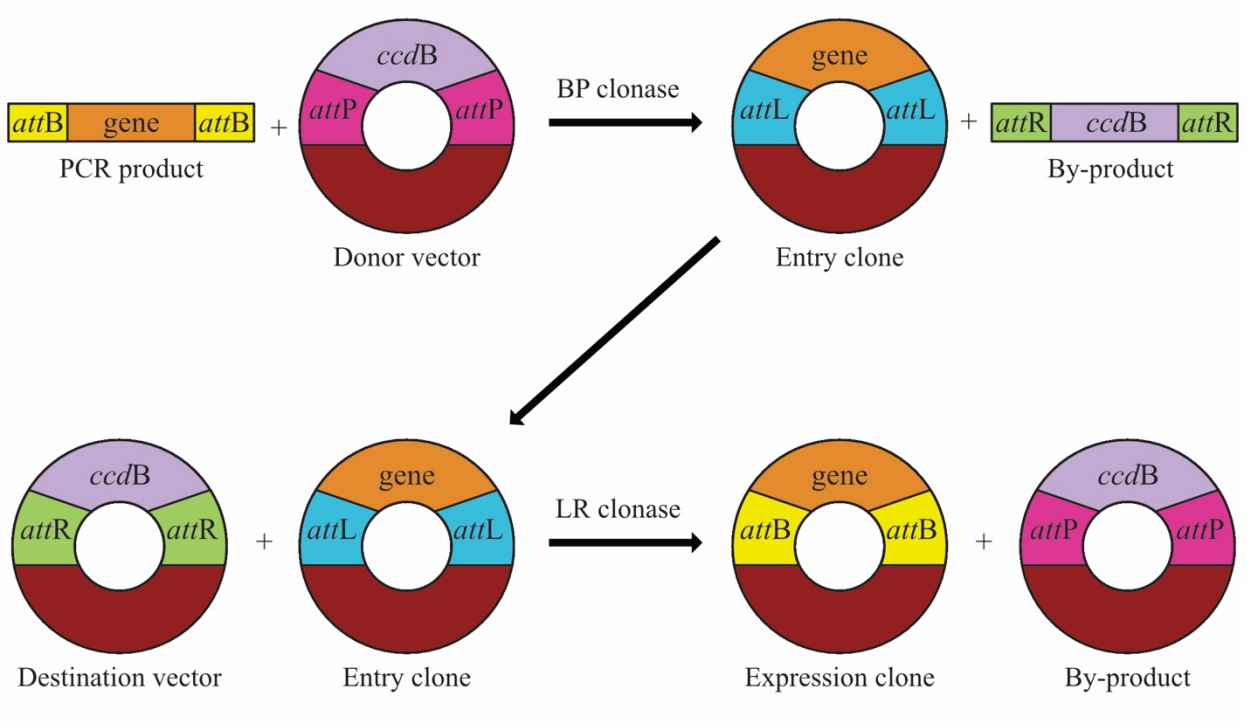

Figure 1.9. Model of the Gateway recombination reactions. The Gateway Cloning System is a technique that allows for efficient DNA transfer into various vectors. The gene of interest is PCR amplified with primers designed to add *att*B sites on both sides of the gene. A BP Clonase enzyme mix is used to mediate a recombination reaction between the *attB* sites on the PCR product and *att*P sites on the donor vector. This generates an entry clone with the gene of interest flanked by *att*L sites. The Gateway cassette (purple) is found in the destination vector and is flanked by two *att*R sites. An LR Clonase enzyme mix catalyses the recombination of the *att*L and the *att*R sites on these to plasmids. This recombination reaction generates an expression clone with the gene of interest. The products of the LR reaction are transformed into *E.coli.* The *ccd*B gene on the by-product encoded for the CcdB protein that interferes with DNA gyrase and inhibits the growth of most *E. coli* strains. Reproduced from ThermoFisher Scientific (2003).

1.10. FiberCell bioreactor system

The FiberCell system is a hollow fiber bioreactor designed to replicate the conditions in which cells grow in vertebrates. The bioreactor cartridge consists of thousands of semi-permeable hollow fibers laid in parallel, surrounded by an exterior shell. Cells are seeded into the area outside of the hollow fibers, known as the extra capillary space. A pump pushes fresh culture media from a bottle through the hollow fibers, providing nutrients and oxygen to the

cells, whilst removing metabolic waste products such as lactic acid and ammonia. Media, from which proteins can be purified, is collected from the extra capillary space using a syringe. The cell density within a FiberCell bioreactor is much higher than in cell culture flask, resulting in an increased concentration of secreted protein in the media (FiberCell Systems, 2017).

1.11. Research objectives

1.11.1. Overarching hypothesis

Attaching the receptor binding domains of ApoB and ApoE to HexM will increase the ability of the protein to cross the BBB, improving the efficacy of the enzyme to reduce GM2 accumulation in the CNS when administered as an ERT and can be augmented using pharmacological chaperones in juvenile and adult-onset forms of the GM2 gangliosidoses.

1.11.2. Research aims

Currently, there are no clinically available treatments to manage the GM2 gangliosidoses (Ou *et al.*, 2020). HexM was created as a potential therapeutic for TSD and SD, overcoming some of the challenges the heterodimeric nature of HexA poses in the development of a therapy *(*Tropak *et al.*, 2016). However, the limited permeability of the BBB impedes the delivery of molecules, including HexM, to the CNS where GM2 accumulation primarily occurs (Oller-Salvia *et al.*, 2016). Consequently, the aim of this thesis was to further develop HexM for use in ERT by assessing the delivery of chimeric HexM-fusion proteins across the BBB by transcytosis. To achieve this, three main objectives were established:

1. To develop a novel method for obtaining and purifying human HexA, which has traditionally been isolated from placentas, providing a consistent source of the protein for use in structural studies and as a control in HexM enzymatic studies.

2. To expand on the novel HexA purification scheme to create an αG269S mutant, the most common mutation in adult-onset TSD, for pharmacological chaperone studies.
3. To produce and characterize HexM-ApoB and HexM-ApoE fusion proteins, then investigate their potential to cross the blood-brain barrier using an *in vitro* model.

2. Materials and Methods

2.1. Generating expression plasmids

2.1.1. HexA

Synthetic DNA fragments encoding the *HEXA* and *HEXB* genes (Table 2.1) were obtained from Integrated DNA Technologies (IDT). The *HEXA* fragment was amplified in a two-step polymerase chain reaction (PCR) to add a C-terminal FLAG-tag and *att*B sites flanking the 5' and the 3' ends of the gene. Primers used for the reactions are listed in Table 2.2 and were obtained from IDT. The first reaction mixture contained 10 µl 5X Q5 reaction buffer, 4 µl 2.5 mM dNTPs, 1 µl 10 µM forward primer, 2 µl 5 µM reverse primer (*HEXA* FLAG-tag), 1 µl template DNA (503.3 ng), 0.5 µl Q5 high-fidelity DNA polymerase and 31.5 µl nuclease-free water. The DNA was initially denatured at 98°C for 30 seconds, followed by 10 cycles of 98°C for 10 seconds and 72°C for 80 seconds. The recommended annealing temperature for the primers was 72°C. For that reason, annealing and elongation were combined into a single step. The product of the first PCR was used for the subsequent amplification. The second reaction mixture contained 4 µl 5X Q5 reaction buffer, 3 µl 2.5 mM dNTPs, 4 µl 10 µM forward primer, 4 µl 10 µM reverse primer (universal *att*B), 10 µl template DNA from the first PCR, 0.5 µl Q5 high-fidelity DNA polymerase and 24.5 µl nuclease free water. The initial denaturation was at

98°C for 30 seconds, followed by 5 cycles at 98°C for 10 seconds, 45°C for 30 seconds, 68°C for 50 seconds, then 20 cycles at 98°C for 10 seconds, 55°C for 30 seconds, 68°C for 50 seconds and a final extension of 72°C for 10 minutes. The amplified DNA was purified using the QIAquick PCR Purification Kit (Qiagen). To add a C-terminal His_6 tag and flanking *att*B sites to *HEXB,* a two-step PCR was carried out by Dr. Brian Mark, using the *HEXB* His_6 tag and the universal *att*B primers.

The PCR-amplified *HEXA* and *HEXB* genes were inserted into pDONR201 vectors using the BP recombination reaction of the Gateway Cloning System. For the *HEXA* reaction, 1.5 µl amplified *HEXA* (150 ng), 0.9 µl pDONR201 (150 ng) and 2 µl Gateway BP Clonase II Enzyme mix (Invitrogen) were added to a PCR tube. Elution buffer was added to bring the sample volume to 10 µl and the tube was incubated at 25°C for 1 hour. The reaction was terminated by adding 1 µl Proteinase K (Invitrogen) and incubating the tube at 37°C for 10 minutes. The plasmid was transformed into *E. coli* DH5α and successful transformants were selected for using kanamycin. Insertion of *HEXB* into pDONR201 was performed by Dr. Brian Mark. The *HEXA* and *HEXB* genes were transferred from the pDONR201 to pB-T-RfA, a mammalian cell expression plasmid (Li *et al*., 2013), using the LR recombination reaction of the Gateway Cloning System. For the reactions, either 0.4 µl pDONR201-*HEXA* (151.5 ng) or 0.9 µl pDONR201-*HEXB* (150.4 ng) were added to PCR tubes with 0.4 µl of pB-T-RfA (149.8 ng) and 2 µl Gateway LR Clonase II Enzyme mix (Invitrogen). Elution buffer was added to bring the total volume to 10 µl. The resulting pB-T-RfA-*HEXA* and pB-T-RfA-*HEXB* plasmids were transformed into *E. coli* DH5α under ampicillin selection and verified by Sanger sequencing (The Center for Applied Genomics, Toronto). The universal pB-T-RfA primers were used to

sequence pB-T-RfA-*HEXB*. For pB-T-RfA-*HEXA*, the internal *HEXA* and the universal pB-T-RfA primers were used for sequencing.

Table 2.1. Synthetic DNA fragments used to generate β-hexosaminidase enzymes.

Protein	Sequence (5'-3')
HexA G269S	GATATACATATGAGAGCTTCACTTTTCCAGAGCTCATGAGAAAGGGGTCCTACAACCCTGTCA CCCACATCTACACAGCACAGGATGTGAAGGAGGTCATTGAATACGCACGGCTCCGGGGTATC CGTGTGCTTGCAGAGTTTGACACTCCTGGCCACACTTTGTCCTGGGGACCAAGTATCCCTGGA TTACTGACTCCTTGCTACTCTGGGTCTGAGCCCTCTGGCACCTTTGGACCAGTGAATCCCAGT CTCAATAATACCTATGAGTTCATGAGCACATTCTTCTTAGAAGTCAGCTCTGTCTTCCCAGATT TTTATCTTCATCTTGGAGGAGATGAGGTTGATTTCACCTGCTGGAAGTCCAACCCAGAGATCC AGGACTTTATGAGGAAGAAAGGCTTCGGTGAGGACTTCAAGCAGCTGGAGTCCTTCTACATC CAGACGCTGCTGGACATCGTCTCTTCTTATGGCAAGGGCTATGTGGTGTGGCAGGAGGTGTTT GATAATAAAGTAAAGATTCAGCCAGACACAATCATACAGGTGTGGCGAGAGGATATTCCAGT GAACTATATGAAGGAGCTGGAACTGGTCACCAAGGCCGGCTTCCGGGCCCTTCTCTCTGCCCC CTGGTACCTGAACCGTATATCCTATGGCCCTGACTGGAAGGATTTCTACGTAGTGGAACCCCT GGCATTTGAAGGTACCCCTGAGCAGAAGGCTCTGGTGATTGGTGGAGAGGCTTGTATGTGGG GAGAATATGTGGACAACACAAACCTGGTCCCCAGGCTCTGGCCCAGAGCAGGGGCTGTTGCC GAAAGGCTGTGGAGCAACAAGTTGACATCTGACCTGACATTTGCCTATGAACGTTTGTCACA CTTCCGCTGTGAGTTGCTGAGGCGAGGTGTCCAGGCCCAACCCCTCAATGTAGGCTTCTGTGA GCAGGAGTTTGAACAGACCGATTACAAGGACGACGATGACAAGTGATGAGACCCAGCTTTCT TGTACAAAGTGGTGATAAACCCGCTGATCAGCCTCGACTGTGCCTTCTAGTTGCCAGCCATCT GTTGTTTGCCCCTCCCCCGTGCCTTCCTTGACCCTGGAAGGTGCCACTCCCACTGTCCTTTCCT AATAAAATGAGGAAATTGCATCGCATTGTCTGAGTAGGTGTCATTCTATTCTGGGGGGTGGG GTGGGGCAGGACAGCAAGGGGGAGGATTGGGAAGACAATAGCAGGCATGCTGGGGATGCGG TGGGCTCTATGGCTTCTGAGGCGGAAAGAACCAGCTGGGGCTCTAGGGGGTATCCCCACGCG CCCTGTAGCGGCGCATTAAGCGCGGCGGGTGTGGTGGTTACGCGCAGCGTGACCGCTACACT TGCCAGCGCCCTAGCGCCCGCTCCTTTCGCTTTCTTCCCTTCCTTTCTCGCCACGTTCGCCGGC TTTCCCCGTCAAGCTCTAAATCGGGGGCTCCCTTTAGGGTTCCGATTTAGTGCTTTACGGCAC CTCGACCCCAAAAAACTTGATTAGGGTGATGGTTCACGTACCTAGAAGTTCCTATTCCGAAGT TCCTATTCTCTAGAAAGTATAGGAACTTCCTTGGCCAAAAAGACCGGTGATATA
HexM-myc	GATATAAGCGCTCCATGGTATCTCAACCGGATATCCTACGGCCAGGACTGGAGAAAATTTTA CAAAGTAGAGCCCCTGGCATTCGAAGGCACCCCTGAACAGAAAGCCCTTGTGATCGGCGGTG AAGCGTGTATGTGGGGTGAATACGTGGACGCAACTAATCTCGTCCCCAGGTTGTGGCCGCGC GCTGGGGCCGTCGCTGAACGCCTGTGGAGCAACAAGCTGACCCGAGATATGGATGACGCGTA CGATCGCCTGAGCCACTTCCGGTGCGAATTGGTTAGACGGGGAGTAGCTGCGCAGCCTCTCT ACGCTGGTTATTGTAACCAGGAGTTCGAGCAAACAATCGAGGGAAGACACCACCACCATCAT CATGAGCAGAAACTCATCAGCGAAGAGGACCTTTGAGACCCAGCTTTCTTGTACAAAGTGGT GATAAACCCGCTGATCAGCCTCGACTGTGCCTTCTAGTTGCCAGCCATCTGTTGTTTGCCCCTC CCCCGTGCCTTCCTTGACCCTGGAAGGTGCCACTCCCACTGTCCTTTCCTAATAAAATGAGGA AATTGCATCGCATTGTCTGAGTAGGTGTCATTCTATTCTGGGGGGTGGGGTGGGGCAGGACA GCAAGGGGGAGGATTGGGAAGACAATAGCAGGCATGCTGGGGATGCGGTGGGCTCTATGGC TTCTGAGGCGGAAAGAACCAGCTGGGGCTCTAGGGGGTATCCCCACGCGCCCTGTAGCGGCG CATTAAGCGCGGCGGGTGTGGTGGTTACGCGCAGCGTGACCGCTACACTTGCCAGCGCCCTA GCGCCCGCTCCTTTCGCTTTCTTCCCTTCCTTTCTCGCCACGTTCGCCGGCTTTCCCCGTCAAG CTCTAAATCGGGGGCTCCCTTTAGGGTTCCGATTTAGTGCTTTACGGCACCTCGACCCCAAAA AACTTGATTAGGGTGATGGTTCACGTACCTAGAAGTTCCTATTCCGAAGTTCCTATTCTCTAG AAAGTATAGGAACTTCCTTGGCCAAAAAGACCGGTGATATA

HexM-ApoB	GATATAAGCGCTCCATGGTATCTCAACCGGATATCCTACGGCCAGGACTGGAGAAAATTTTA CAAAGTAGAGCCCCTGGCATTCGAAGGCACCCCTGAACAGAAAGCCCTTGTGATCGGCGGTG AAGCGTGTATGTGGGGTGAATACGTGGACGCAACTAATCTCGTCCCCAGGTTGTGGCCGCGC GCTGGGGCCGTCGCTGAACGCCTGTGGAGCAACAAGCTGACCCGAGATATGGATGACGCGTA CGATCGCCTGAGCCACTTCCGGTGCGAATTGGTTAGACGGGGAGTAGCTGCGCAGCCTCTCT ACGCTGGTTATTGTAACCAGGAGTTCGAGCAAACAATCGAGGGAAGACACCACCACCATCAT CATGAGCAGAAACTCATCAGCGAAGAGGACCTTCTGGGAGGCGGAGGCAGTGGAGGCGGTG GCTCTGGTGGGGGGGGAAGTGGCGGCGGCGGGTCTTCCGTTATTGATGCACTGCAGTATAAG CTGGAAGGGACCACCCGACTGACGCGAAAGAGAGGCCTTAAGCTCGCCACCGCTCTGTCACT GTCAAACAAGTTTGTCGAGGGTAGCTGAGACCCAGCTTTCTTGTACAAAGTGGTGATAAACC CGCTGATCAGCCTCGACTGTGCCTTCTAGTTGCCAGCCATCTGTTGTTTGCCCCTCCCCCGTGC CTTCCTTGACCCTGGAAGGTGCCACTCCCACTGTCCTTTCCTAATAAAATGAGGAAATTGCAT CGCATTGTCTGAGTAGGTGTCATTCTATTCTGGGGGGGTGGGGTGGGGCAGGACAGCAAGGGG GAGGATTGGGAAGACAATAGCAGGCATGCTGGGGATGCGGTGGGCTCTATGGCTTCTGAGGC GGAAAGAACCAGCTGGGGCTCTAGGGGGTATCCCCACGCGCCCTGTAGCGGCGCATTAAGCG CGGCGGGTGTGGTGGTTACGCGCAGCGTGACCGCTACACTTGCCAGCGCCCTAGCGCCCGCT CCTTTCGCTTTCTTCCCTTCCTTTCTCGCCACGTTCGCCGGCTTTCCCCGTCAAGCTCTAAATCG GGGGCTCCCTTTAGGGTTCCGATTTAGTGCTTTACGGCACCTCGACCCCAAAAAACTTGATTA GGGTGATGGTTCACGTACCTAGAAGTTCCTATTCCGAAGTTCCTATTCTCTAGAAAGTATAGG AACTTCCTTGGCCAAAAAGACCGGTGATATA
HexM-ApoE	GATATAAGCGCTCCCTGGTATCTCAACCGCATCTCCTACGGCCAAGACTGGCGGAAGTTTTAC AAGGTGGAACCGCTGGCATTCGAGGGGACTCCTGAGCAGAAGGCACTGGTAATTGGGGGAG AAGCCTGCATGTGGGGAGAGTATGTCGACGCCACCAATCTGGTCCCCCGGCTGTGGCCCAGA GCCGGGGCCGTTGCCGAAAGGCTGTGGTCCAACAAGTTGACAAGGGACATGGATGATGCCTA CGATAGGCTGTCCCACTTCCGGTGCGAACTTGTAAGAAGGGGAGTCGCTGCTCAGCCACTCT ACGCTGGGTACTGCAATCAAGAATTTGAGCAGACTATTGAAGGGCGACACCATCACCACCAT CATGAACAGAAGCTTATTAGTGAGGAGGATCTGCTGGGCGGAGGTGGAAGTGGAGGCGGCG GTTCTGGTGGAGGAGGATCTGGGGGCGGCGGCAGTCTCCGCAAGCTCCGCAAACGGCTGTTG CTCCGGAAGCTCCGAAAACGCCTGCTGTGAGACCCAGCTTTCTTGTACAAAGTGGTGATAAA CCCGCTGATCAGCCTCGACTGTGCCTTCTAGTTGCCAGCCATCTGTTGTTTGCCCCTCCCCCGT GCCTTCCTTGACCCTGGAAGGTGCCACTCCCACTGTCCTTTCCTAATAAAATGAGGAAATTGC ATCGCATTGTCTGAGTAGGTGTCATTCTATTCTGGGGGGGTGGGGTGGGGCAGGACAGCAAGG GGGAGGATTGGGAAGACAATAGCAGGCATGCTGGGGATGCGGTGGGCTCTATGGCTTCTGAG GCGGAAAGAACCAGCTGGGGCTCTAGGGGGTATCCCCACGCGCCCTGTAGCGGCGCATTAAG CGCGGCGGGTGTGGTGGTTACGCGCAGCGTGACCGCTACACTTGCCAGCGCCCTAGCGCCCG CTCCTTTCGCTTTCTTCCCTTCCTTTCTCGCCACGTTCGCCGGCTTTCCCCGTCAAGCTCTAAAT CGGGGGCTCCCTTTAGGGTTCCGATTTAGTGCTTTACGGCACCTCGACCCCAAAAAACTTGAT TAGGGTGATGGTTCACGTACCTAGAAGTTCCTATTCCGAAGTTCCTATTCTCTAGAAAGTATA GGAACTTCCTTGGCCAAAAAGACCGGTGATATA

Table 2.2. Primers used in this work.

Target	Forward primer (5'-3')	Reverse primer (5'-3')
HEXA FLAG-tag	AAAAAGCAGGCTCCAAAGCCACCATGACA AGCTCCAGGCTTTGG	AGAAAGCTGGGTCTCACTTGTCATCGTCTC CTTGTAATCGGTCTGTTCAAACTCCTGTC
Universal *att*B	GGGGACAAGTTTGTACAAAAAAGCAGGC	GGGGACCACTTTGTACAAGAAAGCTGGG
HEXB His_6 tag	AAAAAGCAGGCTCCAAAGCCACCATGGAG CTGTGCGGGCTGGGG	AGAAAGCTGGGTCTTAATGATGATGATGA TGATGTCTACCCTCGATCATGTTCTCATGG TTAC
Universal pB-T-RfA	GACCTCCATAGAAGACACCGG	AAACAACAGATGGCTGGCAAC
Internal *HEXA*	ATTGAGGACTTTCCCCGCTTTC	TATCCTCTCGCCACACCTGTATG
HexM gBlock	GGAGGACATCCCAGTGAAC	CGGGACTATGGTTGCTGAC

2.1.2. HexA G269S

The pB-T-RfA-*HEXA* plasmid was digested with NdeI and AgeI-HF (New England BioLabs [NEB]). For the reaction, 1 µl of each restriction enzyme was incubated with 18.3 µl pB-T-RfA-*HEXA* (7000 ng), 5 µL 10X CutSmart buffer and 24.7 µl nuclease-free water for 3 hours at 37°C followed by 20 minutes at 65°C.

A 0.8% agarose gel was used to separate the digested DNA and the band containing the pB-T-RfA-*HEXA* plasmid backbone was excised from the gel. The DNA was purified from the agarose using the PureLink Quick Gel Extraction and PCR Purification Combo Kit (Invitrogen) according to the manufacturer's instructions.

A synthetic DNA fragment (IDT) encoding the αG269S mutation (100 ng) was directionally cloned into the pB-T-RfA-*HEXA* backbone (70.5 ng) using 5 µl Instant Sticky-end Ligase Master Mix (NEB). The construct was transformed into $CaCl_2$-competent *E. coli* DH5α and transformants were selected for using ampicillin. Sanger sequencing (The Center for Applied Genomics, Toronto) with the internal *HEXA* primers was conducted to verify the resulting pB-T-RfA-*HEXA*-G269S construct.

2.1.3. HexM-ApoB, HexM-ApoE and HexM-myc

A pB-T-RfA plasmid encoding *HEXM* (pB-T-RfA-*HEXM*) was generously donated to the lab by Dr. Michael Tropak (SickKids Hospital, Toronto). The pB-T-RfA-*HEXM* plasmid was digested using the restriction enzymes AfeI and AgeI-HF (NEB). The reaction mixture contained 27.9 µl pB-T-RfA-*HEXM* (7000 ng), 1 µl AfeI, 1 µl AgeI-HF and 5 µL 10X CutSmart buffer. The total volume was brought to 50 µl with nuclease-free water and the tube was incubated at 37°C for 1 hour. The 5' ends of the digested DNA were dephosphorylated by adding 3 µl

Antarctic phosphatase (AnP) and 6 µl 10X AnP buffer (NEB) to the tube and incubating it for 30 minutes at 37°C, then at 80°C for 5 minutes. The digested DNA fragments were separated on a 0.8% agarose gel. The band corresponding to the pB-T-RfA-*HEXM* backbone was excised and purified using the PureLink Quick Gel Extraction and PCR Purification Combo Kit (Invitrogen) as per the manufacturer's directions.

Synthetic DNA fragments encoding a C-terminal myc tag and the receptor binding domain of ApoB (13.4 ng), a C-terminal myc tag with the ApoE binding domain (9 ng) and a fragment encoding a C-terminal myc tag (14.8 ng) were obtained from IDT and were directionally cloned into the pB-T-RfA-*HEXM* backbone (160 ng, 160 ng and 100 ng respectively) using 5 µl of Instant Sticky-end Ligase Master Mix (NEB) (**Fig. 2.1**). The resulting constructs were transformed into $CaCl_2$-competent *E. coli* DH5α under ampicillin selection. The fidelity of the resulting pB-T-RfA- *HEXM*-ApoB, pB-T-RfA- *HEXM*-ApoE and pB-T-RfA-*HEXM*-myc constructs was verified by Sanger sequencing (The Center for Applied Genomics, Toronto). The HexM gBlock primers were used for sequencing. The design of the synthetic DNA fragments used to generate these plasmids, including a linker sequence and both Apo sequences, were based on previous studies aiming to deliver therapeutics across the BBB (Böckenhoff *et al*., 2014; Sorrentino *et al*., 2013; D. Wang *et al.*, 2013).

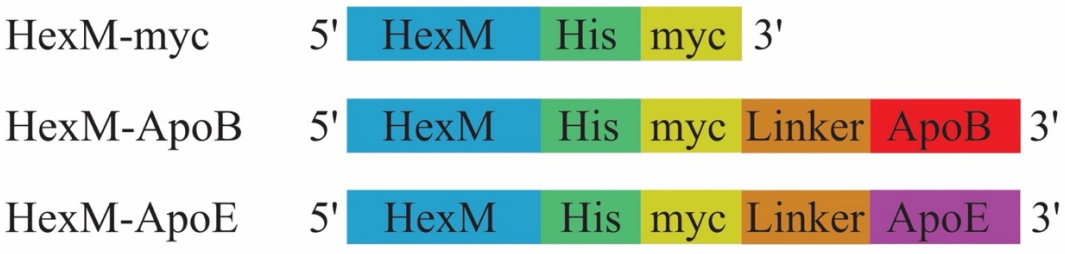

Figure 2.1. Model of DNA used to generate HexM-ApoB, HexM-ApoE and HexM-myc. A His_6 tag, followed by a myc tag was added to the 3' end of the HexM sequence. For HexM-ApoB and ApoE, a linker sequence and receptor binding domains were also added.

2.2. Transfections

2.2.1. HexA

A line of human embryonic kidney 293T (HEK293T) cells deficient in the *HEXA* and *HEXB* genes (HEK293T-ABKO) was previously generated using CRISPR-based genome editing (Tropak *et al*., 2016). HEK293T-ABKO cells were revived from stocks frozen in liquid nitrogen. The cells were frozen in DMEM (Gibco) supplemented with 10% (v/v) FBS (Gibco), 1 % (v/v) Penicillin-Streptomycin and 5% (v/v) dimethyl sulfoxide (DMSO) (Sigma-Aldrich). Prior to thawing the cells, the medium was equilibrated by adding 14 ml DMEM (Gibco) supplemented with 10% (v/v) FBS (Gibco) and 1 % (v/v) Penicillin-Streptomycin was added to a T75 flask (ThermoFisher Scientific) and incubated for 1 hour at 37ºC with 5% CO_2. This incubation step helps ensure the medium is at an optimal temperature and pH for the cells. Afterwards, 4 ml equilibrated medium was transferred to a 50 ml conical centrifuge tube (Corning). A cryovial containing HEK293T-ABKO cells was removed from the liquid nitrogen storage dewar and placed into a 37ºC water bath. Once the cells were thawed, the contents of the cryovial were immediately pipetted into the tube with medium and was centrifuged for 5 minutes at 355 x *g*. The supernatant was decanted, and the cell pellet was resuspended with equilibrated media. The cells were transferred into the T75 flask and incubated at 37ºC with 5% CO_2.

HEK293T-ABKO cells growing in T75 flasks (ThermoFisher Scientific) were resuspended with DMEM (Gibco) supplemented with 10% (v/v) FBS (Gibco), 1 % (v/v) Penicillin-Streptomycin and 1 µg/ml doxycycline. The concentration of resuspended cells was determined using a Cedex XS cell counter (Roche Innovatis) and a total of 1.0 x 10^6 cells was plated per well in a 6-well tissue culture-treated polystyrene plate (Corning Life Sciences). The volume of medium inside each well was brought to 3 ml by adding DMEM (Gibco)

supplemented with 10% (v/v) FBS (Gibco), 1 % (v/v) Penicillin-Streptomycin and 1 µg/ml doxycycline (Li *et al*., 2013). The plate was incubated at 37ºC with 5% CO_2 for 24 hours to allow the cells to adhere to the bottom of the wells.

The following day, 2500 ng pB-T-RfA-*HEXA*, 1500 ng pB-T-RfA-*HEXB*, 500 ng pB-RB and 500 ng pBase (5:3:1:1 ratio) were incubated with 15 µl transfecting agent polyethylenimine (PEI) (Polysciences, cat #: 23966-2) in a glass tube for 15 minutes at room temperature. Serum-free DMEM (Gibco) was used to bring the volume of the plasmid-PEI mixture to 250 µl. A glass tube was prepared for each well containing cells. The plasmid-PEI mixture was gently added to the HEK293T-ABKO cells growing in DMEM (Gibco) supplemented with 10% (v/v) FBS (Gibco), 1 % (v/v) Penicillin-Streptomycin and 1 µg/ml doxycycline (Li *et al*., 2013). The tissue culture plate was incubated at 37ºC with 5% CO_2 for 24 hours.

After a day, the medium was removed from the HEK293T-ABKO cells and replaced with 2.5 ml DMEM (Gibco) with 10% (v/v) FBS (Gibco), 1 % (v/v) Penicillin-Streptomycin and 1 µg/ml doxycycline. The new medium was carefully added to the wells in order to avoid resuspending the cells. The 6-well plate was incubated for 24 hours at 37ºC with 5% CO_2.

Following the incubation, the medium was removed from the wells without resuspending the HEK293T-ABKO cells and 1 ml of phosphate-buffered saline (PBS) was added. The cell culture plate was slowly swirled. The PBS was pipetted up from the wells and 1 ml TrypLE Select enzyme (Gibco) was added. The cells were resuspended and transferred to T75 flasks (ThermoFisher Scientific) with 10 ml DMEM (Gibco) supplemented with 10% (v/v) FBS (Gibco), 1 % (v/v) Penicillin-Streptomycin and 1 µg/ml doxycycline. The T75 flasks were incubated at 37ºC with 5% CO_2 for 24 hours.

The following day, the medium was replaced with 10 ml DMEM (Gibco) with 10% (v/v) FBS (Gibco), 1 % (v/v) Penicillin-Streptomycin, 1 µg/ml doxycycline, 10 µg/ml puromycin (ThermoFisher Scientific) and 5 µg/ml blasticidin S (ThermoFisher Scientific) to select for transformants (Li *et al*., 2013). The resulting HEK293T-ABKO-HexA cell line was grown in this selection medium for 1 month, then medium without puromycin or blasticidin S was used. The cells were passaged every 3-4 days.

Frozen stocks of the HEK293T-ABKO-HexA cell line were made. HEK293T-ABKO-HexA cells growing in T75 flasks (ThermoFisher Scientific) at approximately 80% confluency were resuspended by pipetting up and down. The cells were then transferred into a 50 ml conical tube (Corning) and centrifuged for 5 minutes at 355 x *g*. The supernatant was decanted. For each T75 flask of cells being frozen, 1 ml DMEM (Gibco) with 10% (v/v) FBS (Gibco), 1 % (v/v) Penicillin-Streptomycin, 1 µg/ml doxycycline, 10 µg/ml puromycin (ThermoFisher Scientific), 5 µg/ml blasticidin S (ThermoFisher Scientific) and 5% (v/v) DMSO (Sigma-Aldrich) was used to resuspend the cell pellet. The cells were then aliquoted into cryovials and stored in an isopropanol chamber at -80ºC for 3 days. The cryovials were then transferred to a liquid nitrogen storage dewar.

2.2.2. HexA G269S, HexM-ApoB, HexM-ApoE and HexM-myc

HEK293T-ABKO cells were plated into 6-well tissue culture plates as described above and were incubated for 24 hours at 37ºC with 5% CO_2. The HEK293T-ABKO-HexA-G269S, the HEK293T-ABKO-HexM-ApoB, HEK293T-ABKO-HexM-ApoE and the HEK293T-ABKO-HexM-myc cell lines were generated by transfecting HEK293T-ABKO cells using Lipofectamine 2000 Transfection Reagent (Invitrogen) as per the manufacturer's directions. To

produce the HEK293T-ABKO-HexA-G269S cell line, the cells were transfected with 2000 ng of pB-T-RfA-*HEXA*-G269S, 1200 ng pB-T-RfA-*HEXB,* 400 ng pB-RB and 400 ng pBase (5:3:1:1 ratio). The knockout cells were transfected with 3200 ng pB-T-RfA-*HEXM*-ApoB, 400 ng pB-RB and 400 ng pBase (8:1:1 ratio) to generate the HEK293T-ABKO-HexM-ApoB cell line. To generate the HEK293T-ABKO-HexM-ApoE cell line, the knockout cells were transfected with 3200 ng pB-T-RfA-*HEXM*-ApoE, 400 ng pB-RB and 400 ng pBase (8:1:1 ratio). HEK293T-ABKO-HexM-myc cells were generated by transfecting the knockout cells with 3200 ng pB-T-RfA-*HEXM*-myc, 400 ng pB-RB and 400 ng pBase (8:1:1 ratio) (Li *et al*., 2013). The 6-well plates were incubated at 37ºC with 5% CO_2 and 48 hours after adding the plasmids to the cells, the medium was changed to 10 ml DMEM (Gibco) with 10% (v/v) FBS (Gibco), 1 % (v/v) Penicillin-Streptomycin, 1 µg/ml doxycycline, 10 µg/ml puromycin (ThermoFisher Scientific) and 5 µg/ml blasticidin S (ThermoFisher Scientific). Transfected cells were transferred to T75 flasks (ThermoFisher Scientific) after 24 hours in selection medium. The generated cell lines were grown in the selection medium for approximately 1 month, after which cells were grown in DMEM (Gibco) with 10% (v/v) FBS (Gibco), 1 % (v/v) Penicillin-Streptomycin and 1 µg/ml doxycycline. Cell lines were passaged every 3-4 days.

2.3. FiberCell inoculation and media harvests

The HEK-293T-ABKO-HexA, HEK-293T-ABKO-HexM-ApoB and HEK-293T-ABKO-HexM-ApoE cell lines were inoculated into medium-sized FiberCell bioreactor cartridges with a 20 kDa molecular weight cut-off (C2011) as per the manufacturer's instructions (FiberCell Systems Inc, Maryland). The medium was changed to DMEM (Gibco) supplemented with 10% chemically defined medium for high density (CDM-HD) serum replacement powder (FiberCell

Systems Inc, Maryland), 1 % (v/v) Penicillin-Streptomycin and 1 µg/ml doxycycline. The medium was changed every 1-2 days along with a high glucose harvest as described in the manufacturer's protocol. Medium collected from the bioreactor was filtered using a 0.2 µm Nalgene single use bottle top filter (ThermoFisher Scientific) then centrifuged for 5 minutes at 355 x *g*. The supernatant containing the secreted protein was stored at -20ºC.

2.4. Protein purification

2.4.1. HexA purification

A two-step purification procedure was used to isolate HexA. A gravity column containing nickel-nitrilotriacetic acid (Nickel-NTA) resin (Qiagen) was equilibrated at room temperature with 10 column volumes of 10 mM phosphate buffer (5.78 mM $Na_2HPO_4 \bullet 7H_20$, 4.22 mM $NaH_2PO_4 \bullet H_20$; pH 7). The equilibrated resin was added to a 50 ml tube (Fisher Scientific) containing thawed medium from the FiberCell bioreactor and the mixture was incubated via end-over-end rotation for 1 hour at 4ºC. The slurry pipetted into the column and the media was eluted. The resin was washed with 10 column volumes of 10 mM phosphate buffer. The resin was incubated with 5 column volumes of 10 mM phosphate buffer supplemented with 250 mM imidazole (pH 7.0) for 20 minutes. The elution fractions containing HexA were pooled together and dialyzed overnight at 4°C against tris-buffered saline (50 mM Tris-HCl, 150 mM NaCl; pH 7.4). The dialyzed protein was subsequently run through a column containing anti-FLAG affinity resin (Sigma-Aldrich) as per the manufacturer's protocol.

2.4.2. HexM-ApoB and HexM-ApoE purification

Medium collected from the FiberCell bioreactor was thawed in a water bath at 37ºC. Purifications were done at room temperature using a gravity column loaded with Nickel-NTA Superflow resin (Qiagen). The resin was equilibrated with 10 column volumes of Bis-Tris buffer (10 mM Bis-Tris, 100 mM NaCl; pH 6). The resin was then incubated with medium from the FiberCell via end-over-end rotation for 1 hour at 4ºC. Afterwards, the cell culture medium was run through the gravity column and the resin was washed with 10 column volumes of Bis-Tris buffer. The Nickel-NTA resin was incubated with 5 column volumes of Bis-Tris buffer supplemented with 250 mM of imidazole (pH 7.5) for 20 minutes, after which the proteins were eluted with a slow drip. The elution fractions collected from the Nickel-NTA column were pooled together and dialyzed overnight at 4ºC against Bis-Tris buffer to remove excess imidazole.

2.4.3. HexM-myc purification

DMEM (Gibco) supplemented with 10% CDM-HD serum replacement powder (FiberCell Systems Inc, Maryland), 1 % (v/v) Penicillin-Streptomycin and 1 µg/ml doxycycline was collected from HEK293T-ABKO-HexM-myc cells growing in T75 flasks (ThermoFisher Scientific). The medium was run through a 0.2 µm Nalgene single use bottle top filter (ThermoFisher Scientific) then centrifuged for 5 minutes at 355 x *g*. The volume of medium was concentrated from 150-300 ml to approximately 20 ml using an Amicon stirred cell (MilliporeSigma). The protein was then purified as described above for HexM-ApoB and HexM-ApoE.

2.5. Determining protein concentrations

Concentrations (mg/ml) of the purified β-hexosaminidase proteins were verified using a NanoDrop One (ThermoFisher). The concentrations were determined by measuring the absorbance at $\lambda = 280$ nm, taking into account the extinction coefficient (ε) and the molecular weight (MW) of each protein (Table 2.3). The ProtParam tool from ExPASy Bioinformatics Resource Portal was used to calculate the extinction coefficients and theoretical molecular weights of each enzyme.

Table 2.3. Molecular weights and extinction coefficients used to determine protein concentrations.

Protein	Molecular weight (Da)	ε_{280} ($M^{-1}cm^{-1}$)
HexA	124,780	233,510
HexM-ApoB	137,380	128,730
HexM-ApoE	133,780	127,240
HexM-myc	126,320	127,240
HexM	121,380	254,480
phosHexM	121,380	254,480

2.6. SDS-PAGE and western blots

Proteins were denatured by incubating a 1:1 ratio of samples and Laemmli buffer at 98°C for 10 minutes. Afterwards, the samples were subjected to SDS-PAGE on a 12% bis-acrylamide gel. Protein bands were visualized by staining with Coomassie brilliant blue (Fisher Scientific).

For the western blots, purified proteins (100 ng) were loaded onto SDS-PAGE gels with 12% acrylamide. After gel electrophoresis was complete, the SDS-PAGE gels and nitrocellulose membranes (Pall Corporation, Pensacola, Florida) were equilibrated in western blot transfer buffer (25 mM Tris, 192 mM glycine, 20% [v/v] methanol; pH 8.3) for 15 minutes at room temperature. The proteins were then transferred to membranes using a semi-dry transfer system (Bio-Rad). Proteins were transferred for 25 minutes with 25 volts and 1 ampere. Membranes

were then incubated in skim milk blocking buffer (5% [w/v] skim milk powder, 20 mM Tris, 150 mM NaCl, 0.1% [v/v] Tween 20; pH 7.6) for 1 hour at room temperature with gentle shaking. Membranes were incubated in a 1:1000 dilution of rabbit polyclonal anti-HexA Ab (Abcam, Cat. #: ab91624) followed by a 1:3000 dilution of goat-anti-rabbit IgG (H+L)-HRP Conjugate Ab (Bio-Rad, Cat #: 1706515) for the anti-HexA western blots. The anti-HexB western blots were done by incubating the membrane in 1:1000 a dilution of rabbit monoclonal anti-HexB Ab (Abcam, Cat. #: ab140649) followed by a 1:3000 dilution of the goat-anti-rabbit IgG (H+L)-HRP Conjugate Ab. A 1:1000 dilution of monoclonal mouse anti-FLAG M2 Ab (Sigma-Aldrich, Cat #: F3165) followed by a 1:5000 dilution of goat-anti-mouse IgG (H+L)-HRP Conjugate Ab (Bio-Rad, Cat #: 1706516) was used for the anti-FLAG blots. For the anti-myc western blots, the membranes were incubated in a 1:667 dilution of c-myc 9E10 monoclonal Ab (Invitrogen, Cat. #: MA1-980) followed by a 1:5000 dilution of goat-anti-mouse IgG (H+L)-HRP Conjugate Ab. All antibodies were diluted in skim milk blocking buffer. Membranes were incubated with the primary antibody overnight at 4°C, then washed in TBST (20 mM Tris, 150 mM NaCl, 0.1% [v/v] Tween 20; pH 7.6) for 15 minutes, three times. Membranes were subsequently incubated in the secondary antibody for 1 hour at room temperature which was followed by three washes in TBST for 15 minutes each. The chemiluminescent Immobilon Forte Western HRP Substrate (Millipore) was added to the menbranes and bands were visualized using a ChemiDoc Imaging System (Bio-Rad).

2.7. HexA crystallization trials

HexA was purified by Nickel-NTA resin followed by anti-FLAG affinity resin as described above. Elution fractions containing protein from the anti-FLAG column were pooled

and a 50 MWCO centrifugal filter was used to concentrate HexA to 7.5 mg/ml. JBScreen JCSG++ HTS (Jena Bioscience) was used to screen for crystals, which were grown by the sitting-drop vapour diffusion method using a Crystal Gryphon robot (Art Robbins Instruments) (Stewart & Mueller-Dieckmann, 2014). The protein was mixed in a 1:1 ratio with the well solution (0.5 µl protein and 0.5 µl solution). Optimal crystals appeared in 20% polyethylene glycol (PEG) 3350 (w/v), 200 mM sodium thiocyanate (pH 6.9), which appeared approximately 5 days after incubation at 20°C.

Crystal optimization was attempted using the hanging-drop vapour diffusion method (Stewart & Mueller-Dieckmann, 2014). In a 24 well plate, 1000 µl varying crystallization conditions (19-21% [w/v] PEG 3350 and 0.15-0.25 mM sodium thiocyanate) were added to each reservoir. Two drops were added onto the top of a clear plastic cover slip. Each drop contained 1 µl crystallization condition from a specific well and either 0.5 µl or 1 µl HexA. The cover slip was inverted and sealed to the well of the 24 well plate using a small amount of Vaseline. The plate was then incubated at 20°C. Optimization of crystallization conditions was attempted with HexA concentrations between 4 and 11 mg/ml.

2.8. Determining the melting temperatures of β-hexosaminidase proteins

The melting temperatures (T_m) of HexM-ApoB, HexM-ApoE and HexM-myc were determined by analyzing thermal unfolding using the Prometheus NT.48 (NanoTemper). Each enzyme (HexM-ApoB = 1.041 mg/ml and HexM-ApoE = 1.094 mg/ml) in PBS (pH 7.2) was loaded into capillary tubes in triplicate. The samples were heated to 20°C and the temperature was increased to 95°C at a rate of 1°C per minute. The fluorescence intensity was recorded at 330 nm and 350 nm. The first derivative of the 350/330 ratio was plotted against temperature and

the T_m was determined by the point of inflection. The reported T_m of each enzyme is the average of each replicate.

2.9. Dynamic light scattering analysis of the HexM fusion proteins

Purified HexM-ApoB (1.041 mg/ml) and HexM-ApoE (1.094 mg/ml) in 10 mM Bis-Tris, 100 mM NaCl (pH 6.0) were aliquoted into a low-volume quartz cuvette ZEN2112 (Hellma Analytics). A volume of 40 µl was added to each cuvette and the samples were analyzed with a Zetasizer Nano S (Malvern Instruments Ltd) at 25°C (material refractive index = 1.25, material absorption = 0.001).

2.10. MUGS and MUG activity assays

The activity of the recombinantly produced β-hexosaminidase enzymes was assessed using a previously established kinetic assay (Hou *et al*., 1996; Sharma *et al.*, 2001; Shulman *et al*., 1980). The activity assays were performed in opaque polystyrene 96-well plates (Corning, New York USA). Enzymes were aliquoted into each well with a final concentration of 100 pM. One of the synthetic substrates, MUG or MUGS, was added to the wells with a final concentration between 0.09 mM to 4 mM. Citrate-phosphate buffer (82.8 mM Na_2HPO_4, 58.6 mM citric acid; pH 4.2) supplemented with 0.5% (w/v) bovine serum albumin was used to bring the total volume of each well to 100 µl. The assays were performed with three technical replicates and were run for 30-60 minutes at 37°C in a SpectraMax iD5 plate reader (Molecular Devices) by monitoring the fluorescence ($\lambda_{excitation}$: 365 nm, $\lambda_{emission}$: 450 nm). The data was collected using SoftMax Pro software.

One of the challenges of monitoring the activity of β-hexosaminidase isoforms with fluorescence is the inner-filter effects due to significant substrate absorbance. To overcome this, the product concentrations were calculated using the degree of conversion (DOC) formula described by Shulman *et al*. (1980):

$$DOC = \frac{total\ emission\ (\mathrm{t}) - substrate\ emission\ (0)}{substrate\ emission\ (0) \times\ 120} \times 100\%$$

Total emission (t) represents the fluorescence intensity measured at a given time, while substrate emission (0) is the initial fluorescence intensity measured without any enzyme present. A fluorogenic product called 4-methylumbelliferone (4-MU) is released when MUGS or MUG is cleaved by β-hexosaminidase. The DOC was then used to calculate the concentration of 4-MU formed using the following formula:

$$[product\ (t)] = [DOC][substrate\ (0)]$$

The quantity of 4-MU formed at a given time is indicated by product(t) and the initial concentration of MUG or MUGS is denoted by substrate (0). Microsoft Excel was used to plot product (t) against time. Lines of best fit were added to the plot to determine product formation rates. Normalized reaction rates (NRR) were calculated according to the formula below and GraphPad Prism 8 was used to fit the Michaelis Menten equation to the data.

$$NRR = \frac{product\ formation\ rate}{total\ enzyme\ concentration}$$

2.11. HexA and HexM two-week stability assay

HexM was purified by Graeme Benzie, a former graduate student in the laboratory. HexA and HexM were diluted to a concentration of 1 nM using 10 mM phosphate buffer (5.78 mM $Na_2HPO_4 \bullet 7H_20$, 4.22 mM $NaH_2PO_4 \bullet H_20$; pH 5.5 and pH 7). The two different pH values were chosen to reflect those of the lysosome and blood. The enzymes were incubated at 37ºC for 14 days. Every second day, an aliquot of each sample was collected and stored at -20ºC. Kinetic assays were carried out as described in the previous section using the synthetic substrate MUGS to assess the activity of each enzyme.

2.12. *In vitro* BBB model with the HexM fusion proteins

HexM-ApoB, HexM-ApoE and HexM-myc were purified using Nickel-NTA affinity chromatography as described above. Afterwards, each enzyme was dialyzed overnight at 4ºC against PBS (pH 7.2). The purified protein samples (HexM-ApoB = 2.087 mg/ml, HexM-ApoE = 1.977 mg/ml and HexM-myc = 2.131 mg/ml) were frozen at -20°C and sent to the National Research Council (NRC) of Canada (Ottawa, Ontario) on dry ice.

An established *in vitro* BBB model with BMECs derived from human amniotic fluid pluripotent stem cells was used (Ribecco-Lutkiewicz *et al*., 2018) to assess the ability of the HexM-fusion proteins to cross the barrier. All work conducted with the BBB model was performed by Eric Brunette and Dr. Willard Costain at the NRC. A 2X input containing 2.5 µM enzyme (HexM-ApoB, HexM-ApoE or HexM-myc), 2.5 µM FC5 and 2.5 µM A20.1 was prepared in transport buffer (Hanks' balanced salt solution [HBSS], 5 mM $MgCl_2$, 10 mM 4-(2-hydroxyethyl)-1-piperazineethanethanesulfonic acid [HEPES]; pH 7.4). FC5 is a llama single domain antibody capable of transcytosis across human brain endothelial cells (Abulrob *et al.*,

2005), which was used as a positive control for the BBB model. As a negative control, A20.1 was used. A20.1 is a non-transmigrating antibody raised against *Clostridium difficile* toxin A (Ribecco-Lutkiewicz *et al*., 2018; Webster *et al.*, 2016). A monolayer of BMECs were grown on Transwell inserts with 1 ml endothelial media (serum-free endothelium media with 1% FBS and 20 ng/ml basic fibroblast growth factor [bFGF]) on top of the inserts. The inserts were transferred to a new plate with 2 ml transport buffer on the bottom. Then, 500 µl medium was removed from the top of the insert and replaced with 500 µl 2X input (final protein concentration was 1.25 µM). The cells were incubated at 37ºC for 90 minutes. The Transwell BBB transport assay was run in triplicate for each enzyme. Samples from the top and bottom of the inserts, as well as the 2X inputs were sent to the University of Manitoba on dry ice then stored at -20ºC.

MUGS activity assays were performed on the 2X inputs, on the samples from the top and the samples from the bottom of the insert. The 2X inputs were diluted to 1 nM using citrate-phosphate buffer. As the concentrations of protein in the samples taken from the top and bottom of the Transwell insert were unknown, hypothetical concentrations of 1.25 µM and 0.625 µM were respectively assigned to them. These hypothetical values were chosen based on what the protein concentration would have been if 100% of the enzyme remained in the top layer or if 100% of the enzyme was transported across the insert. The samples were diluted to 1 nM using the assigned concentration values. MUGS activity assays were continued as described above. For western blots, 10 µl sample was subjected to SDS-PAGE on a 12% bis-acrylamide gel and the procedure was continued as described above.

2.13. Statistical analysis

All data points on kinetic plots are the mean ± standard deviation, calculated using GraphPad Prism 8. For each experiment, three technical replicates were used. For the HexA and HexM two-week stability assay, the data was analyzed using a paired two-tailed t-test.

3. Results

3.1. Expression and purification of β-hexosaminidase enzymes

3.1.1. Heterodimeric HexA is isolated in a two-step purification procedure

The first aim of this thesis was to develop a method for recombinant HexA production. HexA has traditionally been purified from human placenta and recombinant protein production provides us with a constant source of HexA for structural and kinetic studies. HEK293T cells (HEK293T-ABKO) lacking endogenous *HEXA* and *HEXB* genes (Tropak *et al*., 2016) were transfected using the *piggyBac* transposon-based mammalian cell expression system (Li *et al*., 2013). Mammalian cells were selected for recombinant protein production, rather than bacteria such as *E. coli*, due to the organelles needed for the post-translational modifications required to produce functional HexA. Plasmids encoding *HEXA* with a C-terminal FLAG-tag and *HEXB* with a C-terminal His_6 tag were transfected into HEK293T-ABKO in a 5:3 ratio to favour HexA (αβ-subunits) production, rather than the more stable HexB (ββ-subunits). The resulting HEX293T-ABKO-HexA cells secreted HexA directly into the cell culture media with addition of doxycycline (**Fig 3.1a**), an inducer for protein expression in the *piggyBac* system .

HexA was isolated from cell culture medium collected from a FiberCell Systems hollow fiber bioreactor in a two-step purification procedure (**Fig 3.2**). Media amassed from HEK293T-

ABKO-HexA cells was run through a column containing Nickel-NTA affinity resin, capturing HexA and HexB, whilst removing any possible HexS (αα-subunits) and other unwanted proteins or nucleic acids. Subsequently, the eluted protein (HexA and HexB) was loaded on a column containing anti-FLAG affinity resin, effectively removing any HexB from the sample. Purity of the protein samples collected from the Nickel-NTA and the anti-FLAG columns was verified by SDS-PAGE (**Fig 3.1b**) and by western blots (**Fig 3.3**).

A yield of ~3 mg of HexM per 20 ml FiberCell medium extraction was reported by Graeme Benzie, a former graduate student in the laboratory. This value was determined after purification using Nickel-NTA resin and size exclusion chromatography. For the HEK293T-ABKO-HexA cells, the protein yield after Nickel-NTA affinity chromatography (HexA and HexB isoforms) was ~2.55 mg per 20 ml medium extraction from the FiberCell. Given that all potential HexS was removed from the sample, it was expected that enzyme yield would be lower than for the homodimeric HexM. Further, after the removal of HexB using the anti-FLAG resin, the HexA yield was ~0.4 mg for a 20 ml extraction. Very little protein precipitation was observed throughout the HexA purification procedure.

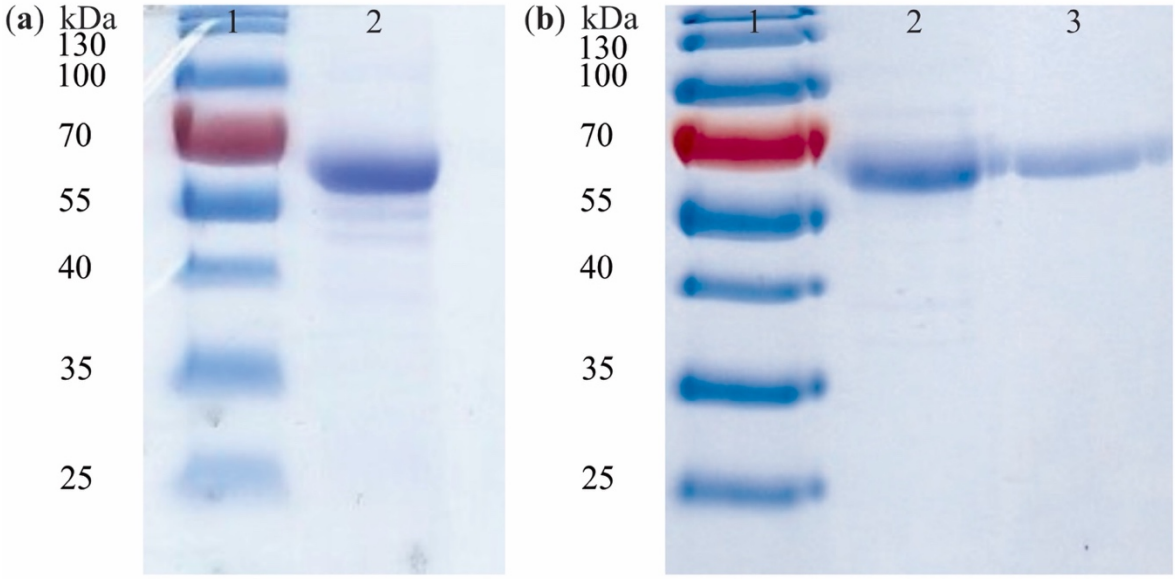

Figure 3.1. Isolation of HexA throughout the two-step purification procedure. (**a**) Medium from the FiberCell was subjected to SDS-PAGE to ensure the HEK293T-ABKO-HexA cells were expressing and secreting HexA (~60 kDa subunits). Lane 1 is PageRuler^{TM} Prestained Protein Ladder, 10 to 180 kDa (ThermoFisher Scientific). Lane 2 is 10 µl 1:100 dilution of DMEM 10% CDM-HD, 1 % (v/v) Penicillin-Streptomycin and 1 µg/ml doxycycline collected from the FiberCell bioreactor, containing HexA (αβ-subunits), HexB (ββ-subunits) and HexS (αα-subunits). (**b**) SDS-PAGE analysis of HexA purity (subunits are ~60 kDa). Lane 1 is PageRuler^{TM} Prestained Protein Ladder, 10 to 180 kDa (ThermoFisher Scientific). Lane 2 is the elution fraction from the Ni-NTA column (3270 ng), capturing HexA (αβ-subunits) and HexB (ββ-subunits). Lane 3 is HexA from an elution fraction from the anti-FLAG affinity resin (1980 ng). The gels both contained 12% acrylamide and were stained with Coomassie brilliant blue.

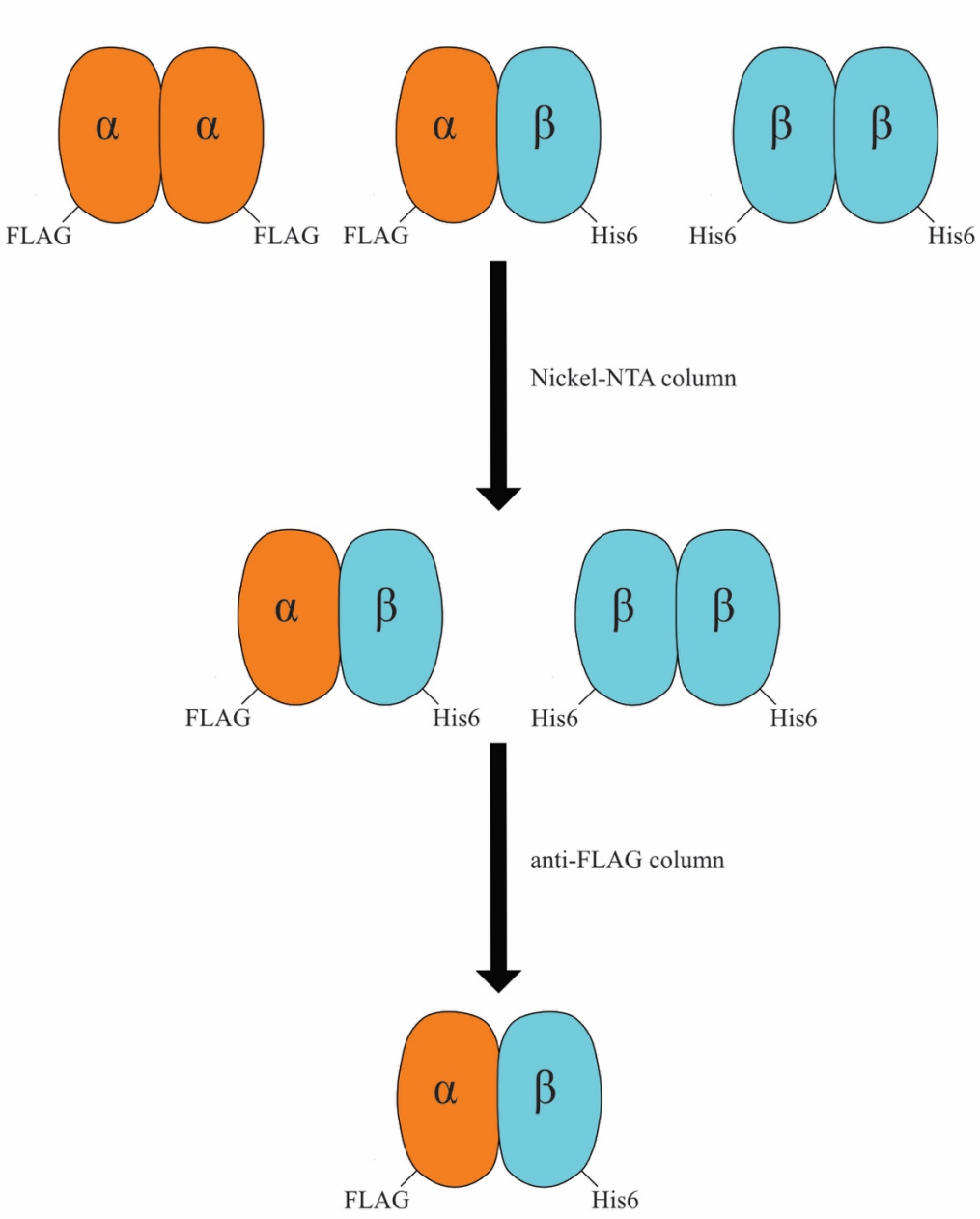

Figure 3.2. HexA two-step purification schematic. Cell culture medium collected from the FiberCell was run through a column containing Nickel-NTA resin, removing any potential HexS (αα-subunits), as the α-subunit lacks a His_6 tag. The eluted protein was subsequently dialized overnight and run through a column containing anti-FLAG immunoaffinity resin. HexB (ββ-subunits) lacks an anti-FLAG tag and therefore did not bind to the column, sucessfully isolating HexA (αβ-subunits).

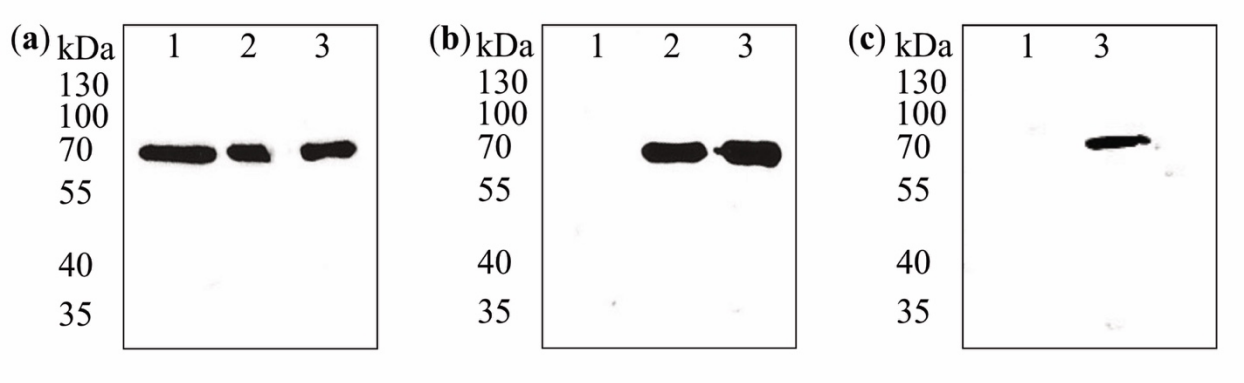

Figure 3.3. HexA purification. Western blots using an (**a**) anti-HexA antibody, an (**b**) anti-HexB antibody and an (**c**) anti-FLAG antibody. Lane 1 contains 100 ng of purified HexM (μμ-subunits). Lane 2 contains 100 ng of HexA (αβ-subunits) and HexB (ββ-subunits) isoforms eluted from the Nickel-NTA column. Lane 3 contains 100 ng of HexA eluted from the anti-FLAG column.

3.1.2. HEK293T-ABKO-HexA-G269S cells express and secrete HexA G269S into media

HEK293T-ABKO cells were transfected with a plasmid encoding the αG269S variant of *HEXA* with a C-terminal FLAG-tag and the plasmid encoding *HEXB* with a C-terminal His_6 tag in a 5:3 ratio to favour the formation of the heterodimeric enzyme. To generate the HEK293T-ABKO-HexA-G269S cell line, the transfecting agent was changed from PEI (used to generate HEK293T-ABKO) to Lipofectamine 2000. This adjustment was made because Lipofectamine 2000 has a slightly higher transfection efficiency in HEK293T cells (Dang *et al.*, 2011) and the procedure was less time consuming than with PEI. Lipofectamine 2000 was subsequently used for all other transfections. Medium collected from the transfected cells was used for the initial assessment of HexA G269S expression by western blot (**Fig 3.4**). A pronounced band appeared in the lane containing medium collected from the HEK293T-ABKO-HexA-G269S cells, while none appeared in the lane loaded with media from HEK293T-ABKO cells. The western blot with medium from the HEK293T-ABKO cells was used to ensure that the band observed from the HEK293T-ABKO-HexA-G269S cell media was not solely due to proteins in the FBS.

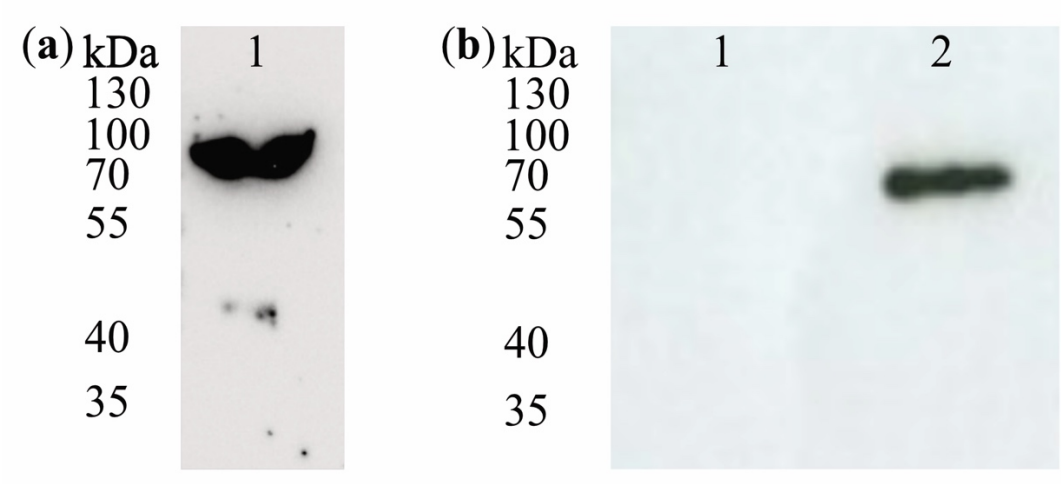

Figure 3.4. Initial assessment of HexA G269S expression. (**a**) Western blot of medium in which the HEK293T-ABKO-HexA-G269S cell line was growing. Lane 1 contains 4 µl of DMEM 10% FBS, 1 % (v/v) Penicillin-Streptomycin and 1 µg/ml doxycycline media collected from HEK293T-ABKO-HexA-G269S cells. (**b**) Western blot of media in which HEK293T-ABKO cells were growing. Lane 1 contains 4 µl DMEM 10% FBS, 1 % (v/v) Penicillin-Streptomycin and 1 µg/ml doxycycline collected from a flask of HEK293T-ABKO cells. Lane 2 contains 100 ng of purified HexA used as a positive control. An anti-HexA antibody (Abcam, Cat. #: ab91624) was used to visualize bands on the blots.

3.1.3. HexM-ApoB, HexM-ApoE and HexM-myc can be purified to homogeneity from transfected cells

The second aim of this thesis was to produce HexM-ApoB and HexM-ApoE fusion proteins. HEK293T-ABKO cells were transfected with plasmids encoding *HEXM* and the required C-terminal tags. HexM-ApoB, HexM-ApoE and HexM-myc were isolated directly from cell culture media. The first attempts at purifying the enzymes were by Nickel-NTA chromatography followed by size exclusion chromatography. Multiple peaks were visible on the chromatogram when either HexM-ApoB or HexM-ApoE were run through the size exclusion column. Each chromatogram also lacked a major peak where the proteins would normally elute based on their size (**Fig. 3.5**). HexM-ApoB and HexM-ApoE should have eluted from the column at ~72 ml; however, very little enzyme eluted at that volume, which suggested the

modified HexM proteins were aggregating and possibly unstable. In contrast, HexM-myc was eluted from the size exclusion column in one large peek containing the enzyme (**Fig. 3.6**).

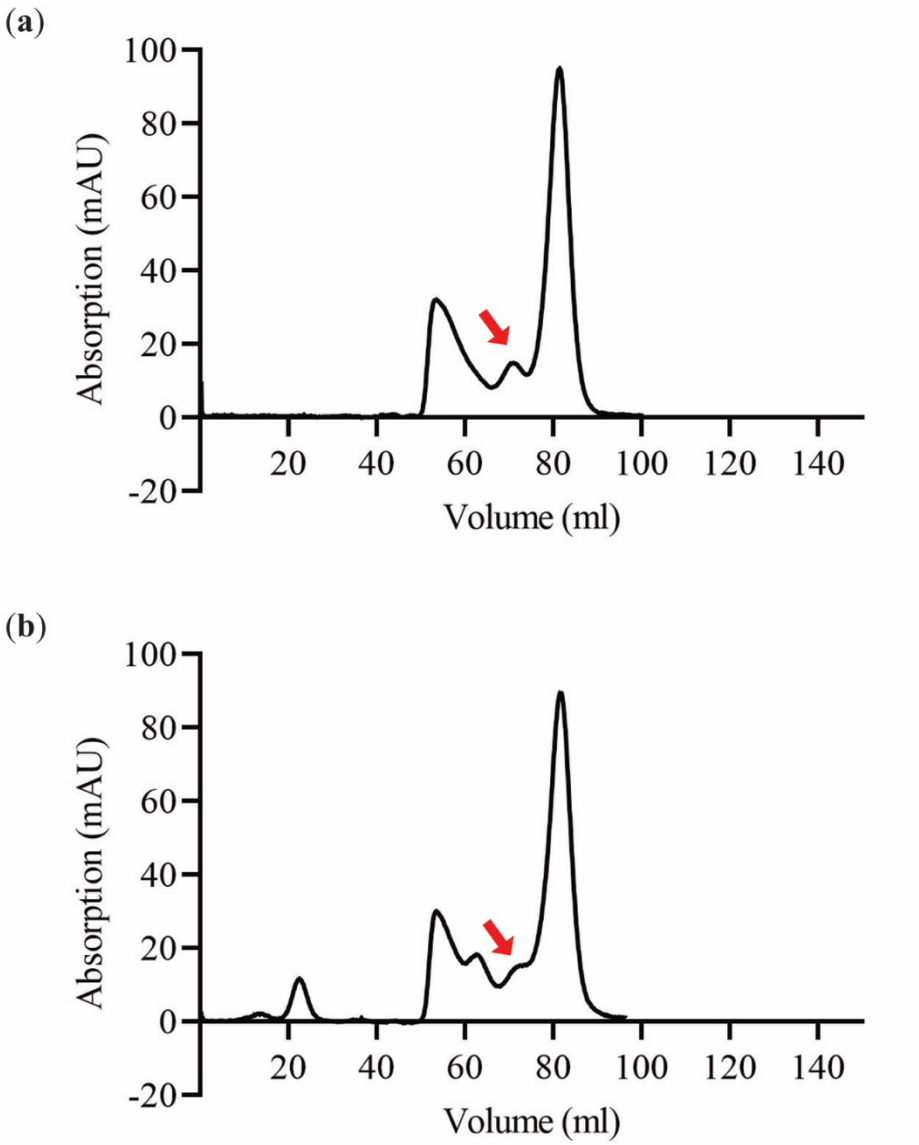

Figure 3.5. Gel filtration column run of the HexM fusion proteins. Proteins were purified using Nickel-NTA resin and dialyzed overnight. Proteins were concentrated using a 30 kDa molecular weight cut-off centrifugal filter then loaded onto a HiLoad 16/600 Superdex 200 (GE Life Sciences) gel filtration column. (**a**) Chromatogram of HexM-ApoB. (**b**) Chromatogram of HexM-ApoE. For both enzymes, ~1.2 mg of protein was loaded onto the size exclusion column. Respectively, HexM-ApoB and HexM-ApoE are indicated by the red arrow.

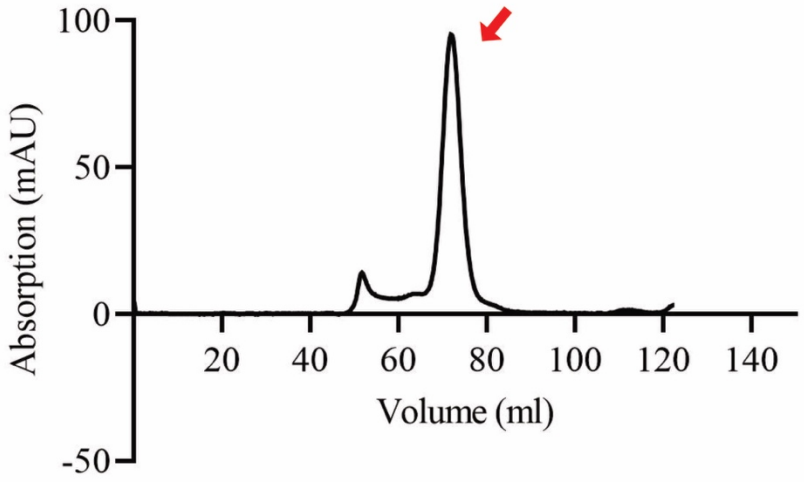

Figure 3.6. Chromatogram of HexM-myc on a gel filtration column. HexM-myc was purified using Nickel-NTA affinity resin. The protein was dialyzed overnight and concentrated using a 30 kDa molecular weight cut-off centrifugal filter. A total of ~1.2 mg of protein was loaded onto a HiLoad 16/600 Superdex 200 (GE Life Sciences) gel filtration column. HexM-myc is indicated by the red arrow.

To assess the presence and the purity of HexM-ApoB, HexM-ApoE and HexM-myc after Nickel-NTA affinity chromatography, without the final gel-filtration polishing step, SDS-PAGE (**Fig 3.7**) and western blots (**Fig 3.8**) were done. These demonstrated that both enzymes could successfully be isolated from cell culture media by Nickel-NTA.

The HexM-ApoB and HexM-ApoE protein yields were ~3 mg per 20 ml media extraction from the FiberCell bioreactor growing HEK293T-ABKO-HexM-ApoB and HEK293T-ABKO-HexM-ApoE cells, respectively. As HexM-ApoB and HexM-ApoE are homodimers, it was expected that these values would be similar to the yield of ~3 mg per 20 ml extraction reported for HexM by Graeme Benzie. From ~500 ml of media collected from T75 flasks, the yield of HexM-myc was ~1.5 mg. A larger volume of medium was required to obtain this quantity of HexM-myc as cell density is much higher in the FiberCell bioreactor than in tissue culture flasks (FiberCell Systems, 2017).

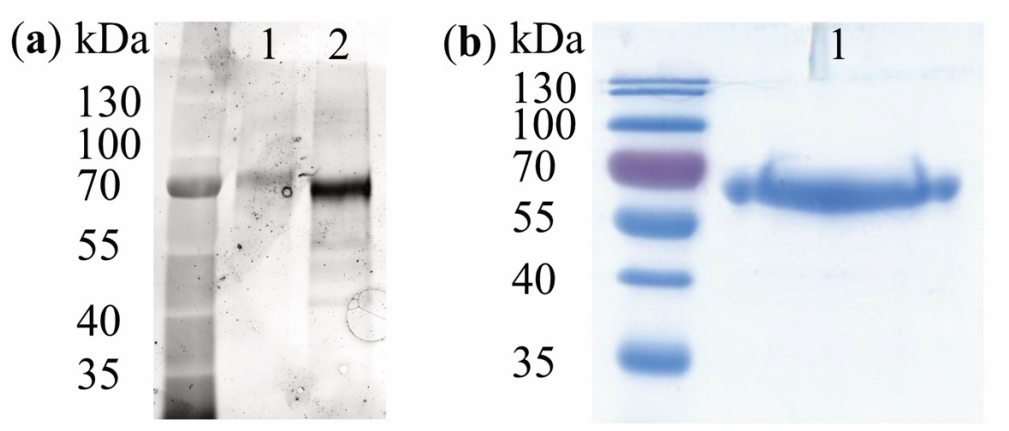

Figure 3.7. Purification of the HexM fusion proteins after Nickel-NTA. (**a**) Isolation of HexM-ApoB and HexM-ApoE. Lane 1 contains HexM-ApoB (1930 ng). Lane 2 contains HexM-ApoE (4760 ng). The samples were run on a 10% mini-PROTEAN TGX stain-free precast gel and imaged using a ChemiDoc Imaging System (Bio-Rad). The stain-free gel has a comparable sensisitivity to Coomassie brilliant blue. (**b**) Isolation of HexM-myc. Lane 1 contains approximately 1800 ng of purified HexM-myc. The sample was run on a 12% acrylamide gel and stained with Coomassie brilliant blue.

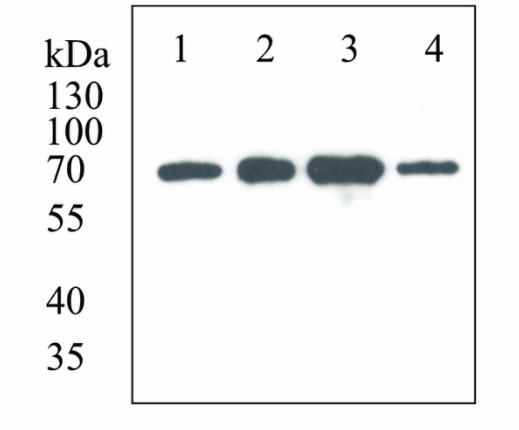

Figure 3.8. Confirmation of the presence of HexM-ApoB, HexM-ApoE and HexM-myc after Nickel-NTA. Western blot using an anti-HexA antibody. Lane 1 contains purified HexM-ApoB. Lane 2 was loaded with HexM-ApoE. Lane 3 contains with HexM-myc and lane 4 contains recombinant HexA. Each well was loaded with 100 ng of protein.

3.1.4. HexM-ApoB and HexM-ApoE are stable in a wide variety of buffer conditions

As it was surprising that HexM-ApoB and HexM-ApoE were not eluted from the gel-filtration column in a single peak, the stability of the enzymes was assessed in a variety of

solutions with a range of pH values in a protein solubility and stability screen (Hampton Research). This was done to ensure that the enzymes were stable in the buffer used. HexM-ApoB and HexM-ApoE were stable in most conditions, including the Bis-Tris buffer (10 mM Bis-Tris, 100 mM NaCl; pH 6) used with the Nickel-NTA resin and during the gel-filtration chromatography attempts.

The enzymes were then analyzed by dynamic light scattering (DLS) to determine if there was any protein aggregation after Nickel-NTA chromatography, which could explain the multiple peaks observed on the chromatograms from the size exclusion column. DLS analysis indicated that both HexM-ApoB and HexM-ApoE were for the most part monodisperse in Bis-Tris buffer (**Fig 3.9** and **Fig 3.10**). Based on the intensity distribution, HexM-ApoB had an average diameter of 15.02 nm, while some aggregates with an 87.95 nm diameter were observed (**Fig 3.9a**). However, the aggregates were only represented by a small peak on the size distribution by volume graph indicating that while there was some aggregation, it was only present in small concentrations (**Fig 3.9b**). Therefore HexM-ApoB was the predominant protein within the solution.

Similar trends were observed for HexM-ApoE. When the particle sizes were determined by intensity distribution, HexM-ApoE had an average diameter of 15.90 nm and aggregates with a diameter of 77.63 nm and 301.9 nm were observed (**Fig 3.10a**). The volume weighted distribution indicates that HexM-ApoE was the main protein found in the solution and while there were some aggregates, they were found in low concentrations (**Fig. 3.10b**).

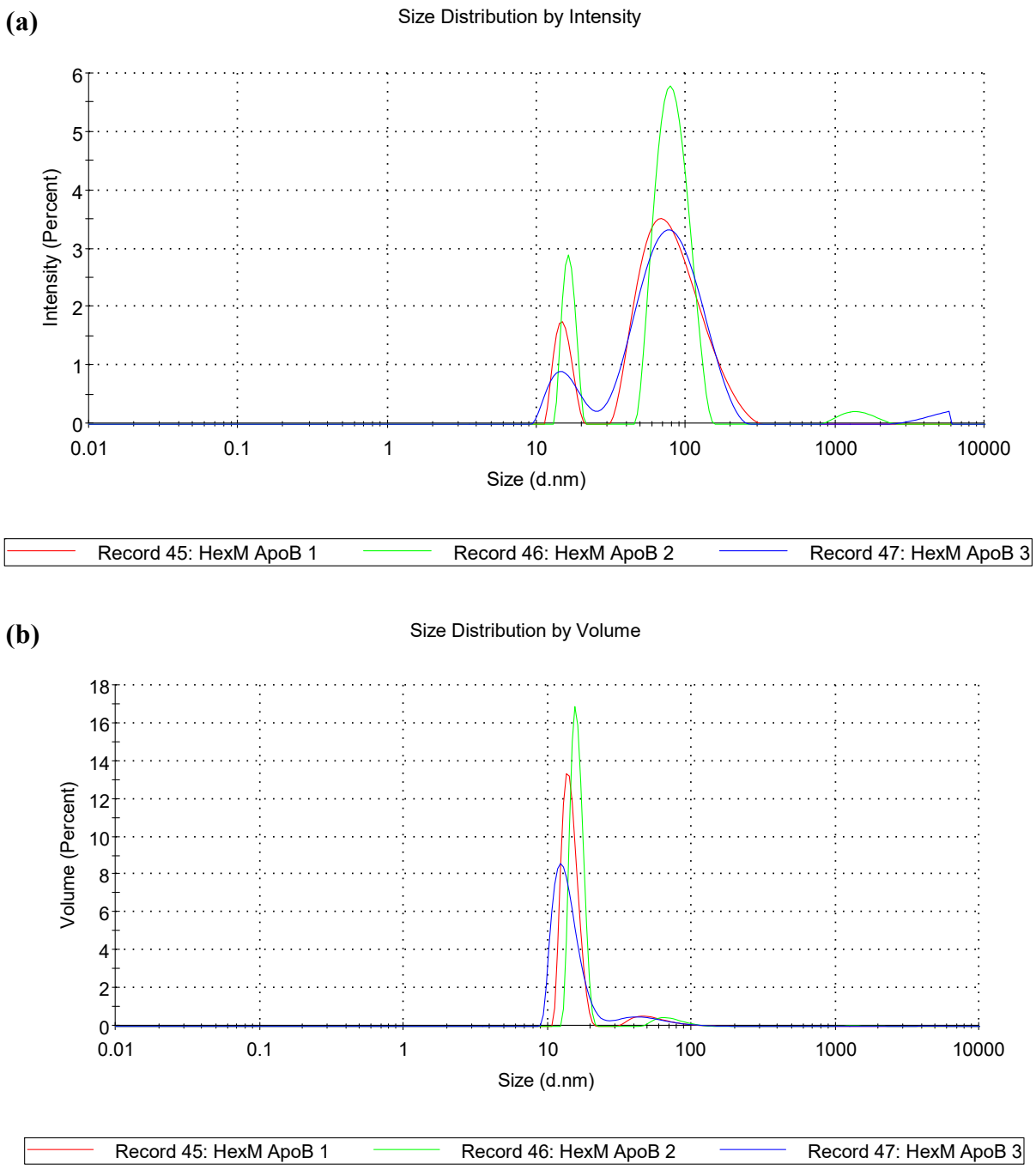

Figure 3.9. Dynamic light scattering analysis of HexM-ApoB for aggregation after Nickel-NTA purification. A 1.041 mg/ml concentration of HexM-ApoB in 10 mM Bis-Tris, 100 mM NaCl (pH 6) was used for DLS analysis. Measurements were recorded at 25°C and in triplicate. (**a**) The size distribution of HexM-ApoB measured by intensity. (**b**) The size distribution of HexM-ApoB measured by volume.

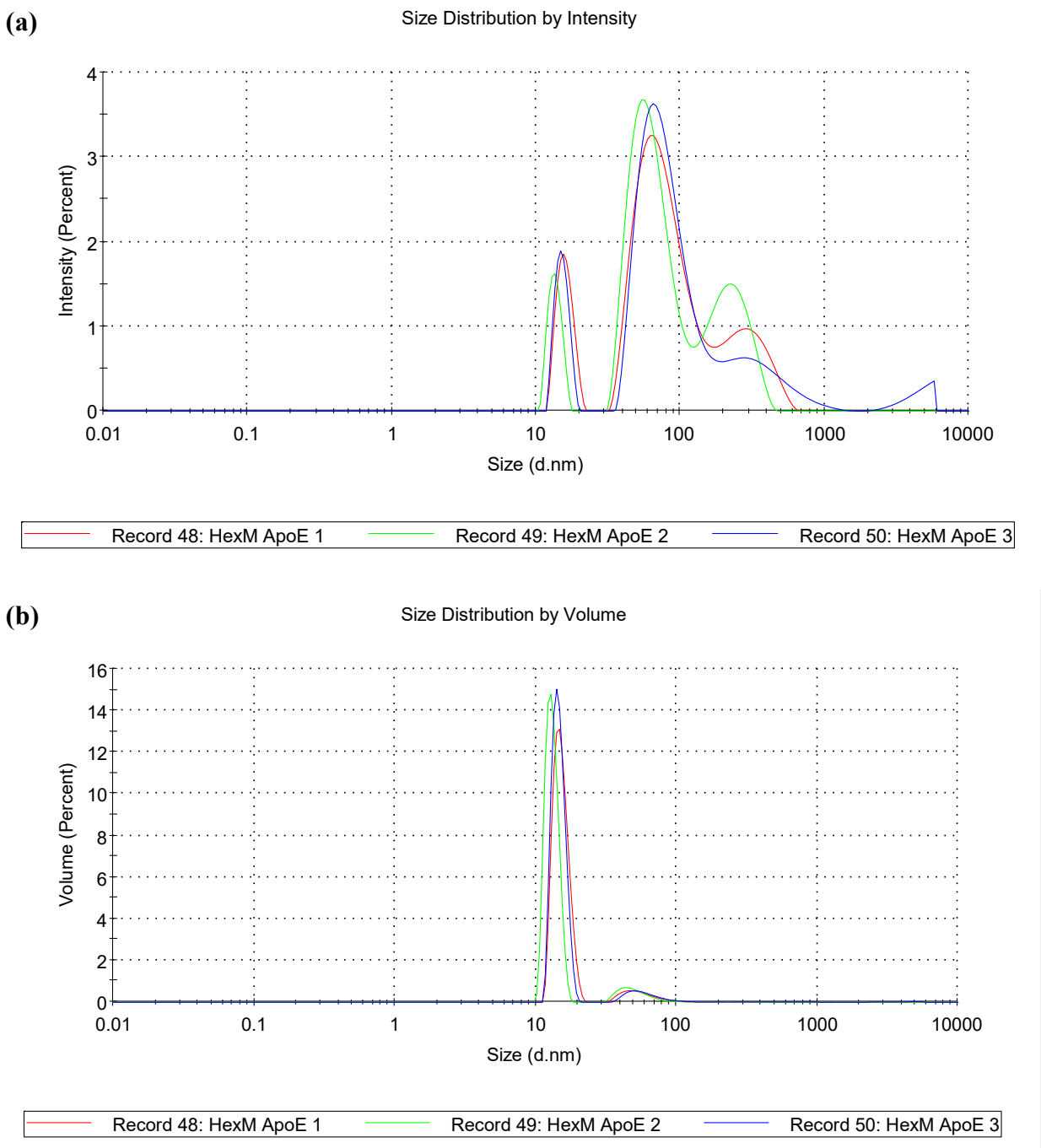

Figure 3.10. Dynamic light scattering analysis of HexM-ApoE for aggregation after Nickel-NTA purification. A 1.094 mg/ml concentration of HexM-ApoE in 10 mM Bis-Tris, 100 mM NaCl (pH 6) was used for analysis. DLS measurements were recorded at 25°C and in triplicate. (**a**) The size distribution of HexM-ApoE measured by intensity. (**b**) The size distribution of HexM-ApoE measured by volume.

3.2. HexA crystallization trials

3.2.1. HexA forms crystals that can diffract

Initially, HexA crystals were obtained using commercial crystallization screens. Crystals formed in 5 different conditions; however, the best ones were observed in 20% PEG 3350, 200 mM sodium thiocyanate, pH 6.9 (**Fig 3.11a**), which appeared approximately 5 days after incubation at 20°C. Attempts to optimize the crystals were made using the hanging-drop vapour diffusion method and by changing the protein concentration (between 4-11 mg/ml) as well as the crystallization conditions (19-21% PEG 3350, 0.15-0.25 mM sodium thiocyanate). None of the crystals that formed during the optimization attempts were much bigger or different in shape than the initial crystals. A crystal from the initial crystallization screen was mounted on the X-ray diffractometer and a diffraction pattern with a resolution of 4.02 Å was obtained (**Fig 3.11b**). Similarly, a previous report indicated that the majority of attempts to crystallize lysosomal HexA from human placenta resulted in a diffraction of approximately 4 Å (Lemieux *et al.*, 2006).

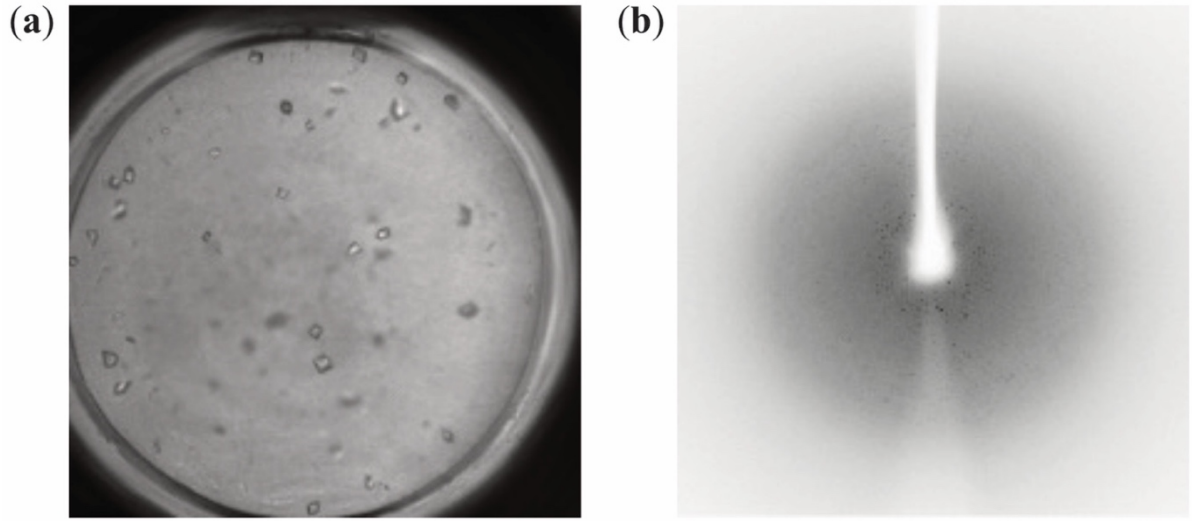

Figure 3.11. Initial HexA crystallization trials. (**a**) Crystals from purified HexA (7.5 mg/ml) produced by sitting drop method. The crystallization condition was 20% PEG 3350, 200 mM sodium thiocyanate (pH 6.9). Brightfield image of crystals were taken with a UVEX-M microscope (JanSci) at 10x magnification. (**b**) Diffraction pattern of a HexA crystal with a resolution of 4.02 Å.

3.3. HexA kinetic activity

3.3.1. Michaelis-Menten comparison of recombinant HexA and HexM

To ensure that the recombinantly produced HexA behaved similarly to lysosomal HexA, which is typically purified from human placenta, kinetic assays were used to assess enzyme activity. Recombinant HexA was evaluated using the synthetic substrates MUG and MUGS, and its activity was compared to that of HexM (**Fig 3.12**). The active sites of the α- and the β-subunits are known to exhibit differences in affinity towards MUG and MUGS (Hou *et al*., 1996; Kytzia & Sandhoff, 1985). Previous studies demonstrated that human HexA from placenta and HexM had almost identical K_m values for MUGS, but the V_{max} for HexM was almost double that of HexA (Tropak *et al.*, 2016). The negatively charged β-subunit active site has a low affinity for the negatively charged MUGS (Kytzia & Sandhoff, 1985) and therefore does not significantly affect the K_m value for HexA. However, HexM has two α-subunit active sites which can hydrolyze MUGS, resulting in a higher V_{max} than HexA (Tropak *et al*., 2016). In the previous report, it was noted that the K_m of HexA was lower than that of HexM for MUG. However, the V_{max} of HexA was approximately double the V_{max} of HexM (Tropak *et al*., 2016). Both the α- and the β-subunits can degrade the neutral substrate MUG, however a higher affinity is observed for the β-subunit (Hou *et al*., 1996). This results in HexA having a lower K_m and a higher V_{max} then HexM (Tropak *et al*., 2016).

As expected, similar trends were observed when recombinant HexA was assessed kinetically (**Table 3.1**). When the substrate MUGS was used, the K_m values were almost identical at 1.252 mM and 1.242 mM for HexA and HexM, respectively. The V_{max} determined for HexA was 2.62 X 10^{-5} mM/s and that of HexM was almost double at 4.79 X 10^{-5} mM/s. The K_m values calculated when using MUG as the substrate were 1.365 mM for HexA and 2.096 mM

for HexM. The V_{max} values for HexM and HexA were respectively 9.34 X 10^{-5} mM/s and 1.25 X 10^{-4} mM/s.

Each β-hexosaminidase isoform has a unique MUG/MUGS activity ratio, which can be used to distinguish the enzymes from each other. The ratio for HexB is approximately 300:1. HexA has a ratio of 4:1 and HexS has a ratio of roughly 1:1 (Hou *et al*., 1996). Recombinant HexA has a MUG/MUGS ratio of 4.8:1, which is consistent with the previously published ratio for placental HexA. These results highlight that both the α- and the β-subunit of the recombinantly produced HexA are active and behave the same as lysosomal human HexA.

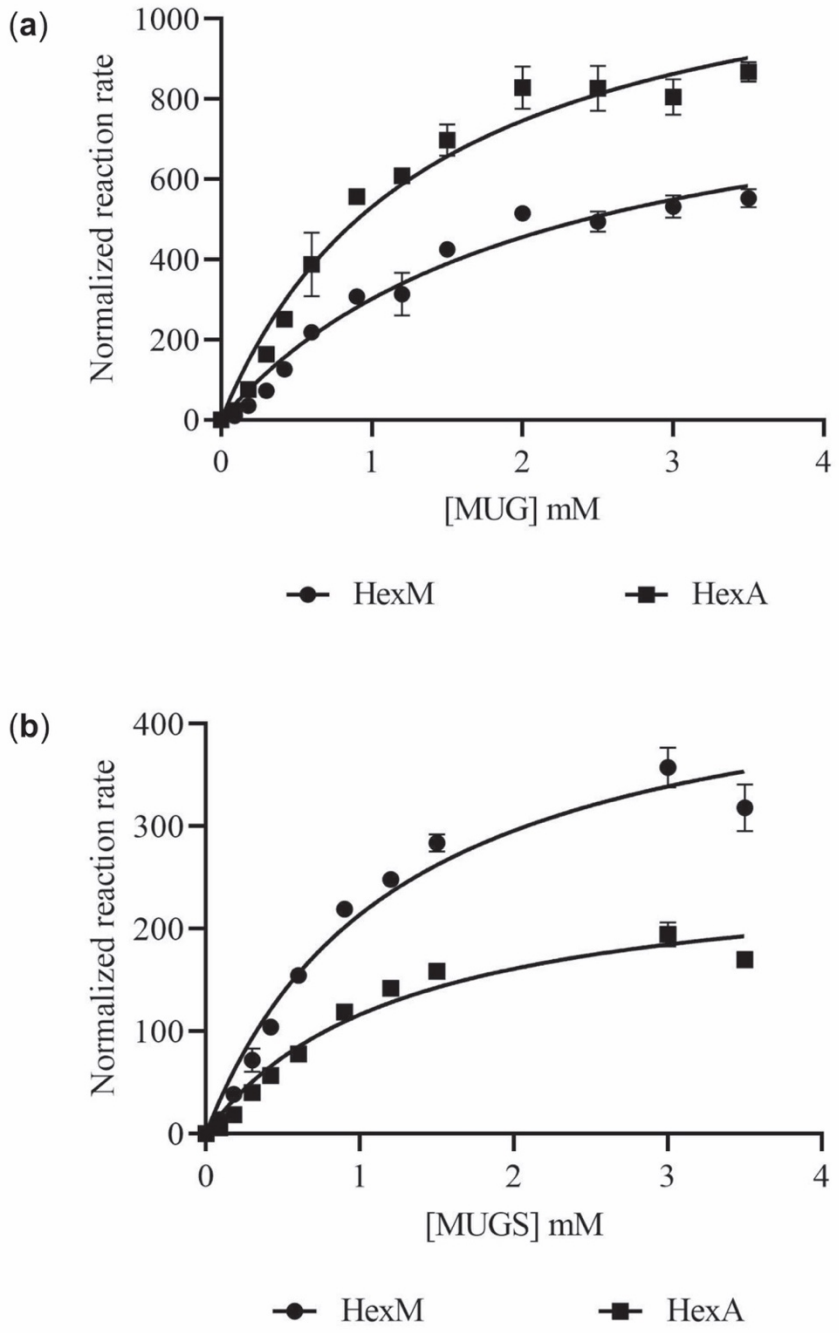

Figure 3.12. Michaelis-Menten kinetics of HexA and HexM against the synthetic substrates MUG and MUGS. Various concentrations of (**a**) MUG and (**b**) MUGS by were incubated with 100 pM of HexM (circles) or HexA (squares). The fluorogenic product 4-MU is released when either substrate is cleaved by β-hexosaminidase isoforms. The normalized reaction rate (NRR) was obtained by dividing the product formation rate by the total enzyme concentration. Data points represent the average of three technical replicates and standard deviation is indicated by error bars. For points where the error bars are not shown, the standard deviations fall within the data point dimensions. GraphPad Prism 8 was used to fit the Michaelis-Menten equation to the data.

Table 3.1. Comparison of Michaelis-Menten kinetics of HexM and HexA.

Substrate	MUG		MUGS	
Isoform	HexA	HexM	HexA	HexM
K_m[a]	1.37 ± 0.17	2.10 ± 0.31	1.25 ± 0.17	1.24 ± 0.15
V_{max}[b]	$1.26 \times 10^{-4} \pm 6.74 \times 10^{-6}$	$9.34 \times 10^{-5} \pm 7.23 \times 10^{-6}$	$2.62 \times 10^{-5} \pm 1.60 \times 10^{-6}$	$4.79 \times 10^{-5} \pm 2.59 \times 10^{-6}$
k_{cat}[c]	627.7 ± 33.72	467.0 ± 36.15	130.9 ± 8.00	239.7 ± 12.94

[a] Experiment was performed in triplicate, ± values represent standard deviation. Units for these values are mM. [b] Units are mM/s, ± values represent standard deviation. [c] Units for these values are s^{-1}, ± values represent standard deviation.

3.3.2. Stability of HexA and HexM in therapeutically relevant conditions

To assess the potential of HexM as an ERT, a two-week enzyme stability assay was conducted in physiologically relevant conditions. HexA and HexM were found to be stable when incubated in phosphate buffer pH 5.5 and pH 7 at 37ºC (**Fig 3.13**). No significant changes in the activity of either enzyme was observed over the course of 14 days (paired two-tailed t-test, $P > 0.05$).

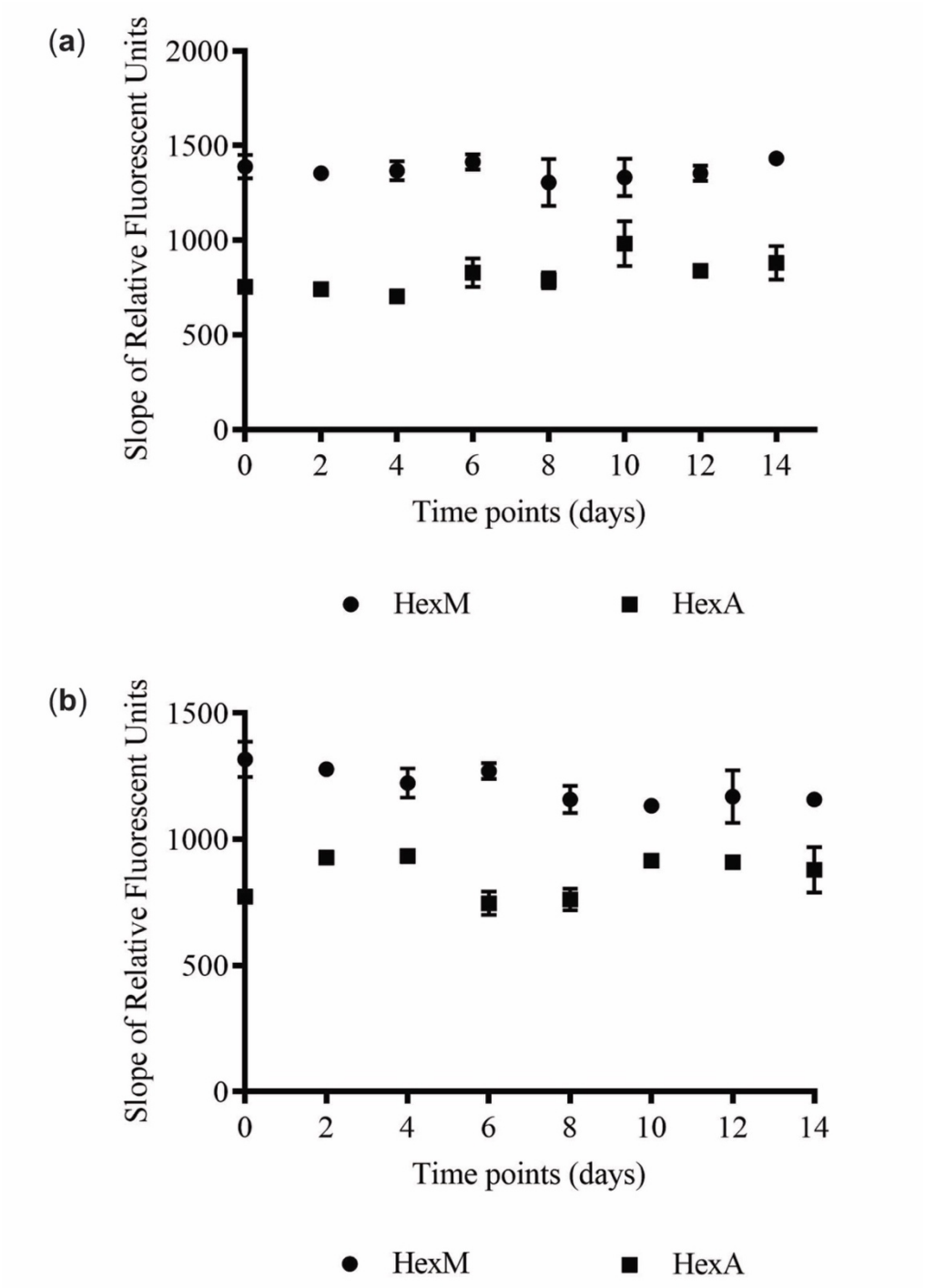

Figure 3.13. HexM and HexA activity after incubation at 37ºC for 14 days. HexM (circles) and HexA (squares) were incubated in phosphate buffer (**a**) pH 5.5 and (**b**) pH 7 for 14 days at 37ºC. Every second day, an aliquot of each sample was removed and stored at -20ºC. Kinetic assays were performed using MUGS. Enzyme activity was assessed by observing the change in RFU over the course of 30 minutes. Data points are represented by three technical replicates and the error bars indicate standard deviation. For points where the error bars are not shown, the standard deviations fall within the data point dimensions.

3.4. Thermal stability of the β-hexosaminidase fusion proteins

3.4.1. The melting temperatures of HexM-ApoB and HexM-ApoE are relatively high

As stability is one of the key features of HexM, the melting temperatures (T_m) of the modified HexM proteins were determined to ensure that the additional tags do not affect the enzymes. The Prometheus NT.48 (NanoTemper) was used to measure the fluorescence intensity of the samples at 330 nm and 350 nm as the temperature increased. The maximum point on a plot of the first derivative of the 350/330 nm ratios (**Fig 3.14b**) was used to determine that the T_m of recombinant HexM-ApoB and HexM-ApoE had melting temperatures of 63.9ºC and 64.4ºC, respectively (**Table 3.2**). These values are slightly higher than the previously reported T_m of 62ºC for HexM (Tropak *et al*., 2016), demonstrating that the extra tags do not greatly impact the stability of the HexM-fusion proteins.

Table 3.2. Melting temperatures of β-hexosaminidase isoforms.

β-hexosaminidase isoform	Onset (°C)[a]	T_m (°C)[a]
HexM-ApoB	52.60 ± 2.52	63.90 ± 0.10
HexM-ApoE	48.10 ± 1.57	64.43 ± 0.06

[a] Values represent the average of three technical replicates; ± represents the standard deviation

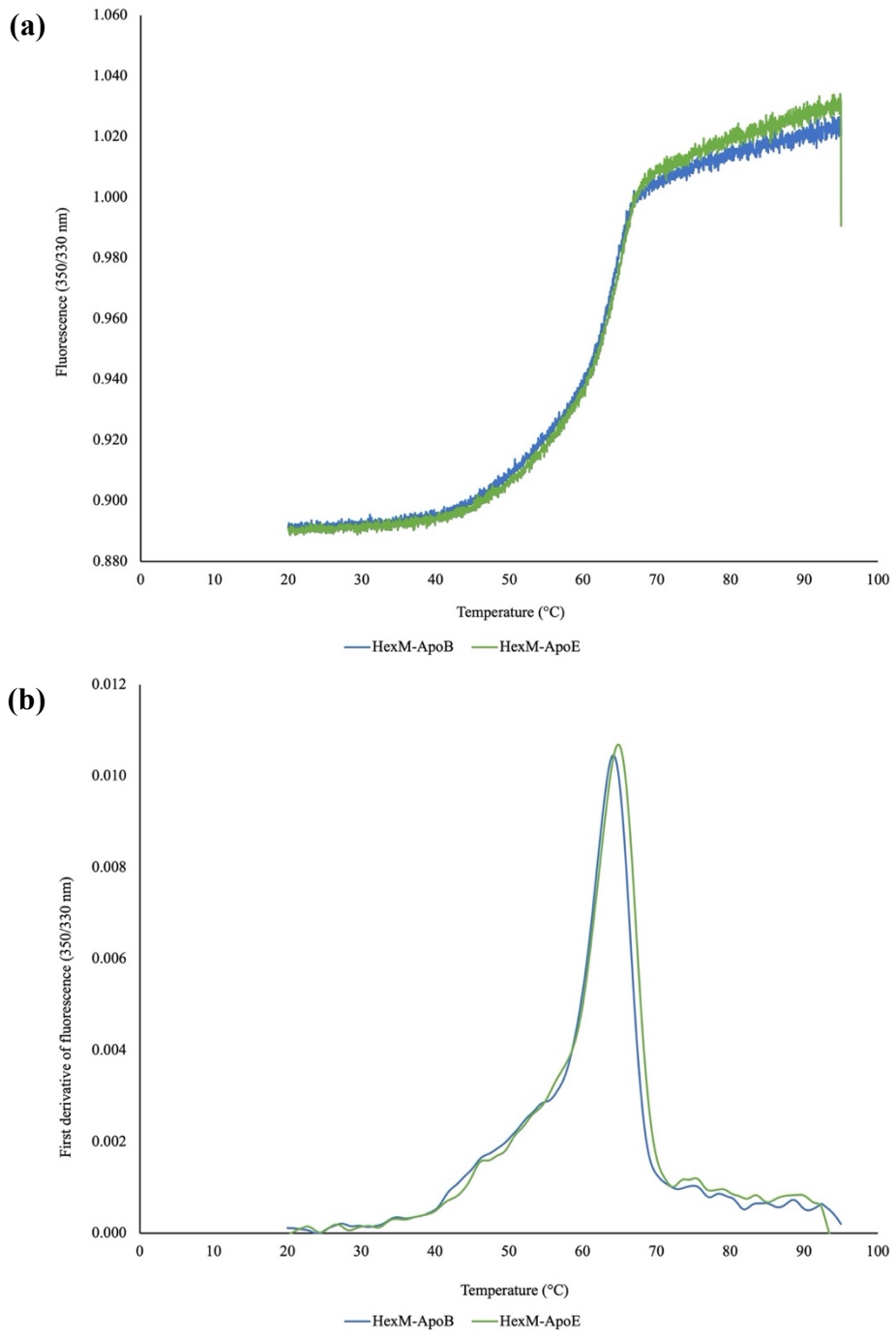

Figure 3.14. Determining the melting temperatures of various forms of β-hexosaminidase. Samples in a 1 mg/ml concentration were loaded into capillary tubes and the temperature was increased from 20°C to 95°C at a rate of 1°C per minute. The fluorescence intensity was measured at 330 nm and 350 nm to measure shifts in tryptophan emission when unfolding. (**a**) The ratio of the fluorescence intensities measured at 350/330 nm, where the T_m is indicated by the inflection point. (**b**) The first derivative of the 350/330 nm ratio. The maximum point indicates the T_m. While samples were run in triplicate, the curves represent one technical replicate for each enzyme.

3.5. Kinetics assays of the upper and lower layer of the BBB model

3.5.1. The enzymes in the 2X inputs are active against the artificial substrate MUGS

Kinetic assays done on HexM so far in this thesis have been done on enzymes which have been stored in 10 mM Bis-Tris, 100 mM NaCl (pH 6) (**Fig 3.15**), which is relatively close to the acidic pH of the lysosome (pH 4.5-5). To ensure that the enzymes were active in the 2X inputs loaded onto the BBB model, in which the buffer was at physiological pH (pH 7.4), a MUGS assay was performed (**Fig 3.16**). Similar activity was observed in HexM-ApoB and HexM-ApoE, while HexM-myc was slightly more active. These results are consistent with the Michaelis-Menten plots obtained from these enzymes.

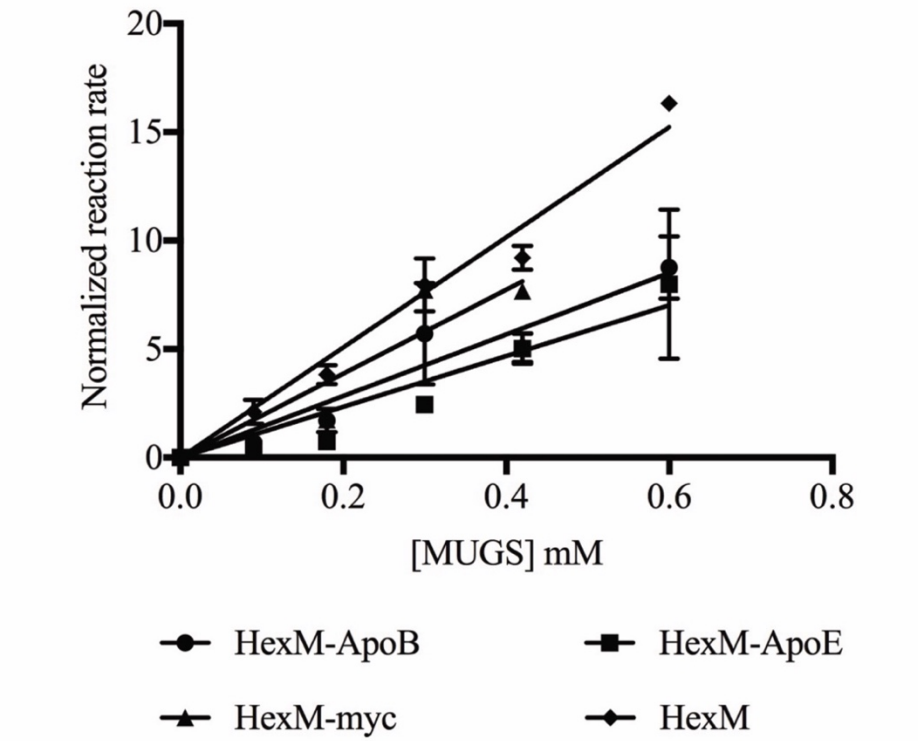

Figure 3.15. Comparison of the kinetic activity of the various forms of HexM against MUGS. Various concentrations of MUGS were incubated with 100 pM HexM (diamond), HexM-ApoB (circles), HexM-ApoE (squares) and HexM-myc (triangles). NRR was obtained by dividing the product formation rate by the total enzyme concentration. Data points represent the average of three technical replicates and standard deviation is indicated by error bars. GraphPad Prism 8 was used to fit the Michaelis-Menten equation to the data.

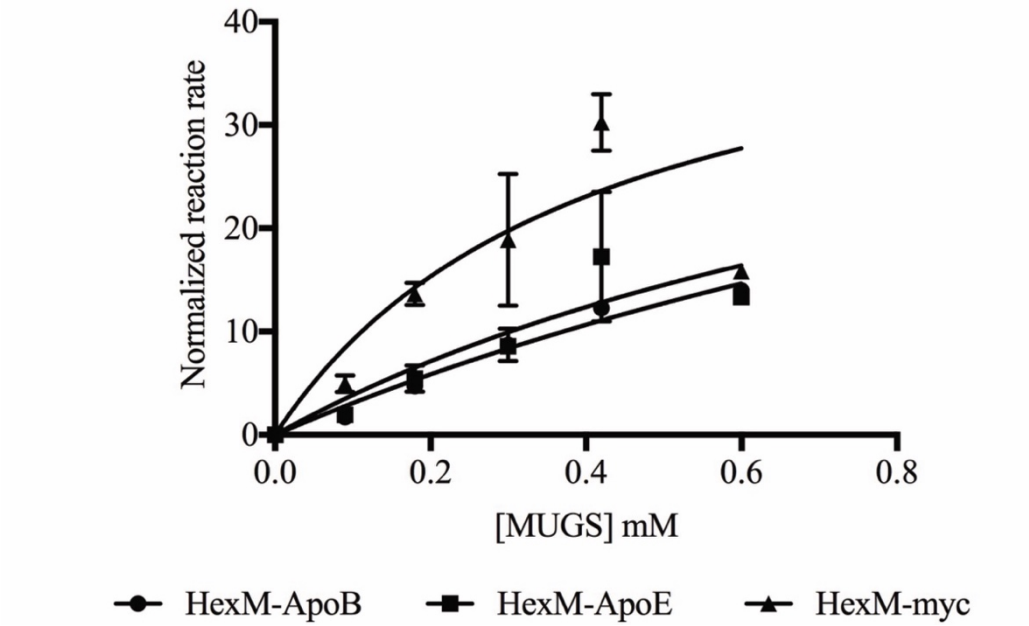

Figure 3.16. MUGS activity assay of the 2X HexM-ApoB, HexM-ApoE and HexM-myc inputs for the BBB model. Various concentrations of the synthetic substrate MUGS were incubated with 100 pM of HexM-ApoB (circles), HexM-ApoE (squares) and HexM-myc (triangles). NRR was obtained by dividing the product formation rate by the total enzyme concentration. Data points represent the average of three technical replicates. Standard deviation is indicated by error bars and for points where the error bars are not shown, the standard deviations fall within the data point dimensions in the graph. GraphPad Prism 8 was used to fit the Michaelis-Menten equation to the plot.

3.5.2. HexM-ApoB and HexM-ApoE do not cross the BBB in an *in vitro* model

Kinetic assays were performed on samples taken from the upper and lower chambers of the BBB model. Consistently, HexM-ApoB, HexM-ApoE and HexM-myc activity was observed on the top of the insert containing the BMECs (**Fig 3.17a**, **Fig 3.18a** and **Fig 3.19a**) but not on the bottom (**Fig 3.17b**, **Fig 3.18b** and **Fig 3.19b**). These results were unexpected, as previous studies have shown the uses of these tags to deliver lysosomal enzymes across various BBB models (Böckenhoff *et al*., 2014; Wang *et al*., 2013).

When analyzed by western blot, both the upper and the lower chambers lit up (**Fig 3.20**). However, the exposure time to see a band on the samples taken from the bottom had a longer exposure time than the bands on the top (~90 seconds vs ~4 seconds). While the presence of each

protein in the top well and the HexM fusion proteins (HexM-ApoB and HexM-ApoE) in bottom well was anticipated, it was unexpected to see any bands from samples taken from the bottom chamber of the wells containing HexM-myc, as it does not contain any tags to help facilitate transcytosis across the BBB.

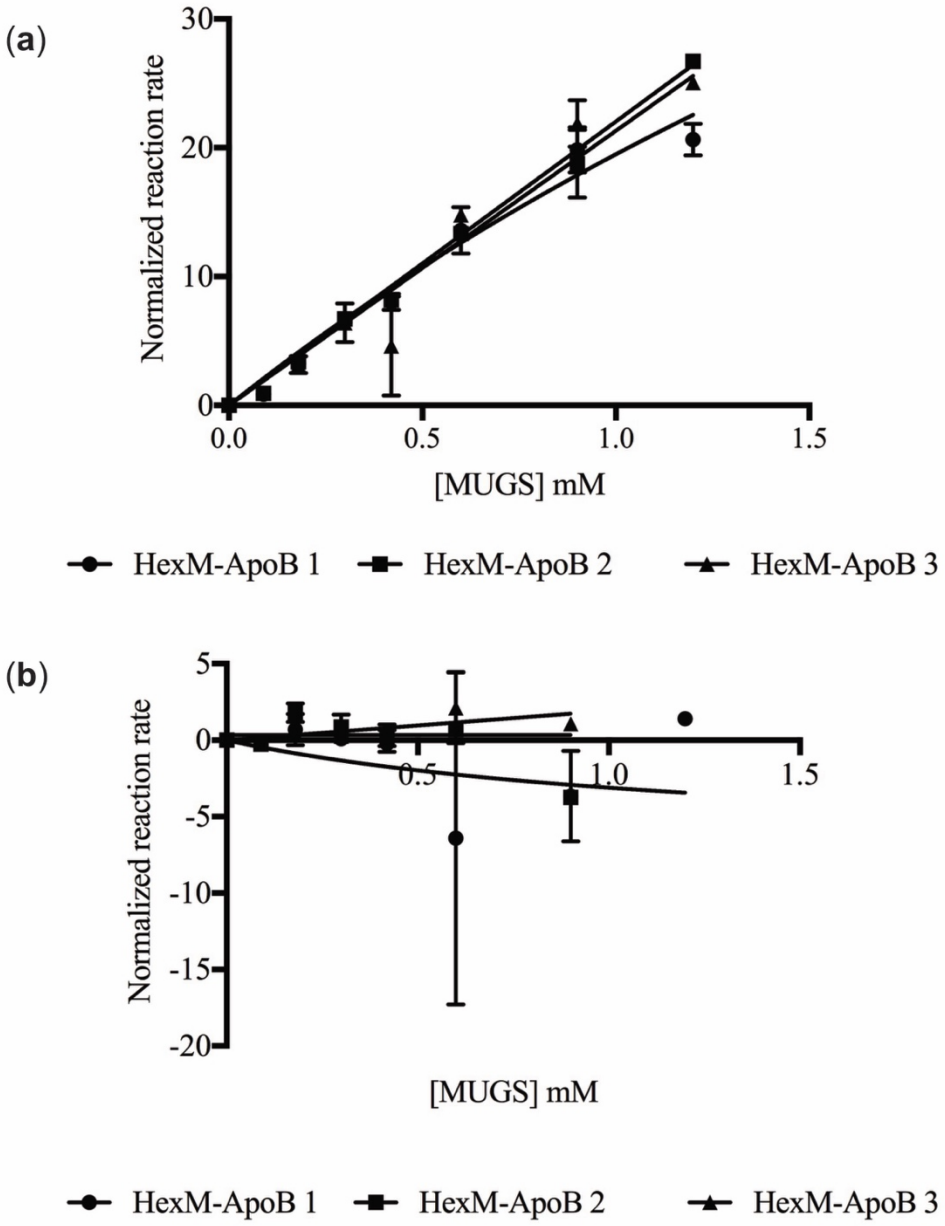

Figure 3.17. Activity assay of HexM-ApoB in the in vitro BBB model. (**a**) Samples from the top (**b**) and the bottom of the insert on which the BMECs were growing were assayed with the synthetic substrate MUGS. As the concentration of HexM-ApoB in each chamber was unknown, the samples were diluted the same as the 2X inputs. NRR was obtained by dividing the product formation rate by the total enzyme concentration. Data points represent the average of three technical replicates and standard deviation is indicated by error bars. For points where the error bars are not visible, the standard deviations fall within the data point dimensions in the graph. GraphPad Prism 8 was used to fit the Michaelis-Menten equation to the plot.

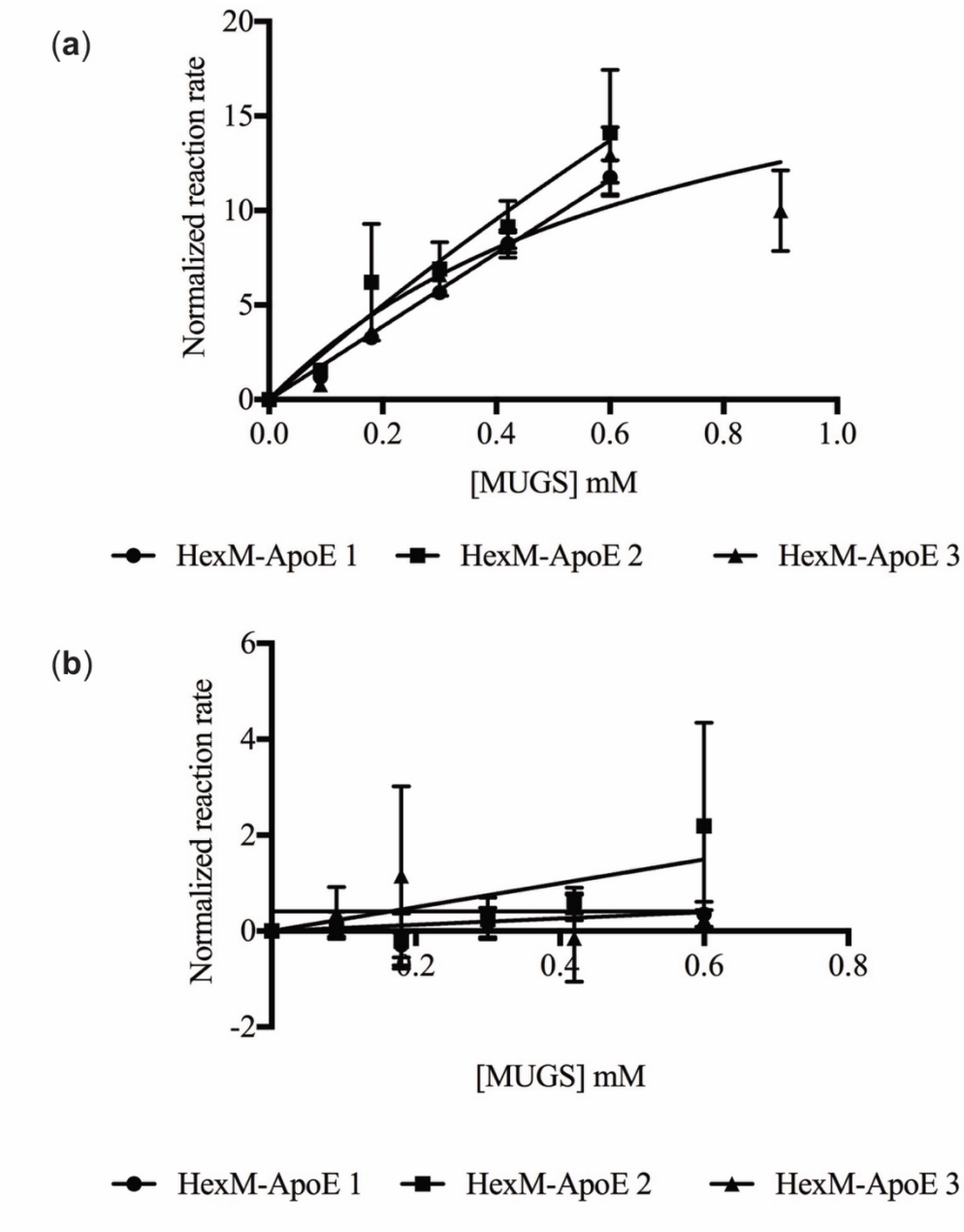

Figure 3.18. Activity assay of HexM-ApoE in the in vitro BBB model. (**a**) Samples from the top (**b**) and the bottom of the insert on which the BMECs were growing were assayed with the synthetic substrate MUGS. As the concentration of HexM-ApoE in each chamber was unknown, the samples were diluted the same as the 2X inputs. NRR was obtained by dividing the product formation rate by the total enzyme concentration. Data points represent the average of three technical replicates. Standard deviation is indicated by error bars and for points where the error bars are not shown, the standard deviations fall within the data point dimensions in the graph. GraphPad Prism 8 was used to fit the Michaelis-Menten equation to the plot.

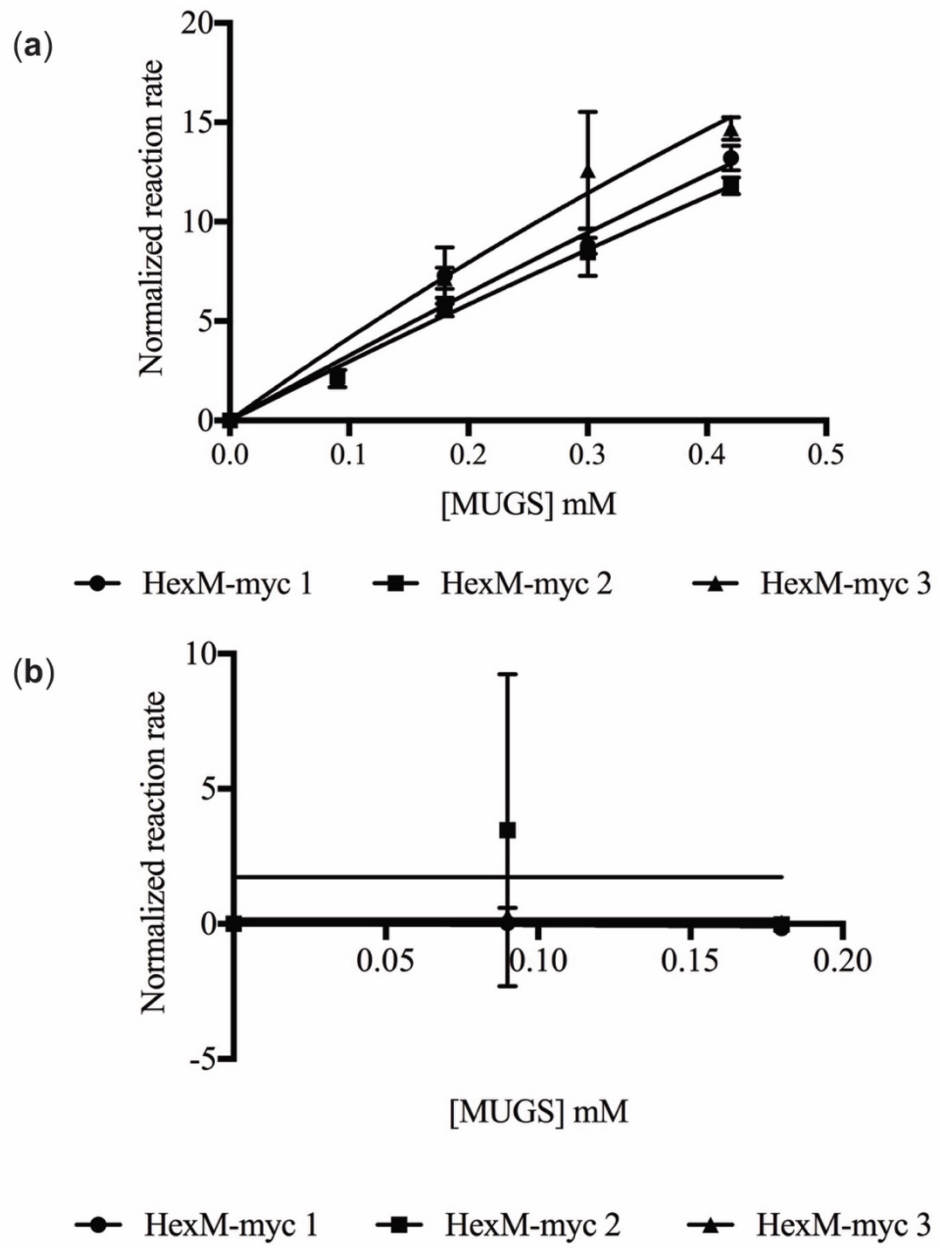

Figure 3.19. Activity assay of HexM-myc in the in vitro BBB model. (**a**) Samples from the top (**b**) and the bottom of the insert on which the BMECs were growing were assayed with the synthetic substrate MUGS. As the concentration of HexM-myc in each chamber was unknown, the samples were diluted the same as the 2X inputs. NRR was obtained by dividing the product formation rate by the total enzyme concentration. Data points represent the average of three technical replicates and standard deviation is indicated by error bars. For points where the error bars are not visible, the standard deviations fall within the data point dimensions in the graph. GraphPad Prism 8 was used to fit the Michaelis-Menten equation to the plot.

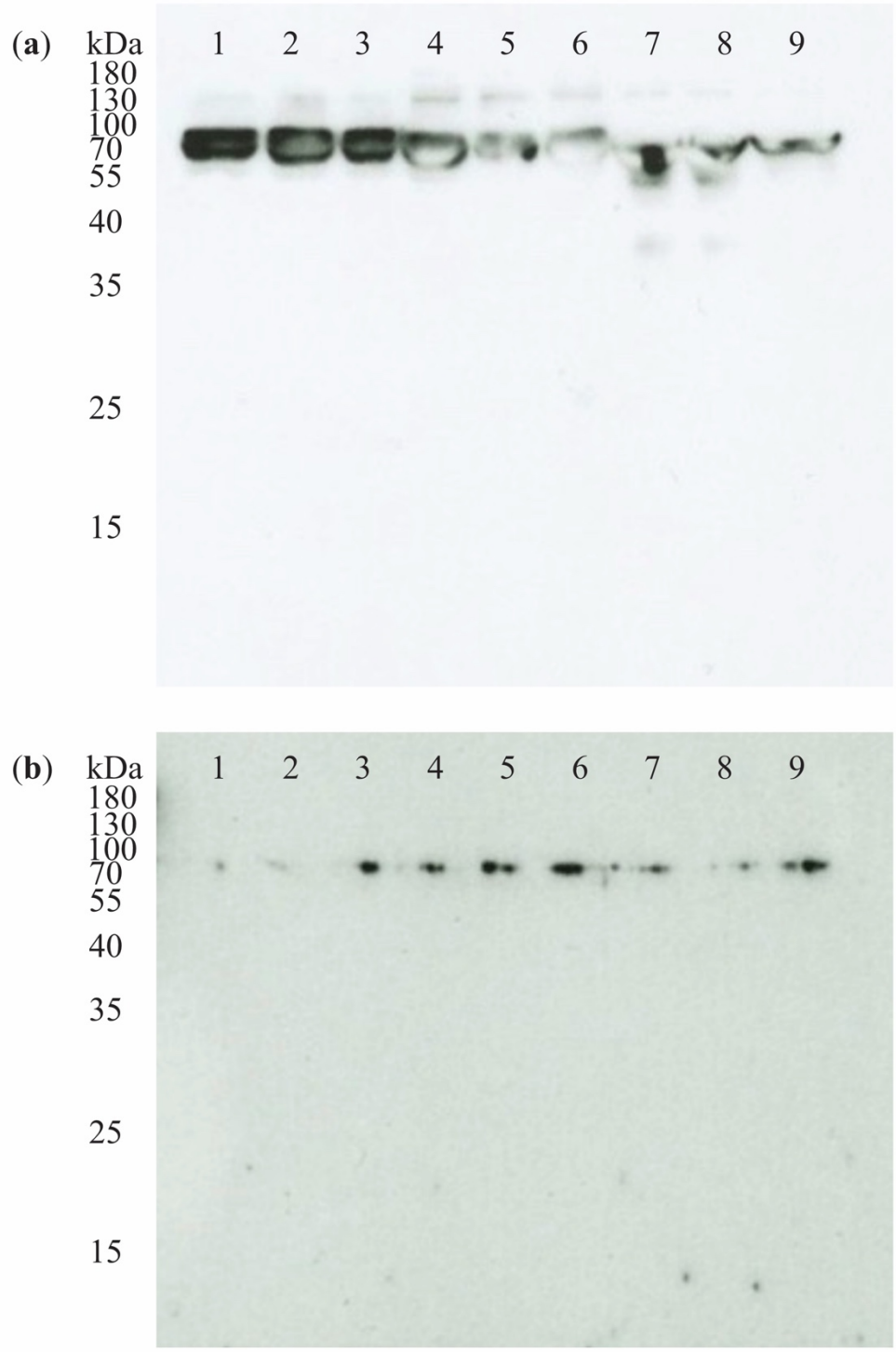

Figure 3.20. Determining the presence of HexM-ApoB, HexM-ApoE and HexM-myc by western blot. (**a**) Samples (10 µl) from the top and (**b**) the bottom of the insert on which the BMECs were growing were subjected to SDS-PAGE on 12% acrylamide gels. Lanes 1-3 contain replicates of HexM-ApoB in the BBB model. Lanes 4-6 contain replicates of HexM-ApoE and lanes 7-9 contain replicates of HexM-myc in the BBB model. The bands were visualized using an anti-HexA antibody.

4. Discussion

4.1. Protein expression, purification and characterization

4.1.1. Recombinant protein production provides a novel method for obtaining HexA

Lysosomal HexA has traditionally been purified from human placenta for medical research purposes. For the development of therapeutics, a consistent source of the enzyme which can be produced in large quantities is necessary. Consequently, the first goal of this thesis was to produce recombinant HexA, which could be used as a control for kinetic assays with HexM and for future pharmacological chaperone therapy studies. The HEK293T-ABKO-HexA cells were found to produce HexA and in the FiberCell system, almost 3 mg of protein per week could be obtained from the culture media, producing enough enzyme for kinetic assays and crystallization trials. However, the HexA protein yield is lower than the yield of HexM from a previously established cell line (Tropak *et al*., 2016). There are a few reasons this discrepancy occurs. The primary reason being that HexA (αβ-subunits) is a heterodimer and has to be isolated from other isoforms, while HexM (μμ-subunits) is a homodimer and does not need to be separated from other forms. The HEK293T-ABKO-HexA cells were transfected with the *HEXA* and *HEXB* genes and therefore produces the HexA (αβ-subunits), HexB (ββ-subunits) and HexS (αα-subunits) isoforms. During the purification procedure, the HexB and HexS isoforms are removed. In comparison, the HEK293T-ABKO-HexM cells were only transfected with the *HEXM* gene and are only capable of making one isoform and almost all the protein is captured during the purification procedure. Another potential reason for the difference in enzyme yields is that the HexA purification procedure requires the use of an anti-FLAG affinity resin, which has a relatively low binding capacity (>0.6 mg/ml resin binding capacity). If HexA quantities larger than what is currently being produced are needed, using a higher volume of the affinity resin

may increase the yield of HexA, due to protein lost on the column. Another way of potentially increasing the HexA yield would be to use a larger FiberCell cartridge which has a capacity for a larger quantity of cells to grow (FiberCell Systems, 2017).

To judge enzyme purity and to carry out future structure-based design of HexA pharmacological chaperones, I carried out crystallization trials of the enzyme. HexA crystals formed in several different crystallization conditions. Fluorescence was detected when the crystals were exposed to ultraviolet (UV) light, which confirmed they were protein crystals rather than salt as aromatic amino acids, especially tryptophan, absorb UV light strongly, whereas salts do not (Dierks *et al.*, 2010). Though the structure of lysosomal HexA from human placenta has already been determined (Lemieux *et al*., 2006), solving the structure of the recombinant enzyme would be interesting to ensure that there are no major changes in protein folding, since the recombinant form of the enzyme will not have been fully processed in the lysosome, where residues $M_1 \rightarrow A_{22}$ and $S_{75} \rightarrow H_{88}$ of the α-subunit are proteolytically cleaved, while residues $M_1 \rightarrow S_{49}$, $F_{108} \rightarrow K_{121}$, and $R_{312} \rightarrow K_{315}$ of the β-subunit are removed (Mark *et al*., 2003). Instead, the recombinant enzyme is secreted directly to the medium due to saturation of the lysosomal targeting pathway. If the two forms of the protein are nearly identical structurally, it may be possible to use recombinant HexA as a therapeutic for ERT or gene therapy. This could be especially beneficial for patients with the juvenile or late-onset forms of TSD or SD, as they produce some HexA, but not enough to prevent GM2 accumulation, lower quantities of the recombinant protein would be needed than for patients diagnosed with the infant-onset forms of GM2 gangliosidoses. Although HexM is more stable and is easier to purify, it is currently unknown how the human immune system responds to the hybrid enzyme. Recombinant HexA

could potentially be used as a therapeutic, especially in patients which produce some form of the full-length enzyme, until further immunological studies are conducted on HexM.

The enzymatic activity of recombinant HexA and HexM produced from the transfected HEK293T-ABKO cell lines was assessed using MUG and MUGS. The kinetic activity of both enzymes follows Michaelis-Menten kinetics (**Fig. 3.12**). The affinity of HexA and HexM towards the negatively charged MUGS was similar. This affinity is primarily influenced by the α-subunit active site, which is positively charged (Kytzia & Sandhoff, 1985). The turnover rate for HexM was almost twice that of HexA. This was expected as HexM has two α-subunit active sites which can degrade MUGS, while HexA only has one active site which effectively degrades the substrate. HexA exhibited a slightly higher affinity towards the neutral MUG than HexM, which is consistent with a previous report indicating that while both the α- and the β-subunit are active against MUG, the β-subunit has a higher affinity towards the substrate (Hou *et al*., 1996). A higher turnover rate was also observed for HexA. Similar trends were observed by Tropak *et a*l. (2016) when comparing the activity of HexA from placentas to that of HexM produced from the same cell line used in this thesis. This demonstrates that although recombinant HexA is a precursor form of the enzyme, it exhibits similar kinetic behavior as the mature form of lysosomal HexA purified from placenta. This is not surprising as previous studies demonstrated virtually no difference in HexB enzyme activity when using the precursor form of the protein compared to the mature form (Hou *et al*., 1996). The similarity in enzyme activity highlights an exciting new method of safely obtaining milligram quantities of human HexA, which by-passes the need to work with human tissues. Having access to cell lines which can constantly produce the enzyme ensures that the protein is available whenever needed, and the availability of HexA for studies is not limited by the quantity of placentas available.

Proteins produced for ERTs to treat TSD and SD must be stable long enough for the therapeutic to be delivered to the lysosome, where the enzyme can reduce GM2 storage. The stability of HexM and HexA was tested in buffers chosen to replicate physiological conditions in the human body. The pHs of the buffers were selected to reflect the pH of the lysosome (~4.5-5) and that of human blood (~7.35-7.45). No significant decrease in HexM and HexA activity was observed in either buffer (phosphate buffer; pH 5.5 and pH 7) over the course of 14 days. The activity of HexM was greater than that of HexA, presumably due to HexM having two active sites capable of hydrolyzing MUGS. These results highlight the potential for HexM to be used in ERT.

4.1.2. HexA G269S producing cells secrete the enzyme directly into media

Culture media collected from HEK293T-ABKO-HexA-G269S cells produced a visible band on a western blot at ~70 kDa, while media taken from flasks of *HEXA* and *HEXB* knockout cells (HEK293T-ABKO) did not (**Fig 3.4**). These results suggest that the α-HexA antibody was not binding to a component of the FBS but rather the transfected cell line was producing and secreting the HexA G269S mutant directly into the medium. In humans, most HexA mutations which cause protein misfolding, including the αG269S mutation, result in the enzyme being eliminated through the ERAD pathway (Tropak & Mahuran, 2007). Since the HEK293T-ABKO-HexA-G269S cell line was generated with overexpression cassettes (Li *et al.*, 2013), it is likely that the ERAD pathway became saturated by the amount of HexA G269S produced. Therefore, not all the enzyme was marked for degradation and could be secreted from the cells into the medium.

Various small molecules, such as pyrimethamine, have been shown to increase the activity of certain HexA mutants against MUGS (Maegawa *et al.*, 2007; Tropak *et al*., 2004) These mutants typically have a functional α-subunit active site, but the mutation results in protein misfolding. Pharmacological chaperones are thought to bind to the enzyme in a manner which leads to the proper conformation (Tropak & Mahuran, 2007). From my experiments with recombinant wild-type HexA, it is conceivable that the αG269S mutant could be purified in the required concentrations for structural studies and *in vitro* binding assays with pharmacological chaperones such as pyrimethamine. Crystallizing HexA G269S in the presence of pharmacological chaperones could also provide information on how the enzyme is stabilized by these small molecules and could potentially lead to the discovery of additional therapeutic small molecules that rescue HexA folding mutants.

4.1.3. HexM-ApoB and HexM-ApoE can be purified and are relatively stable

The first purification attempts for HexM-ApoB, HexM-ApoE and HexM-myc were done by Nickel-NTA chromatography followed by size exclusion chromatography. Each protein appeared pure by SDS-PAGE analysis and had kinetic activity against the synthetic substrates MUGS and MUG after Nickel-NTA chromatography. However, running HexM-ApoB and HexM-ApoE through the size exclusion column resulted in the formation of several different peaks, without a major peak where the protein would typically be eluted based on its size (**Fig. 3.5**). HexM-ApoB and HexM-ApoE should have eluted from the column at ~72 ml; however, very little enzyme eluted at that volume, which suggested the modified HexM proteins were aggregating and possibly unstable. In contrast, HexM-myc was eluted from the size exclusion column in one large peek containing the enzyme (**Fig. 3.6**).

A solubility and stability screen (Hampton Research) was used to determine if a more suitable buffer could be used for HexM-ApoB and HexM-ApoE purifications. However, the enzymes had comparable stability in 10 mM Bis-Tris, 100 mM NaCl (pH 6) and 10 mM Bis-Tris, 100 mM NaCl, 250 mM imidazole (pH 6) as with the other buffers assayed, and therefore we decided to continue using the original buffers. The purity of HexM-ApoB and HexM-ApoE samples after Nickel-NTA were then assessed by DLS. On the intensity distribution plots, two peaks were observed for HexM-ApoB (**Fig. 3.9a**) and three peaks were observed for HexM-ApoE (**Fig. 3.10a**). On the volume weighted distribution plot for both HexM-ApoB and HexM-ApoE, a large peak representing the enzyme was observed with a small peak representing the aggregates (**Fig 3.9b** and **3.10b**). While several peaks on the intensity distribution plot indicate that some aggregation was occurring within the samples, the volume weighted distribution suggests that most of the protein present was either monodisperse HexM-ApoB or HexM-ApoE. These results did not explain why several peaks were observed when the enzymes were passed through the size exclusion column.

As HexM-ApoB and -ApoE appeared relatively stable and pure after being run through the Nickel-NTA column with 10 mM Bis-Tris, 100 mM NaCl (pH 6) and 10 mM Bis-Tris, 100 mM NaCl, 250 mM imidazole (pH 6), the final purification step with the size exclusion column was forgone. To maintain consistency, the same was done for HexM-myc despite having no problems running this enzyme through the size exclusion column, since HexM-myc was being used as a control for studies with HexM-ApoB and HexM-ApoE.

One of the key features of HexM is that it was designed to be more stable than HexA (Tropak *et al*., 2016). To ensure that the additional tags did not negatively affect enzyme stability, the T_m of the HexM fusion proteins was determined. HexM-ApoB had a T_m of ~63.9°C

and the T_m of HexM-ApoE was ~64.4°C. HexM had a previously reported T_m of ~62°C. HexB (ββ-subunits) has a higher T_m than HexA (αβ-subunits) mainly due to a stable interface formed between the two β-subunits. The stable interface was included in the design of HexM, causing it to be more stable and have a higher T_m than HexA (Tropak *et al*., 2016). It was expected that the T_m of the HexM fusion proteins would be similar to that of HexM, as the stable β-subunit interface still forms between the subunits of the HexM-Apo proteins. The additional myc-tag and the Apo-tags do not seem to adversely influence the stability of the HexM fusion proteins. Nevertheless, the gel filtration results above still suggested that the HexM fusion proteins were being perturbed in some way, and this appears to be reflected in the slightly lower enzymatic activity of HexM-ApoB and -ApoE compared that of HexM-myc (**Fig. 3.15**). When assayed with MUGS, HexM had more activity then HexM-myc, which in turn consistently had more activity than the HexM-Apo fusion proteins. The μ-subunits, and therefore the active sites, of HexM dimerize in an antiparallel orientation (Benzie, 2020). It is possible that the additional linker sequence and the Apo tags from the adjacent subunit are long enough to partially block the active site at times, therefore making it less accessible to the synthetic substrates. HexM-myc only has the additional myc-tag, potentially making the active site more accessible than the fusion proteins but less so than HexM.

4.2. The *in vitro* blood-brain barrier model

4.2.1. HexM-ApoB and HexM-ApoE are not transported into the lower chamber of the model

Surprisingly, neither HexM-ApoB or HexM-ApoE were found to cross into the lower chamber of the BBB model. Although a few small bands appeared on the western blot of media

collected from the bottom chamber, they were not very convincing (**Fig. 3.20**). Firstly, this western was developed for much longer than the blot of the top chambers (~90 seconds vs ~5 seconds), indicating that most of the enzyme remained in the top chamber. It was also expected that HexM-ApoB and HexM-ApoE would be more effective at crossing the barrier than the control protein, HexM-myc. However, on the western blot, similar bands appear in the wells containing HexM-myc as in the wells containing the HexM-Apo fusion proteins. It is possible that the bands that lit up were from HexA produced by the BMECs or that the HexM fusion proteins were non-selectively being transported across the *in vitro* BBB. Furthermore, when enzyme activity was assayed, activity against MUGS was detected in the upper chamber of the BBB model but not the lower chamber (**Fig. 3.17**, **3.18** and **3.19**). If any enzyme crossed into the lower chamber of the model, it was not significant enough in quantity to produce any detectable activity and therefore is not likely to be beneficial in preventing the storage of GM2 *in vivo*. The enzymes would need to effectively be able to cross the BBB as not all protein will get endocytosed into cells, where it can reduce GM2 accumulation.

These results were unexpected as the HexM fusion protein designs included identical ApoB and ApoE receptor binding domain sequences as in previously published experiments where the tags were fused to different lysosomal enzymes. In one study, IDUA fused to ApoE $(159\text{-}167)_2$ was found to cross a BBB model comprised of bovine brain capillary endothelial cells on collagen-coated Transwell inserts and into the CNS of MPS I mice when injected via mice tail-vein with a liver specific promotor (Wang *et al*., 2013). In another study, ASA-ApoB (3371-3409) and ASA-ApoE $(159\text{-}167)_2$ (which contained a linker sequence separating the protein and the Apo-tag) were found to significantly cross an *in vitro* BBB model consisting of primary porcine brain capillary endothelial cells. ASA-ApoE $(159\text{-}167)_2$ was also found to have

crossed the BBB into the CNS of ASA-knock out mice (Böckenhoff *et al*., 2014). While the same Apo-tags and linker sequence were fused to the C-terminus of HexM, different outcomes were observed. However, there was an additional his-tag attached to the HexM fusion proteins that was not present on ASA or on IDUA. It is possible that the additional tags were too flexible, causing the HexM-Apo proteins to detach from the receptors on the BBB model and therefore resulting in poor transcytosis across the barrier. Another possibility would be that the linker sequence was not long enough for the Apo tags to sufficiently access the receptors.

5. Conclusion

5.1. Summary of findings

TSD and SD are severe neurodegenerative disorders, which result from mutations in the genes encoding the heterodimeric enzyme HexA. Although there are currently no effective treatments available for either disorder, potential therapeutics including ERT and pharmacological chaperone therapy are currently being investigated. To this effect, the objectives of this thesis were focused on furthering research towards the development of possible therapies for the GM2 gangliosidoses.

For research purposes, lysosomal HexA has historically been purified from human placenta. Accordingly, the quantity of enzyme available was limited by the amount of tissue which could be obtained. A novel method for producing and isolating recombinant HexA was developed to maintain a stable and consistent source of the protein. The enzyme could be isolated from the other Hex isoforms in a two-step purification procedure, which yielded

approximately 0.4 mg of protein per daily medium extraction from the FiberCell bioreactor. Recombinant HexA was found to exhibit kinetic activity comparable to that of placental HexA.

The same strategy used to generate recombinant HexA was then applied to develop an αG269S mutant which is overexpressed in HEK293T cells. HexA G269S could be detected in the cell culture media by western blot. It is likely that enough protein is produced to saturate the cellular degradation pathways which target misfolded proteins, resulting in the remaining protein to be secreted. It is expected that purification of the αG269S mutant will be conducted in the same manner as recombinant HexA, as the two enzymes are completely identical with the exception of one amino acid mutation.

To further the development of treatments for TSD and SD, it is essential to discover a method of efficiently delivering the therapeutic to the CNS. The LDLR binding regions of ApoB (3371-3409) and ApoE $(159\text{-}167)_2$ were genetically fused to HexM. The HexM fusion proteins were purified using Nickel-NTA resin and it was determined that the additional tags did not negatively impact protein stability. Unfortunately, the HexM-ApoB and HexM-ApoE were not transcytosed across an *in vitro* BBB model in sufficient quantities to be detected by activity assays.

5.2. Future directions

Originally, the aims of this project included crystallizing recombinant HexA and the αG269S mutant. Determining the structure of HexA purified from HEK293T cells would ensure that there are no major changes between the recombinant protein and human HexA isolated from placenta. Structural differences in the enzyme may be important in case of use of the recombinant enzyme in ERT or GT, as any major changes could elicit a stronger immune response. While HexM degrades GM2 more efficiently, it may be worthwhile to investigate the

use of recombinant HexA as a therapy in patients with juvenile- or adult-onset forms of the GM2 gangliosidoses, as these patients produce some HexA already and may be less likely to have a strong immune response to HexA than towards the hybrid HexM. Also, less enzyme would need to be delivered to cells to reach the 10% threshold required to prevent GM2 storage than in patients which produce almost no HexA.

It has been demonstrated that certain TSD and SD cell lines exhibit a significant increase in HexA activity after incubation with therapeutic concentrations of the potential pharmacological chaperone pyrimethamine (Maegawa *et al.*, 2007). While HexB (ββ-subunits) has been crystallized in the presence of the small molecule (Bateman *et al*., 2011), pyrimethamine has yet to be crystallized with HexA or the αG269S mutant. The next logical step would be to obtain a structure of the αG269S mutant with and without pyrimethamine. This could provide some insight on how the mutation affects the structure of HexA and how binding to the pharmacological chaperone impacts folding, as it is currently unknown exactly how the molecule helps stabilize mutant enzymes. This may also impart a better understanding of which mutations pyrimethamine is effective with, as increased enzyme activity was not observed when the small molecule was incubated in cell lines with αR178H, αR499H or αR499C mutations (Maegawa *et al.,* 2007). Purified HexA G269S could also be used to screen for novel pharmacological chaperones.

The two-week HexA and HexM stability experiment, where the enzymes were incubated at human body temperature for 14 days, could be repeated but with an artificial cerebrospinal fluid buffer instead of PBS. While PBS was chosen to reflect physiological conditions, it may be insightful to repeat the experiment in a buffer which mimics the environment of the CSF as the CNS is the main target of the enzymes. This would provide better insight on whether the proteins

are stable for long periods of time in the area where the therapeutic is most likely to be directly administered or transported to.

Other future experiments would be to redesign the HexM fusion proteins. Some possibilities include moving the Apo-tags to the N-terminus or modifying the length of the linker sequence which separates the tag from the enzyme. Increasing the linker sequence would allow the tag to stick out further, perhaps rendering it more accessible for the receptor. Reducing the linker length may also change the flexibility of the protein, and subsequently receptor binding. There is also the possibility of redesigning the HexM-fusion proteins with different BBB shuttle peptides such as the 19 amino acid oligopeptide, Angiopep-2, which has been used in clinical trials as a BBB shuttle peptide (Oller-Salvia *et al.*, 2016) or the 262 amino acid nontoxic binding domain of the ricinAB toxin (Acosta *et al*., 2015; Medina-Bolivar *et al.*, 2003; Ou *et al*., 2018). Endocytosis assays with TDS fibroblasts would help determine whether the tags affect cellular uptake and whether hyperphosphorylation of the enzymes leads to an increased uptake as it does for HexM (Benzie, 2020). It may also be worth doing pull-down assays to ensure the tags do not prevent GM2AP from interacting with the enzyme. If the redesigned HexM-fusion proteins are capable of crossing the *in vitro* BBB model, then further experiments could be conducted in mice models.

References

Abbott, N. J., Rönnbäck, L., & Hansson, E. (2006). Astrocyte-endothelial interactions at the blood-brain barrier. *Nature Reviews Neuroscience*, *7*(1), 41–53. https://doi.org/10.1038/nrn1824

Abrahao, A., Meng, Y., Llinas, M., Huang, Y., Hamani, C., Mainprize, T., Aubert, I., Heyn, C., Black, S. E., Hynynen, K., Lipsman, N., & Zinman, L. (2019). First-in-human trial of blood–brain barrier opening in amyotrophic lateral sclerosis using MR-guided focused ultrasound. *Nature Communications*, *10*(1), 1–9. https://doi.org/10.1038/s41467-019-12426-9

Abulrob, A., Sprong, H., Van Bergen en Henegouwen, P., & Stanimirovic, D. (2005). The blood-brain barrier transmigrating single domain antibody: Mechanisms of transport and antigenic epitopes in human brain endothelial cells. *Journal of Neurochemistry*, *95*(4), 1201–1214. https://doi.org/10.1111/j.1471-4159.2005.03463.x

Acosta, W., Ayala, J., Dolan, M. C., & Cramer, C. L. (2015). RTB lectin: A novel receptor-independent delivery system for lysosomal enzyme replacement therapies. *Scientific Reports*, *5*(August), 1–11. https://doi.org/10.1038/srep14144

Agha-Mohammadi, S., O'Malley, M., Etemad, A., Wang, Z., Xiao, X., & Lotze, M. T. (2004). Second-generation tetracycline-regulatable promoter: Repositioned tet operator elements optimize transactivator synergy while shorter minimal promoter offers tight basal leakiness. *Journal of Gene Medicine*, *6*(7), 817–828. https://doi.org/10.1002/jgm.566

Alarcon-Martinez, L., Yilmaz-Ozcan, S., Yemisci, M., Schallek, J., Kılıç, K., Can, A., Di Polo,

A., & Dalkara, T. (2018). Capillary pericytes express α-smooth muscle actin, which requires prevention of filamentous-actin depolymerization for detection. *ELife*, *7*, 1–17. https://doi.org/10.7554/eLife.34861

Alroy, J., & Lyons, J. A. (2014). Lysosomal storage diseases. *Journal of Inborn Errors of Metabolism and Screening*, *2*, 731–749. https://doi.org/10.1016/B978-0-12-370491-7.00024-6

Appelmans, F., Wattiaux, R., & de Duve, C. (1955). Tissue fractionation studies. 5. The association of acid phosphatase with a special class of cytoplasmic granules in rat liver. *The Biochemical Journal*, *59*(3), 438–445. https://doi.org/10.1042/bj0590438

Armulik, A., Genové, G., & Betsholtz, C. (2011). Pericytes: developmental, physiological, and pathological perspectives, problems, and promises. *Developmental Cell*, *21*(2), 193–215. https://doi.org/10.1016/j.devcel.2011.07.001

Balabanov, R., Washington, R., Wagnerova, J., & Dore-Duffy, P. (1996). CNS microvascular pericytes express macrophage-like function, cell surface integrin. *Microvascular Research*, *52*(2), 127–142.

Bateman, K. S., Cherney, M. M., Mahuran, D. J., Tropak, M., & James, M. N. G. (2011). Crystal structure of β-hexosaminidase B in complex with pyrimethamine, a potential pharmacological chaperone. *Journal of Medicinal Chemistry*, *54*(5), 1421–1429. https://doi.org/10.1021/jm101443u

Beguinot, L., Lyall, R. M., Willingham, M. C., & Pastan, I. (1984). Down-regulation of the epidermal growth factor receptor in KB cells is due to receptor internalization and

subsequent degradation in lysosomes. *Proceedings of the National Academy of Sciences of the United States of America*, *81*(8 I), 2384–2388. https://doi.org/10.1073/pnas.81.8.2384

Benzie, G. (2020). *Elucidating the structure and improving the cellular uptake of HexM, a candidate for enzyme replacement therapy of GM2 gangliosidosis*. University of Manitoba.

Bernardo, K., Hurwitz, R., Zenk, T., Desnick, R. J., Ferlinz, K., Schuchman, E. H., & Sandhoff, K. (1995). Purification, characterization, and biosynthesis of human acid ceramidase. *Journal of Biological Chemistry*, *270*(19), 11098–11102. https://doi.org/10.1074/jbc.270.19.11098

Beutler, E., Kuhl, W., & Comings, D. (1975). Hexosaminidase isozyme in type O GM2 gangliosidosis (Sandhoff Jatzkewitz disease). *American Journal of Human Genetics*, *27*(5), 628–638.

Böckenhoff, A., Cramer, S., Wölte, P., Knieling, S., Wohlenberg, C., Gieselmann, V., Galla, H. J., & Matzner, U. (2014). Comparison of five peptide vectors for improved brain delivery of the lysosomal enzyme arylsulfatase A. *Journal of Neuroscience*, *34*(9), 3122–3129. https://doi.org/10.1523/JNEUROSCI.4785-13.2014

Bottros, M. M., & Christo, P. J. (2014). Current perspectives on intrathecal drug delivery. *Journal of Pain Research*, *7*, 615–626. https://doi.org/10.2147/JPR.S37591

Brandli, A. W., Hansson, G. C., Rodriguez-Boulan, E., & Simons, K. (1988). A polarized epithelial cell mutant deficient in translocation of UDP-galactose into the Golgi complex. *Journal of Biological Chemistry*, *263*(31), 16283–16290. https://doi.org/10.1016/s0021-9258(18)37590-2

Brem, H., Piantadosi, S., Burger, P. C., Walker, M., Selker, R., Vick, N. A., Black, K., Sisti, M., Brem, S., Mohr, G., Muller, P., Morawetz, R., & Schold, S. C. (1995). Placebo-controlled trial of safety and efficacy of intraoperative controlled delivery by biodegradable polymers of chemotherapy for recurrent gliomas. *The Lancet*, *345*(8956), 1008–1012. https://doi.org/10.1016/S0140-6736(95)90755-6

Bright, N. A., Gratian, M. J., & Luzio, J. P. (2005). Endocytic delivery to lysosomes mediated by cocurrent fusion and kissing events in living cells. *Current Biology*, *15*(4), 360–365.

Brightman, M. W., & Reese, T. S. (1969). Junctions between intimately apposed cell membranes in the vertebrate brain. *The Journal of Cell Biology*, *40*(3), 648–677. https://doi.org/10.1083/jcb.40.3.648

Chen, H., & Konofagou, E. E. (2014). The size of blood-brain barrier opening induced by focused ultrasound is dictated by the acoustic pressure. *Journal of Cerebral Blood Flow and Metabolism*, *34*(7), 1197–1204. https://doi.org/10.1038/jcbfm.2014.71

Chester, M. A. (1999). IUPAC-IUB joint commission on biochemical nomenclature (JCBN) nomenclature of glycolipids: Recommendations 1997. *Glycoconjugate Journal*, *16*(1), 1–6. https://doi.org/10.1023/a:1017225000910

Chiry, O., Pellerin, L., Monnet-Tschudi, F., Fishbein, W. N., Merezhinskaya, N., Magistretti, P. J., & Clarke, S. (2006). Expression of the monocarboxylate transporter MCT1 in the adult human brain cortex. *Brain Research*, *1070*(1), 65–70. https://doi.org/10.1016/j.brainres.2005.11.064

Clarke, D., Pearse, Y., Kan, S. hsin, Le, S. Q., Sanghez, V., Cooper, J. D., Dickson, P. I., &

Iacovino, M. (2018). Genetically corrected iPSC-derived neural stem cell grafts deliver enzyme replacement to affect CNS disease in Sanfilippo B Mice. *Molecular Therapy - Methods and Clinical Development*, *10*(September), 113–127. https://doi.org/10.1016/j.omtm.2018.06.005

Cohen-Pfeffer, J. L., Gururangan, S., Lester, T., Lim, D. A., Shaywitz, A. J., Westphal, M., & Slavc, I. (2017). Intracerebroventricular delivery as a safe, long-term route of drug administration. *Pediatric Neurology*, *67*, 23–35. https://doi.org/10.1016/j.pediatrneurol.2016.10.022

Colegio, O. R., Van Itallie, C. M., McCrea, H. J., Rahner, C., & Anderson, J. M. (2002). Claudins create charge-selective channels in the paracellular pathway between epithelial cells. *American Journal of Physiology - Cell Physiology*, *283*, 142–147. https://doi.org/10.1152/ajpcell.00038.2002

Colegio, O. R., Van Itallie, C., Rahner, C., & Anderson, J. M. (2003). Claudin extracellular domains determine paracellular charge selectivity and resistance but not tight junction fibril architecture. *American Journal of Physiology - Cell Physiology*, *284*(6), 1346–1354. https://doi.org/10.1152/ajpcell.00547.2002

Conzelmann, E., Kytzia, H. J., Navon, R., & Sandhoff, K. (1983). Ganglioside G(M2) N-acetyl-β-D-galactosaminidase activity in cultured fibroblasts of late-infantile and adult G(M2) gangliosidosis patients and of healthy probands with low hexosaminidase level. *American Journal of Human Genetics*, *35*(5), 900–913.

Conzelmann, E., & Sandhoff, K. (1978). AB variant of infantile GM2 gangliosidosis. Deficiency

of a factor necessary for stimulation of hexosaminidase A-catalyzed degradation of ganglioside GM2 and glycolipid GA2. *Proceedings of the National Academy of Sciences of the United States of America*, *75*(8), 3979–3983. https://doi.org/10.1073/pnas.75.8.3979

Coomber, B. L., & Stewart, P. A. (1985). Morphometric analysis of CNS microvascular endothelium. *Microvascular Research*, *30*(1), 99–115. https://doi.org/10.1016/0026-2862(85)90042-1

Cordoncardo, C., Brien, J. P. O., Casals, D., Rittman-Grauert, L., Biedler, J. L., Melamed, M. R., & Bertino, J. R. (1989). Multidrug-resistance (P-glycoprotein) is expressed by endothelial cells at blood-brain barrier sites. *Proceedings of the National Academy of Sciences, 86*(2), 695–698.

Couturier, M., Bahassi, E. M., & Van Melderen, L. (1998). Bacterial death by DNA gyrase poisoning. *Trends in Microbiology*, *6*(7), 269–275. https://doi.org/10.1016/S0966-842X(98)01311-0

Cutillo, G., Saariaho, A. H., & Meri, S. (2020). Physiology of gangliosides and the role of antiganglioside antibodies in human diseases. *Cellular and Molecular Immunology*, *17*(4), 313–322. https://doi.org/10.1038/s41423-020-0388-9

Daneman, R., & Prat, A. (2015). The blood–brain barrier. *Cold Spring Harbor Perspectives in Biology*, *7*(1), 2007–2009. https://doi.org/10.1101/cshperspect.a020412

Daneman, R., Zhou, L., Kebede, A. A., & Barres, B. A. (2016). Pericytes are required for blood-brain barrier integrity during embryogenesis. *Nature*, *468*(7323), 562–566. https://doi.org/10.1049/iet-cvi.2015.0210

Dang, S. P., Wang, R. X., Qin, M. De, Zhang, Y., Gu, Y. Z., Wang, M. Y., Yang, Q. L., Li, X. R., & Zhang, X. G. (2011). A novel transfection method for eukaryotic cells using polyethylenimine coated albumin microbubbles. *Plasmid*, *66*(1), 19–25. https://doi.org/10.1016/j.plasmid.2011.03.003

Dashkoff, J., Lerner, E. P., Truong, N., Klickstein, J. A., Fan, Z., Mu, D., Maguire, C. A., Hyman, B. T., & Hudry, E. (2016). Tailored transgene expression to specific cell types in the central nervous system after peripheral injection with AAV9. *Molecular Therapy - Methods and Clinical Development*, *3*, 16081. https://doi.org/10.1038/mtm.2016.81

de Baecque, C. M., Suzuki, K., Rapin, I., Johnson, A. B., Whethers, D. L., & Suzuki, K. (1975). GM2-gangliosidosis, AB variant. *Acta Neuropathologica*, *33*(3), 207–226. https://doi.org/10.1007/bf00688395

de Duve, C. (1975). Exploring cells with a centrifuge. *Science*, *189*(4198), 186–194. https://doi.org/10.1126/science.1138375

de Duve, C., Pressman, B. C., Gianetto, R., Wattiaux, R., & Appelmans, F. (1955). Tissue fractionation studies. 6. Intracellular distribution patterns of enzymes in rat-liver tissue. *The Biochemical Journal*, *60*(4), 604–617. https://doi.org/10.1042/bj0600604

Deer, T. R., Pope, J. E., Hanes, M. C., & McDowell, G. C. (2019). Intrathecal therapy for chronic pain: A review of morphine and ziconotide as firstline options. *Pain Medicine*, *20*(4), 784–798. https://doi.org/10.1093/pm/pny132

Demeule, M., Currie, J. C., Bertrand, Y., Ché, C., Nguyen, T., Régina, A., Gabathuler, R., Castaigne, J. P., & Béliveau, R. (2008). Involvement of the low-density lipoprotein

receptor-related protein in the transcytosis of the brain delivery vector angiopep-2. *Journal of Neurochemistry*, *106*(4), 1534–1544. https://doi.org/10.1111/j.1471-4159.2008.05492.x

Demeule, M., Regina, A., Ché, C., Poirier, J., Nguyen, T., Gabathuler, R., Castaigne, J. P., & Béliveau, R. (2008). Identification and design of peptides as a new drug delivery system for the brain. *Journal of Pharmacology and Experimental Therapeutics*, *324*(3), 1064–1072. https://doi.org/10.1124/jpet.107.131318

Dierks, K., Meyer, A., Oberthür, D., Rapp, G., Einspahr, H., & Betzel, C. (2010). Efficient UV detection of protein crystals enabled by fluorescence excitation at wavelengths longer than 300 nm. *Acta Crystallographica Section F: Structural Biology and Crystallization Communications*, *66*(4), 478–484. https://doi.org/10.1107/S1744309110007153

Doolittle, N. D., Petrillo, A., Bell, S., Cummings, P., & Eriksen, S. (1998). Blood-brain barrier disruption for the treatment of malignant brain tumors: The national program. *The Journal of Neuroscience Nursing*, *30*(2), 81–90. https://doi.org/10.1097/01376517-199804000-00002

Doolittle, Nancy D., Miner, M. E., Hall, W. A., Siegal, T., Hanson, E. J., Osztie, E., McAllister, L. D., Bubalo, J. S., Kraemer, D. F., Fortin, D., Nixon, R., Muldoon, L. L., & Neuwelt, E. A. (2000). Safety and efficacy of a multicenter study using intraarterial chemotherapy in conjunction with osmotic opening of the blood-brain barrier for the treatment of patients with malignant brain tumors. *Cancer*, *88*(3), 637–647. https://doi.org/10.1002/(SICI)1097-0142(20000201)88:3<637::AID-CNCR22>3.0.CO;2-Y

Drousiotou, A., Stylianidou, G., Anastasiadou, V., Christopoulos, G., Mavrikiou, E., Georgiou,

T., Kalakoutis, G., Oladimeji, A., Hara, Y., Suzuki, K., Furihata, K., Ueno, I., Ioannou, P. A., & Fensom, A. H. (2000). Sandhoff disease in Cyprus: Population screening by biochemical and DNA analysis indicates a high frequency of carriers in the Maronite community. *Human Genetics*, *107*(1), 12–17. https://doi.org/10.1007/s004390000324

Erickson, K. D., Garcea, R. L., & Tsai, B. (2009). Ganglioside GT1b is a putative host cell receptor for the Merkel cell polyomavirus. *Journal of Virology*, *83*(19), 10275–10279. https://doi.org/10.1128/jvi.00949-09

Erkhembaatar, M., Gu, D. R., Lee, S. H., Yang, Y. M., Park, S., Muallem, S., Shin, D. M., & Kim, M. S. (2017). Lysosomal Ca2+ signaling is essential for osteoclastogenesis and bone remodeling. *Journal of Bone and Mineral Research*, *32*(2), 385–396. https://doi.org/10.1002/jbmr.2986

FiberCell Systems. (2017). *FiberCell Systems User's Manual*. https://www.fibercellsystems.com/wp-content/uploads/2015/06/FiberCell-Systems-User's-Manual-r2.pdf

Fitterer, B., Hall, P., Antonishyn, N., Desikan, R., Gelb, M., & Lehotay, D. (2014). Incidence and carrier frequency of Sandhoff disease in Saskatchewan determined using a novel substrate with detection by tandem mass spectrometry and molecular genetic analysis. *Molecular Genetics and Metabolism*, *111*(3), 382–389. https://doi.org/10.1016/j.ymgme.2014.01.002

Foley, J. L., Eames, M., Snell, J., Hananel, A., Kassell, N., & Aubry, J. F. (2013). Image-guided focused ultrasound: State of the technology and the challenges that lie ahead. *Imaging in*

Medicine, *5*(4), 357–370. https://doi.org/10.2217/iim.13.38

Fortin, D., Gendron, C., Boudrias, M., & Garant, M. P. (2007). Enhanced chemotherapy delivery by intraarterial infusion and blood-brain barrier disruption in the treatment of cerebral metastasis. *Cancer*, *109*(4), 751–760. https://doi.org/10.1002/cncr.22450

Foust, K. D., Nurre, E., Montgomery, C. L., Hernandez, A., Chan, C. M., & Kaspar, B. K. (2009). Intravascular AAV9 preferentially targets neonatal neurons and adult astrocytes. *Nature Biotechnology*, *27*(1), 59–65. https://doi.org/10.1038/nbt.1515

Frankel, A. D., & Pabo, C. O. (1988). Cellular uptake of the tat protein from human immunodeficiency virus. *Cell*, *55*(6), 1189–1193. https://doi.org/10.1016/0092-8674(88)90263-2

Frigeri, A., Gropper, M. A., Umenishi, F., Kawashima, M., Brown, D., & Verkman, A. S. (1995). Localization of MIWC and GLIP water channel homologs in neuromuscular, epithelial and glandular tissues. *Journal of Cell Science*, *108*(9), 2993–3002.

Futerman, A. H., & Pagano, R. E. (1991). Determination of the intracellular sites and topology of glucosylceramide synthesis in rat liver. *Biochemical Journal*, *280*(2), 295–302. https://doi.org/10.1042/bj2800295

Futerman, Anthony H., & Van Meer, G. (2004). The cell biology of lysosomal storage disorders. *Nature Reviews Molecular Cell Biology*, *5*(7), 554–565. https://doi.org/10.1038/nrm1423

Gao, Y., Chen, Y., Zhan, S., Zhang, W., Xiong, F., & Ge, W. (2017). Comprehensive proteome analysis of lysosomes reveals the diverse function of macrophages in immune responses.

Oncotarget, *8*(5), 7420–7440. https://doi.org/10.18632/oncotarget.14558

Gordon, G. R. J., Howarth, C., & Macvicar, B. A. (2011). Bidirectional control of arteriole diameter by astrocytes. *Experimental Physiology*, *96*(4), 393–399. https://doi.org/10.1113/expphysiol.2010.053132

Gossen, M., Freundlieb, S., Bender, G., Müller, G., Hillen, W., & Bujard, H. (1995). Transcriptional activation by tetracyclines in mammalian cells. *Science*, *268*(5218), 1766–1769. https://doi.org/10.1126/science.7792603

Gravel, R. A., Kaback, M. M., Proia, R. L., Sandhoff, K., Suzuki, K., & Suzuki, K. (2001). The GM2 Gangliosidoses. In C. R. Scriver, A. L. Beaudet, W. S. Sly, & D. Valle (Eds.), *The Metabolic and Molecular Bases of Inherited Disease* (8th ed., pp. 3827–3876). McGraw-Hill.

Gray, S. J., Matagne, V., Bachaboina, L., Yadav, S., Ojeda, S. R., & Samulski, R. J. (2011). Preclinical differences of intravascular AAV9 delivery to neurons and glia: A comparative study of adult mice and nonhuman primates. *Molecular Therapy*, *19*(6), 1058–1069. https://doi.org/10.1038/mt.2011.72

Grossman, S. A., Reinhard, C., Colvin, O. M., Chasin, M., Brundrett, R., Tamargo, R. J., & Brem, H. (1992). The intracerebral distribution of BCNU delivered by surgically implanted biodegradable polymers. *Journal of Neurosurgery*, *76*(4), 640–647. https://doi.org/10.3171/jns.1992.76.4.0640

Hanada, K., Nishijima, M., & Akamatsu, Y. (1990). A temperature-sensitive mammalian cell mutant with thermolabile serine palmitoyltransferase for the sphingolipid biosynthesis.

Journal of Biological Chemistry, *265*(36), 22137–22142. https://doi.org/10.1016/s0021-9258(18)45681-5

Hanada, K., Nishijima, M., Kiso, M., Hasegawa, A., Fujita, S., Ogawa, T., & Akamatsu, Y. (1992). Sphingolipids are essential for the growth of Chinese hamster ovary cells. Restoration of the growth of a mutant defective in sphingoid base biosynthesis by exogenous sphingolipids. *Journal of Biological Chemistry*, *267*(33), 23527–23533. https://doi.org/10.1016/s0021-9258(18)35871-x

Harris, J. P., Burrell, J. C., Struzyna, L. A., Chen, H. I., Serruya, M. D., Wolf, J. A., Duda, J. E., & Cullen, D. K. (2020). Emerging regenerative medicine and tissue engineering strategies for Parkinson's disease. *npj Parkinson's Disease*, *6*(1). https://doi.org/10.1038/s41531-019-0105-5

Hayek, S. M., & Hanes, M. C. (2014). Intrathecal therapy for chronic pain: Current trends and future needs. *Current Pain and Headache Reports*, *18*(1). https://doi.org/10.1007/s11916-013-0388-x

Henninger, D. D., Panés, J., Eppihimer, M., Russell, J., Gerritsen, M., Anderson, D. C., & Granger, D. N. (1997). Cytokine-induced VCAM-1 and ICAM-1 expression in different organs of the mouse. *Journal of Immunology, 158*(4), 1825–1832. http://www.ncbi.nlm.nih.gov/pubmed/9029122

Hladky, S. B., & Barrand, M. A. (2018). Elimination of substances from the brain parenchyma: Efflux via perivascular pathways and via the blood-brain barrier. *Fluids and Barriers of the CNS*, *15*(1), 1–73. https://doi.org/10.1186/s12987-018-0113-6

Holmgren, J., Lonnroth, I., & Svennerholm, L. (1973). Tissue receptor for cholera exotoxin: postulated structure from studies with G(M1) Ganglioside and related glycolipids. *Infection and Immunity*, *8*(2), 208–214. https://doi.org/10.1128/iai.8.2.208-214.1973

Hoogerbrugge, P. M., Brouwer, O. F., Bordigoni, P., Cornu, G., Kapaun, P., Ortega, J. J., O'Meara, A., Souillet, G., Frappaz, D., Blanche, S., Fischer, A., & Ringden, O. (1995). Allogeneic bone marrow transplantation for lysosomal storage diseases. *The Lancet*, *345*(8962), 1398–1402. https://doi.org/10.1016/S0140-6736(95)92597-X

Hou, Y., Tse, R., & Mahuran, D. J. (1996). Direct determination of the substrate specificity of the α-active site in heterodimeric β-hexosaminidase A. *Biochemistry*, *35*(13), 3963–3969. https://doi.org/10.1021/bi9524575

Hrabe, J., Hrabětová, S., & Segeth, K. (2004). A model of effective diffusion and tortuosity in the extracellular space of the brain. *Biophysical Journal*, *87*(3), 1606–1617. https://doi.org/10.1529/biophysj.103.039495

Jeckel, D., Karrenbauer, A., Burger, K. N. J., Van Meer, G., & Wieland, F. (1992). Glucosylceramide is synthesized at the cytosolic surface of various Golgi subfractions. *Journal of Cell Biology*, *117*(2), 259–267. https://doi.org/10.1083/jcb.117.2.259

Jobling, M. G., Yang, Z., Kam, W. R., Lencer, W. I., & Holmes, R. K. (2012). A single native ganglioside GM1-binding site is sufficient for cholera toxin to bind to cells and complete the intoxication pathway. *MBio*, *3*(6), 1–9. https://doi.org/10.1128/mBio.00401-12

Journet, A., Chapel, A., Kieffer, S., Roux, F., & Garin, J. (2002). Proteomic analysis of human lysosomes: Application to monocytic and breast cancer cells. *Proteomics*, *2*(8), 1026–1040.

https://doi.org/10.1002/1615-9861(200208)2:8<1026::AID-PROT1026>3.0.CO;2-I

Joyce, N. C., Haire, M. F., & Palade, G. E. (1985a). Contractile proteins in pericytes. I. Immunoperoxidase localization of tropomyosin. *Journal of Cell Biology*, *100*(5), 1379–1386. https://doi.org/10.1083/jcb.100.5.1379

Joyce, N. C., Haire, M. F., & Palade, G. E. (1985b). Contractile proteins in pericytes. II. immunocytochemical evidence for the presence of two isomyosins in graded concentrations. *Journal of Cell Biology*, *100*(5), 1387–1395. https://doi.org/10.1083/jcb.100.5.1387

Kalaria, R. N., Gravina, S. A., Schmidley, J. W., Perry, G., & Harik, S. I. (1988). The glucose transporter of the human brain and blood-brain barrier. *Annals of Neurology*, *24*(6), 757–764. https://doi.org/10.1002/ana.410240610

Kolter, T. (2012). Ganglioside biochemistry. *ISRN Biochemistry*, *2012*, 1–36. https://doi.org/10.5402/2012/506160

Korneluk, R. G., Mahuran, D. J., Neote, K., Klavins, M. H., O'Dowd, B. F., Tropak, M., Willard, H. F., Anderson, M. J., Lowden, J. A., & Gravel, R. A. (1986). Isolation of cDNA clones coding for the α-subunit of human β-hexosaminidase. Extensive homology between the α- and β-subunits and studies on Tay-Sachs disease. *Journal of Biological Chemistry*, *261*(18), 8407–8413.

Kresse, H., Fuchs, W., Glössl, J., Holtfrerich, D., & Gilberg, W. (1981). Liberation of N-acetylglucosamine-6-sulfate by human β-N-acetylhexosaminidase A. *Journal of Biological Chemistry*, *256*(24), 12926–12932.

Kuhn, R., & Wiegandt, H. (1963). Die Konstitution der Ganglio-N-tetraose und des Gangliosids GI. *Chemische Berichte*, *96*(3), 866–880.

Kytzia, H. J., & Sandhoff, K. (1985). Evidence for two different active sites on human β-hexosaminidase A. Interaction of G(M2) activator protein with β-hexosaminidase A. *Journal of Biological Chemistry*, *260*(12), 7568–7572.

Leavens, M. E., Hill, C. S., Cech, D. A., Weyland, J. B., & Weston, J. S. (1982). Intrathecal and intraventricular morphine for pain in cancer patients: initial study. *Journal of Neurosurgery*, *56*(2), 241–245. https://doi.org/10.3171/jns.1982.56.2.0241

Ledeen, R., & Wu, G. (2018). Gangliosides of the Nervous System. In S. Sonnino & A. Prinetti (Eds.), *Gangliosides: Methods and Protocols* (pp. 19–55). Springer New York. https://doi.org/10.1007/978-1-4939-8552-4_2

Leinekugel, P., Michel, S., Conzelmann, E., & Sandhoff, K. (1992). Quantitative correlation between the residual activity of β-hexosaminidase A and arylsulfatase A and the severity of the resulting lysosomal storage disease. *Human Genetics*, *88*, 513–523.

Lemieux, M. J., Mark, B. L., Cherney, M. M., Withers, S. G., Mahuran, D. J., & James, M. N. G. (2006). Crystallographic structure of human β-hexosaminidase A: Interpretation of Tay-Sachs mutations and loss of GM2 ganglioside hydrolysis. *Journal of Molecular Biology*, *359*(4), 913–929. https://doi.org/10.1016/j.jmb.2006.04.004

Li, Z., Michael, I. P., Zhou, D., Nagy, A., & Rini, J. M. (2013). Simple *piggyBac* transposon-based mammalian cell expression system for inducible protein production. *Proceedings of the National Academy of Sciences of the United States of America*, *110*(13), 5004–5009.

https://doi.org/10.1073/pnas.1218620110

Lieser, M., Harms, E., Kern, H., Bach, G., & Cantz, M. (1989). Ganglioside GM3 sialidase activity in fibroblasts of normal individuals and of patients with sialidosis and mucolipidosis IV. Subcellular distribution and some properties. *Biochemical Journal*, *260*(1), 69–74. https://doi.org/10.1042/bj2600069

Lin, J., Zhou, H., Zhang, N., Yin, B., & Sheng, H. S. (2012). Effects of the implantation of Ommaya reservoir in children with tuberculous meningitis hydrocephalus: A preliminary study. *Child's Nervous System*, *28*(7), 1003–1008. https://doi.org/10.1007/s00381-012-1748-2

Linke, T., Wilkening, G., Sadeghlar, F., Mozcall, H., Bernardo, K., Schuchman, E., & Sandhoff, K. (2001). Interfacial regulation of acid ceramidase activity: Stimulation of ceramide degradation by lysosomal lipids and sphingolipid activator proteins. *Journal of Biological Chemistry*, *276*(8), 5760–5768. https://doi.org/10.1074/jbc.M006846200

Lu, C. T., Zhao, Y. Z., Wong, H. L., Cai, J., Peng, L., & Tian, X. Q. (2014). Current approaches to enhance CNS delivery of drugs across the brain barriers. *International Journal of Nanomedicine*, *9*(1), 2241–2257. https://doi.org/10.2147/IJN.S61288

Luzio, J. P., Pryor, P. R., & Bright, N. A. (2007). Lysosomes: Fusion and function. *Nature Reviews Molecular Cell Biology*, *8*(8), 622–632. https://doi.org/10.1038/nrm2217

Madani, F., Lindberg, S., Langel, Ü., Futaki, S., & Gräslund, A. (2011). Mechanisms of cellular uptake of cell-penetrating peptides. *Journal of Biophysics*, *2011*. https://doi.org/10.1155/2011/414729

Maegawa, G.H.B., Stockley, T., & Tropak, M. (2006). The natural history of juvenile or subacute GM2 gangliosidosis: 21 new cases and literature review of 134 previously reported. *Pediatrics*, *120*(4), 936. https://doi.org/10.1542/peds.2007-0343

Maegawa, G.H.B., Banwell, B. L., Blaser, S., Sorge, G., Toplak, M., Ackerley, C., Hawkins, C., Hayes, J., & Clarke, J. T. R. (2009). Substrate reduction therapy in juvenile GM2 gangliosidosis. *Molecular Genetics and Metabolism*, *98*(1–2), 215–224. https://doi.org/10.1016/j.ymgme.2009.06.005

Maegawa, G.H.B., Tropak, M., Buttner, J., Stockley, T., Kok, F., Clarke, J. T. R., & Mahuran, D. J. (2007). Pyrimethamine as a potential pharmacological chaperone for late-onset forms of GM2 gangliosidosis. *Journal of Biological Chemistry*, *282*(12), 9150–9161. https://doi.org/10.1074/jbc.M609304200

Mahuran, D. J. (1999). Biochemical consequences of mutations causing the GM2 gangliosidoses. *Biochimica et Biophysica Acta - Molecular Basis of Disease*, *1455*(2–3), 105–138. https://doi.org/10.1016/S0925-4439(99)00074-5

Mahuran, D., & Lowden, J. A. (1980). The subunit and polypeptide structure of hexosaminidases from human placenta. *Canadian Journal of Biochemistry*, *58*(4), 287–294. https://doi.org/10.1139/o80-038

Malisan, F., & Testi, R. (2002). GD3 ganglioside and apoptosis. *Biochimica et Biophysica Acta - Molecular and Cell Biology of Lipids*, *1585*(2–3), 179–187. https://doi.org/10.1016/S1388-1981(02)00339-6

Mark, B. L., Mahuran, D. J., Cherney, M. M., Zhao, D., Knapp, S., & James, M. N. G. (2003).

Crystal structure of human β-hexosaminidase B: Understanding the molecular basis of Sandhoff and Tay-Sachs disease. *Journal of Molecular Biology*, *327*(5), 1093–1109. https://doi.org/10.1016/S0022-2836(03)00216-X

Marshall, N. R., Hassiotis, S., King, B., Rozaklis, T., Trim, P. J., Duplock, S. K., Winner, L. K., Beard, H., Snel, M. F., Jolly, R. D., Hopwood, J. J., & Hemsley, K. M. (2015). Delivery of therapeutic protein for prevention of neurodegenerative changes: Comparison of different CSF-delivery methods. *Experimental Neurology*, *263*, 79–90. https://doi.org/10.1016/j.expneurol.2014.09.008

McDannold, N. J., Vykhodtseva, N. I., & Hynynen, K. (2006). Microbubble contrast agent with focused ultrasound to create brain lesions at low power levels: MR imaging and histologic study in rabbits. *Radiology*, *241*(1), 95–106. https://doi.org/10.1148/radiol.2411051170

Medina-Bolivar, F., Wright, R., Funk, V., Sentz, D., Barroso, L., Wilkins, T. D., Petri, W., & Cramer, C. L. (2003). A non-toxic lectin for antigen delivery of plant-based mucosal vaccines. *Vaccine*, *21*(9–10), 997–1005. https://doi.org/10.1016/S0264-410X(02)00551-0

Meier, E. M., Schwarzmann, G., Furst, W., & Sandhoff, K. (1991). The human G(M2) activator protein. A substrate specific cofactor of β-hexosaminidase A. *Journal of Biological Chemistry*, *266*(3), 1879–1887.

Meikle, P. J., Hopwood, J. J., Clague, A. E., & Carey, W. F. (1999). Prevalence of lysosomal storage disorders. *Journal of the American Medical Association*, *281*(3), 249–254. https://doi.org/10.1001/jama.281.3.249

Mercadante, S. (1999). Problems of long-term spinal opioid treatment in advanced cancer

patients. *Pain*, *79*(1), 1–13. https://doi.org/10.1016/S0304-3959(98)00118-3

Miller, G. (2002). Breaking down barriers. *Science*, *297*(5584), 1116–1118.

Neudorfer, O., Pastores, G. M., Zeng, B. J., Gianutsos, J., Zaroff, C. M., & Kolodny, E. H. (2005). Late-onset Tay-Sachs disease: Phenotypic characterization and genotypic correlation in 21 affected patients. *Genetics in Medicine*, *7*(2), 119–123. https://doi.org/10.1097/01.GIM.0000154300.84107.75

Neuwelt, E. A., Frenkel, E. P., Diehl, J., Vu, L. H., Rapoport, S., & Hill, S. (1980). Reversible osmotic blood-brain barrier disruption in humans: Implications for the chemotherapy of malignant brain tumors. *Neurosurgery*, *7*(1), 44–52.

Nicholson, C., Kamali-Zare, P., & Tao, L. (2011). Brain extracellular space as a diffusion barrier. *Computing and Visualization in Science*, *14*(7), 309–325. https://doi.org/10.1007/s00791-012-0185-9

Nielsen, S., Nagelhus, E. A., Amiry-Moghaddam, M., Bourque, C., Agre, P., & Ottersen, O. R. (1997). Specialized membrane domains for water transport in glial cells: High- resolution immunogold cytochemistry of aquaporin-4 in rat brain. *Journal of Neuroscience*, *17*(1), 171–180. https://doi.org/10.1523/jneurosci.17-01-00171.1997

Norflus, F., Suzuki, K., Proia, R. L., Norflus, F., Tifft, C. J., Mcdonald, M. P., Goldstein, G., Crawley, J. N., Hoffmann, A., Sandhoff, K., Suzuki, K., & Proia, R. L. (1998). Bone marrow transplantation prolongs life span and ameliorates neurologic manifestations in Sandhoff disease mice. *Journal of Clinical Investigation*, *101*(9), 1881–1888. https://doi.org/10.1172/JCI2127

Norman, R. M., & Wood, N. (1941). A congenital form of amaurotic family idiocy. *Journal of Neurology, Neurosurgery & Psychiatry*, *4*(3–4), 175–190. https://doi.org/10.1136/jnnp.4.3-4.175

Ohkuma, S., Moriyama, Y., & Takano, T. (1982). Identification and characterization of a proton pump on lysosomes by fluorescein isothiocyanate-dextran fluorescence. *Proceedings of the National Academy of Sciences of the United States of America*, *79*(9), 2758–2762. https://doi.org/10.1073/pnas.79.9.2758

Okada, S., & O'Brien, J. S. (1968). Generalized gangliosidosis: Beta-galactosidase deficiency. *Science*, *160*, 1002–1004.

Okada, S., & O'Brien, J. S. (1969). Tay-Sachs disease : Generalized absence of a beta-D-N-acetylhexosaminidase component. *Science*, *165*(3894), 698–700.

Oldendorf, W. H., Cornford, M. E., & Brown, W. J. (1977). The large apparent work capability of the blood-brain barrier: A study of the mitochondrial content of capillary endothelial cells in brain and other tissues of the rat. *Annals of Neurology*, *1*(5), 409–417.

Oller-Salvia, B., Sánchez-Navarro, M., Giralt, E., & Teixidó, M. (2016). Blood-brain barrier shuttle peptides: An emerging paradigm for brain delivery. *Chemical Society Reviews*, *45*(17), 4690–4707. https://doi.org/10.1039/c6cs00076b

Osmon, K. J. L., Woodley, E., Thompson, P., Ong, K., Karumuthil-Melethil, S., Keimel, J. G., Mark, B. L., Mahuran, D., Gray, S. J., & Walia, J. S. (2016). Systemic gene transfer of a hexosaminidase variant using an scAAV9.47 vector corrects GM2 gangliosidosis in Sandhoff mice. *Human Gene Therapy*, *27*(7), 497–508.

https://doi.org/10.1089/hum.2016.015

Ou, L., Przybilla, M. J., Koniar, B., & Whitley, C. B. (2018). RTB lectin-mediated delivery of lysosomal α-L-iduronidase mitigates disease manifestations systemically including the central nervous system. *Molecular Genetics and Metabolism*, *123*(2), 105–111. https://doi.org/10.1016/j.ymgme.2017.11.013

Ou, L., Przybilla, M. J., Tăbăran, A. F., Overn, P., O'Sullivan, M. G., Jiang, X., Sidhu, R., Kell, P. J., Ory, D. S., & Whitley, C. B. (2020). A novel gene editing system to treat both Tay–Sachs and Sandhoff diseases. *Gene Therapy*, *27*(5), 226–236. https://doi.org/10.1038/s41434-019-0120-5

Ozand, P. T., & Al-essa, M. (2012). Lysosomal Storage Diseases. In *Textbook of Clinical Pediatrics*. https://doi.org/10.1007/978-3-642-02202-9

Palmieri, M., Impey, S., Kang, H., di Ronza, A., Pelz, C., Sardiello, M., & Ballabio, A. (2011). Characterization of the CLEAR network reveals an integrated control of cellular clearance pathways. *Human Molecular Genetics*, *20*(19), 3852–3866. https://doi.org/10.1093/hmg/ddr306

Pardridge, W. M. (1986). Receptor-mediated peptide transport through the blood-brain barrier. *Endocrine Reviews*, *7*(3), 314–330. https://doi.org/10.1210/edrv-7-3-314

Pauwels, A. M., Trost, M., Beyaert, R., & Hoffmann, E. (2017). Patterns, receptors, and signals: regulation of phagosome maturation. *Trends in Immunology*, *38*(6), 407–422. https://doi.org/10.1016/j.it.2017.03.006

Penn, R. D., & Paice, J. A. (1987). Chronic intrathecal morphine for intractable pain. *Journal of Neurosurgery*, *67*(2), 182–186. https://doi.org/10.3171/jns.1987.67.2.0182

Platt, F. M., Boland, B., & van der Spoel, A. C. (2012). Lysosomal storage disorders: The cellular impact of lysosomal dysfunction. *Journal of Cell Biology*, *199*(5), 723–734. https://doi.org/10.1083/jcb.201208152

Platt, F. M., d'Azzo, A., Davidson, B. L., Neufeld, E. F., & Tifft, C. J. (2018). Lysosomal storage diseases. *Nature Reviews Disease Primers*, *4*(1). https://doi.org/10.1038/s41572-018-0025-4

Platt, F. M., Neises, G. R., Dwek, R. A., & Butters, T. D. (1994). N-butyldeoxynojirimycin is a novel inhibitor of glycolipid biosynthesis. *Journal of Biological Chemistry*, *269*(11), 8362–8365. https://doi.org/10.1016/s0021-9258(17)37202-2

Preuss, U., Gu, X., Gu, T., & Yu, R. K. (1993). Purification and characterization of CMP-N-acetylneuraminic acid:lactosylceramide (α2-3) sialyltransferase (G(M3)-synthase) from rat brain. *Journal of Biological Chemistry*, *268*(35), 26273–26278. https://doi.org/10.1016/s0021-9258(19)74311-7

Proia, R. L. (1988). Gene encoding the human β-hexosaminidase β chain: Extensive homology of intron placement in the α- and β-chain genes. *Proceedings of the National Academy of Sciences of the United States of America*, *85*(6), 1883–1887. https://doi.org/10.1073/pnas.85.6.1883

Rapoport, Sanley I. (1970). Effect of concentrated on blood-brain solutions barrier. *American Journal of Physiology*, *219*(1), 270–274.

Rapoport, Stanley I., Hori, M., & Klatzo, I. (1971). Reversible osmotic opening of the blood-brain barrier. *Science*, *173*(4001), 1026–1028. https://www.jstor.org/stable/1732289

Rash, J. E., Yasumura, T., Hudson, C. S., Agre, P., & Nielsen, S. (1998). Direct immunogold labeling of aquaporin-4 in square arrays of astrocyte and ependymocyte plasma membranes in rat brain and spinal cord. *Proceedings of the National Academy of Sciences of the United States of America*, *95*(20), 11981–11986. https://doi.org/10.1073/pnas.95.20.11981

Reddy, A., Caler, E. V., & Andrews, N. W. (2001). Plasma membrane repair is mediated by Ca2+-regulated exocytosis of lysosomes. *Cell*, *106*(2), 157–169. https://doi.org/10.1016/S0092-8674(01)00421-4

Reese, T. S., & Karnovsky, M. J. (1967). Fine structural localization of a blood-brain barrier to exogenous peroxidase. *The Journal of Cell Biology*, *34*(1), 207–217. https://doi.org/10.1083/jcb.34.1.207

Rezai, A. R., Ranjan, M., D'Haese, P. F., Haut, M. W., Carpenter, J., Najib, U., Mehta, R. I., Chazen, J. L., Zibly, Z., Yates, J. R., Hodder, S. L., & Kaplitt, M. (2020). Noninvasive hippocampal blood−brain barrier opening in Alzheimer's disease with focused ultrasound. *Proceedings of the National Academy of Sciences of the United States of America*, *117*(17), 9180–9182. https://doi.org/10.1073/pnas.2002571117

Ribecco-Lutkiewicz, M., Sodja, C., Haukenfrers, J., Haqqani, A. S., Ly, D., Zachar, P., Baumann, E., Ball, M., Huang, J., Rukhlova, M., Martina, M., Liu, Q., Stanimirovic, D., Jezierski, A., & Bani-Yaghoub, M. (2018). A novel human induced pluripotent stem cell blood-brain barrier model: Applicability to study antibody-triggered receptor-mediated

transcytosis. *Scientific Reports*, *8*(1), 1–17. https://doi.org/10.1038/s41598-018-19522-8

Rodriguez, A., Tatter, S. B., & Debinski, W. (2015). Neurosurgical techniques for disruption of the blood–brain barrier for glioblastoma treatment. *Pharmaceutics*, *7*(3), 175–187. https://doi.org/10.3390/pharmaceutics7030175

Roe, K., Orillo, B., & Verma, S. (2014). West nile virus-induced cell adhesion molecules on human brain microvascular endothelial cells regulate leukocyte adhesion and modulate permeability of the in vitro blood-brain barrier model. *PLoS ONE*, *9*(7), 1–12. https://doi.org/10.1371/journal.pone.0102598

Rutenber, E., Ready, M., & Robertus, J. D. (1987). Structure and evolution of ricin B chain. *Nature*, *326*(6113), 624–626. https://doi.org/10.1038/326624a0

Sachs, B. (1887). On arrested cerebral development with special reference to its cortical Pathology. *Journal of Nervous and Mental Disease*, *14*(9), 541–553.

Sachs, B. (1896). A family form of idiocy, generally fatal, associated with early blindness (amaurotic family idiocy). *New York Medical Journal*, *63*, 697.

Sandhoff, K., & Christomanou, H. (1979). Biochemistry and genetics of gangliosidoses. *Human Genetics*, *50*(2), 107–143. https://doi.org/10.1007/BF00390234

Sandhoff, K. (1969). Variation of β-N-acetylhexosaminidase pattern in Tay-Sachs disease. *FEBS Letters*, *4*(4), 351–354.

Sandhoff, Konrad, & Harzer, K. (2013). Gangliosides and gangliosidoses: Principles of molecular and metabolic pathogenesis. *Journal of Neuroscience*, *33*(25), 10195–10208.

https://doi.org/10.1523/JNEUROSCI.0822-13.2013

Sandhoff, Konrad, & Kolter, T. (2003). Biosynthesis and degradation of mammalian glycosphingolipids. *Philosophical Transactions of the Royal Society B: Biological Sciences*, *358*(1433), 847–861. https://doi.org/10.1098/rstb.2003.1265

Sands, M. S., & Davidson, B. L. (2006). Gene therapy for lysosomal storage diseases. *Molecular Therapy*, *13*(5), 839–849. https://doi.org/10.1016/j.ymthe.2006.01.006

Sandvig, K., Pust, S., Skotland, T., & van Deurs, B. (2011). Clathrin-independent endocytosis: Mechanisms and function. *Current Opinion in Cell Biology*, *23*(4), 413–420. https://doi.org/10.1016/j.ceb.2011.03.007

Sango, K., Johnson, O. N., Kozak, C. A., & Proia, R. L. (1995). β-1,4-N-acetylgalactosaminyltransferase involved in ganglioside syntesis: cDNA sequence, expression and chromosome mapping of the mouse gene. *Genomics*, *27*, 362–365.

Schnaar, R. L. (2016). Gangliosides of the vertebrate nervous system. *Journal of Molecular Biology*, *428*(16), 3325–3336. https://doi.org/10.1016/j.jmb.2016.05.020

Sharma, R., Deng, H., Leung, A., & Mahuran, D. (2001). Identification of the 6-sulfate binding site unique to α-subunit-containing isozymes of human β-hexosaminidase. *Biochemistry*, *40*(18), 5440–5446. https://doi.org/10.1021/bi0029200

Shulman, M. L., Kulshin, V. A., & Khorlin, A. Y. (1980). A continuous fluorimetric assay for glycosidase activity: Human N-acetyl-β-D-hexosaminidase. *Analytical Biochemistry*, *101*(2), 342–348. https://doi.org/10.1016/0003-2697(80)90198-0

Siegal, T., Rubinstein, R., Bokstein, F., Schwartz, A., Lossos, A., Shalom, E., Chisin, R., & Gomori, J. M. (2000). *In vivo* assessment of the window of barrier opening after osmotic blood-brain barrier disruption in humans. *Journal of Neurosurgery*, *92*(4), 599–605. https://doi.org/10.3171/jns.2000.92.4.0599

Smith, Q. R., Momma, S., Aoyagi, M., & Rapoport, S. I. (1987). Kinetics of neutral amino acid transport across the blood-brain barrier. *Journal of Neurochemistry*, *49*(5), 1651–1658. https://doi.org/10.1111/j.1471-4159.1987.tb01039.x

Soderquist, R. G., & Mahoney, M. J. (2010). Central nervous system delivery of large molecules: Challenges and new frontiers for intrathecally administered therapeutics. *Expert Opinion on Drug Delivery*, *7*(3), 285–293. https://doi.org/10.1517/17425240903540205

Sommer, B., Karageorgos, N., AlSharif, M., Stubbe, H., & Hans, F. J. (2020). Long-term outcome and adverse events of intrathecal opioid therapy for nonmalignant pain syndrome. *Pain Practice*, *20*(1), 8–15. https://doi.org/10.1111/papr.12818

Sorrentino, N. C., D'Orsi, L., Sambri, I., Nusco, E., Monaco, C., Spampanato, C., Polishchuk, E., Saccone, P., De Leonibus, E., Ballabio, A., & Fraldi, A. (2013). A highly secreted sulphamidase engineered to cross the blood-brain barrier corrects brain lesions of mice with mucopolysaccharidoses type IIIA. *EMBO Molecular Medicine*, *5*(5), 675–690. https://doi.org/10.1002/emmm.201202083

Spector, R., Robert Snodgrass, S., & Johanson, C. E. (2015). A balanced view of the cerebrospinal fluid composition and functions: Focus on adult humans. *Experimental Neurology*, *273*, 57–68. https://doi.org/10.1016/j.expneurol.2015.07.027

Spencer, B. J., & Verma, I. M. (2007). Targeted delivery of proteins across the blood-brain barrier. *Proceedings of the National Academy of Sciences of the United States of America*, *104*(18), 7594–7599. https://doi.org/10.1073/pnas.0702170104

Spencer, B., Marr, R. A., Gindi, R., Potkar, R., Michael, S., Adame, A., Rockenstein, E., Verma, I. M., & Masliah, E. (2011). Peripheral delivery of a CNS targeted, metalo-protease reduces Aβ toxicity in a mouse model of Alzheimer's disease. *PLoS ONE*, *6*(1). https://doi.org/10.1371/journal.pone.0016575

Srivastava, S. K., & Beutler, E. (1973). Hexosaminidase-A and hexosaminidase-B: Studies in Tay-Sachs' and Sandhoff's disease. *Nature*, *241*(5390), 463. https://doi.org/10.1038/241463a0

Stewart, P. S., & Mueller-Dieckmann, J. (2014). Automation in biological crystallization. *Acta Crystallographica Section F:Structural Biology Communications*, *70*(6), 686–696. https://doi.org/10.1107/S2053230X14011601

Stins, M. F., Gilles, F., & Kim, K. S. (1997). Selective expression of adhesion molecules on human brain microvascular endothelial cells. *Journal of Neuroimmunology*, *76*(1–2), 81–90. https://doi.org/10.1016/S0165-5728(97)00036-2

Svennerholm, L. (1963). Chromatographic separation of human brain gangliosides. *Journal of Neurochemistry*, *10*(9), 613–623. https://doi.org/10.1111/j.1471-4159.1963.tb08933.x

Svennerholm, L. (1980). Gangliosides and Synaptic Transmission. In L. Svennerholm, P. Mandel, H. Dreyfus, & P.-F. Urban (Eds.), *Structure and Function of Gangliosides* (pp. 533–544). Springer US. https://doi.org/10.1007/978-1-4684-7844-0_46

Svennerholm, L. (1964). The gangliosides. *Journal of Lipid Research*, *5*(1), 145–155.

Tay, W. (1881). Symmetrical changes in the region of the yellow spot in each eye of an infant. *Transactions of the Opthalmological Society of the United Kingdom*, *1*, 55–57.

ThermoFisher Scientific. (2003). *Gateway® Technology A universal technology to clone DNA sequences for functional analysis and expression in multiple systems*. https://tools.thermofisher.com/content/sfs/manuals/gatewayman.pdf.

Thiebaut, F., Tsuruo, T., Hamada, H., Gottesman, M. M., Pastan, I., & Willingham, M. C. (1989). Immunohistochemical localization in normal tissues of different epitopes in the multidrug transport protein P170: Evidence for localization in brain capillaries and crossreactivity of one antibody with a muscle protein. *Journal of Histochemistry and Cytochemistry*, *37*(2), 159–164. https://doi.org/10.1177/37.2.2463300

Toyokawa, G., Toyozawa, R., Inamasu, E., Kojo, M., Morodomi, Y., Shiraishi, Y., Takenaka, T., Hirai, F., Yamaguchi, M., Seto, T., Takenoyama, M., & Ichinose, Y. (2013). Cystic brain metastasis of non-small-cell lung cancer successfully controlled with Ommaya reservoir placement. *International Cancer Conference Journal*, *2*(2), 89–92. https://doi.org/10.1007/s13691-012-0068-4

Tropak, M. B., Blanchard, J. E., Withers, S. G., Brown, E. D., & Mahuran, D. (2007). High-throughput screening for human lysosomal β-N-acetyl hexosaminidase inhibitors acting as pharmacological chaperones. *Chemistry and Biology*, *14*(2), 153–164. https://doi.org/10.1016/j.chembiol.2006.12.006

Tropak, M. B., & Mahuran, D. (2007). Lending a helping hand, screening chemical libraries for

compounds that enhance β-hexosaminidase A activity in GM2 gangliosidosis cells. *FEBS Journal*, *274*(19), 4951–4961. https://doi.org/10.1111/j.1742-4658.2007.06040.x

Tropak, M. B., Reid, S. P., Guiral, M., Withers, S. G., & Mahuran, D. (2004). Pharmacological enhancement of β-hexosaminidase activity in fibroblasts from adult Tay-Sachs and Sandhoff patients. *Journal of Biological Chemistry*, *279*(14), 13478–13487. https://doi.org/10.1074/jbc.M308523200

Tropak, M. B., Yonekawa, S., Karumuthil-Melethil, S., Thompson, P., Wakarchuk, W., Gray, S. J., Walia, J. S., Mark, B. L., & Mahuran, D. (2016). Construction of a hybrid β-hexosaminidase subunit capable of forming stable homodimers that hydrolyze GM2 ganglioside in vivo. In *Molecular Therapy - Methods and Clinical Development*, 3, 15057. https://doi.org/10.1038/mtm.2015.57

Tsuji, D., Akeboshi, H., Matsuoka, K., Yasuoka, H., Miyasaki, E., Kasahara, Y., Kawashima, I., Chiba, Y., Jigami, Y., Taki, T., Sakuraba, H., & Itoh, K. (2011). Highly phosphomannosylated enzyme replacement therapy for GM2 gangliosidosis. *Annals of Neurology*, *69*(4), 691–701. https://doi.org/10.1002/ana.22262

U.S. Food and Drug Administration (1996). *Gliadel Wafer NDA 20-637 approval letter*. https://www.accessdata.fda.gov/drugsatfda_docs/nda/96/020637Orig1s000.pdf

Vaccaro, A. M., Tatti, M., Ciaffoni, F., Salvioli, R., Barca, A., & Scerch, C. (1997). Effect of saposins A and C on the enzymatic hydrolysis of liposomal glucosylceramide. *Journal of Biological Chemistry*, *272*(27), 16862–16867. https://doi.org/10.1074/jbc.272.27.16862

Van Itallie, C., Rahner, C., & Anderson, J. M. (2001). Regulated expression of claudin-4

decreases paracellular conductance through a selective decrease in sodium permeability. *Journal of Clinical Investigation*, *107*(10), 1319–1327. https://doi.org/10.1172/JCI12464

Vivès, E., Brodin, P., & Lebleu, B. (1997). A truncated HIV-1 tat protein basic domain rapidly translocates through the plasma membrane and accumulates in the cell nucleus. *Journal of Biological Chemistry*, *272*(25), 16010–16017. https://doi.org/10.1074/jbc.272.25.16010

Vlachos, F., Tung, Y. S., & Konofagou, E. (2011). Permeability dependence study of the focused ultrasound-induced blood-brain barrier opening at distinct pressures and microbubble diameters using DCE-MRI. *Magnetic Resonance in Medicine*, *66*(3), 821–830. https://doi.org/10.1002/mrm.22848

Vrijens, P., Noppen, S., Boogaerts, T., Vanstreels, E., Ronca, R., Chiodelli, P., Laporte, M., Vanderlinden, E., Liekens, S., Stevaert, A., & Naesens, L. (2019). Influenza virus entry via the GM3 ganglioside-mediated platelet-derived growth factor receptor β signalling pathway. *Journal of General Virology*, *100*(4), 583–601. https://doi.org/10.1099/jgv.0.001235

Walia, J. S., Altaleb, N., Bello, A., Kruck, C., LaFave, M. C., Varshney, G. K., Burgess, S. M., Chowdhury, B., Hurlbut, D., Hemming, R., Kobinger, G. P., & Triggs-Raine, B. (2015). Long-term correction of Sandhoff disease following intravenous delivery of rAAV9 to mouse neonates. *Molecular Therapy*, *23*(3), 414–422. https://doi.org/10.1038/mt.2014.240

Wang, D., El-Amouri, S. S., Dai, M., Kuan, C. Y., Hui, D. Y., Brady, R. O., & Pan, D. (2013). Engineering a lysosomal enzyme with a derivative of receptor-binding domain of apoE enables delivery across the blood-brain barrier. *Proceedings of the National Academy of Sciences of the United States of America*, *110*(8), 2999–3004.

https://doi.org/10.1073/pnas.1222742110

Wang, E., Norred, W. P., Bacon, C. W., Riley, R. T., & Merrill, A. H. (1991). Inhibition of sphingolipid biosynthesis by fumonisins. Implications for diseases associated with Fusarium moniliforme. *Journal of Biological Chemistry*, *266*(22), 14486–14490. https://doi.org/10.1016/s0021-9258(18)98712-0

Wang, J., Cui, Y., Yu, Z., Wang, W., Cheng, X., Ji, W., Guo, S., Zhou, Q., Wu, N., Chen, Y., Chen, Y., Song, X., Jiang, H., Wang, Y., Lan, Y., Zhou, B., Mao, L., Li, J., Yang, H., Guo, W. & Yang, X. (2019). Brain endothelial cells maintain lactate homeostasis and control adult hippocampal neurogenesis. *Cell Stem Cell*, *25*(6), 754-767.e9. https://doi.org/10.1016/j.stem.2019.09.009

Wang, W., Lin, C., Lu, D., Ning, Z., Cox, T., Melvin, D., Wang, X., Bradley, A., & Liu, P. (2008). Chromosomal transposition of *PiggyBac* in mouse embryonic stem cells. *Proceedings of the National Academy of Sciences of the United States of America*, *105*(27), 9290–9295. https://doi.org/10.1073/pnas.0801017105

Webster, C. I., Caram-Salas, N., Haqqani, A. S., Thom, G., Brown, L., Rennie, K., Yogi, A., Costain, W., Brunette, E., & Stanimirovic, D. B. (2016). Brain penetration, target engagement, and disposition of the blood-brain barrier-crossing bispecific antibody antagonist of metabotropic glutamate receptor type 1. *FASEB Journal*, *30*(5), 1927–1940. https://doi.org/10.1096/fj.201500078

Wei, B., Qian, C., Liu, Y., Lin, X., Wan, J., & Wang, Y. (2017). Ommaya reservoir in the treatment of cryptococcal meningitis. *Acta Neurologica Belgica*, *117*(1), 283–287.

https://doi.org/10.1007/s13760-016-0682-6

Westergaard, E., & Brightman, M. W. (1973). Transport of proteins across normal cerebral arterioles. *Journal of Comparative Neurology*, *152*(1), 17–44. https://doi.org/10.1002/cne.901520103

Wilkening, G., Linke, T., Uhlhorn-Dierks, G., & Sandhoff, K. (2000). Degradation of membrane-bound ganglioside GM1: Stimulation by bis(monoacylglycero)phosphate and the activator proteins SAP-B and GM2-AP. *Journal of Biological Chemistry*, *275*(46), 35814–35819. https://doi.org/10.1074/jbc.M006568200

Yam, G. H.-F., Zuber, C., & Roth, J. (2005). A synthetic chaperone corrects the trafficking defect and disease phenotype in a protein misfolding disorder. *The FASEB Journal*, *19*(1), 12–18. https://doi.org/10.1096/fj.04-2375com

Zschoche, A., Fürst, W., Schwarzmann, G., & Sandhoff, K. (1994). Hydrolysis of lactosylceramide by human galactosylceramidase and GM1-β-galactosidase in a detergent-free system and its stimulation by sphingolipid activator proteins, sap-B and sap-C Activator proteins stimulate lactosylceramide hydrolysis. *European Journal of Biochemistry*, *222*(1), 83–90. https://doi.org/10.1111/j.1432-1033.1994.tb18844.x